Synthesis of Gold Nanoparticle-Hydrogel Nanocomposites with Controlled Cytotoxicity and Unique Cell-Adhesive Properties

Vorgelegt von
M.Sc. Fang Ren
aus Hunan

Von der Fakultät II - Mathematik und Naturwissenschaften

der Technischen Universität Berlin

zur Erlangung des akademischen Grades

Doktor der Ingenieurwissenschaften
Dr.-Ing.

genehmigte Dissertation

Promotionsausschuss:

Vorsitzender: Prof. Dr. Janina Maultzsch

Berichter/Gutachter: Prof. Dr. Ir. Marga C. Lensen

Berichter/Gutachter: Prof. Dr. Ulla Wollenberger

Tag der wissenschaftlichen Aussprache: 9. September 2016

Berlin 2016

Table of contents

List of abbreviations

3D	Three dimensional
8PEG	8arm star-shaped poly(ethylene glycol) with acrylate-end groups
8PEG-NH_3	Hydrogels synthesized by mixing of 8PEG and NH_3
8PEG-UV	The UV-curing 8PEG hydrogels via photopolymerization
Au NPs	Gold nanoparticles
AFM	Atomic force microscopy
APTES	(3-aminopropyl) triethoxysilane
BC	Before Christ
BSA	Bovine serum albumin
CNTs	Carbon nanotubes
CVD	Chemical vapor deposition
DTT	DL-dithiothreitol
DAPI	4',6-diamidino-2-phenylindole
DMEM	Dulbecco's modified eagle's medium
DNA	Deoxyribonucleic acid
e.g.	*exempli gratia*
et al.	e*t altera*
ECM	Extracellular matrix
FA	Focal adhesion
FBS	Fetal bovine serum
FDA	Fluorescein diacetate

FN	Fibronectin
FTIR	Fourier transform infrared spectroscopy
GO	Graphene oxide
h	hour
i.e.	*id est*
HA	Hyaluronic acid
LDH	Lactate dehydrogenase
MTT	3-(4,5-dimethyl-2-thiazolyl)-2,5-diphenyl-2-H-tetrazolium bromide
Mw	Molecular weight
NPs	Nanoparticles
PBS	Phosphate buffered saline solution
PEG	Poly(ethylene glycol)
PVA	Poly(vinyl alcohol)
PAA	Polyacrylic acid
PI	Propidium iodide
PLL	Poly(L-lysine)
PNIPAAm	Poly(N-isopropylacrylamide)
QDs	Quantum dots
RPMI	Roswell park memorial institute
r.t.	room temperature
RGD	Tripepti acid arginine–glycine–aspartic
SAMs	Self-assembled monolayers
SEM	Scanning electron microscope

starPEG	Star-shaped poly(ethylene glycol)
-SH	Thiol
TEM	Transmission electron microscope
TCPS	Tissue culture polystyrene
UV	Ultraviolet
UV-vis	Ultraviolet-visible
VN	Vitronectin
VS	Vinyl sulfone
V/V	Volume/Volume
W/V	Weight/Volume

Scope and organization of the thesis

The overall topic of this thesis is **Synthesis of Gold Nanoparticle-Hydrogel Nanocomposites with Controlled Cytotoxicity and Unique Cell-Adhesive Properties**. In recent years, the properties and structure of gold nanoparticles (Au NPs) make them useful for a wide array of biological applications. However, studies to address their potential cytotoxicity and control cell behaviors are few in comparison. In the present work, the cytotoxicity effects of Au NPs with different sizes have been firstly studied. Subsequently, these Au NPs have been immobilized or patterned on the cyto-compatible hydrogels to synthesize novel nanocomposite hydrogels, which have been applied in cancer treatment, and to control cell behavior mainly on cell adhesion.

In **Chapter 1**, the properties of Au NPs and their chemical assays, biomedical and medicine applications are introduced. Different methods for study of cytotoxicity of Au NPs are briefly discussed. Secondly, several preparation approaches of nanocomposite hydrogels and their biomedical applications are introduced. At last, some factors for controlling cell adhesion on the different hydrogels are discussed.

In **Chapter 2**, Au NPs with different sizes are synthesized, and their cytotoxic effects to murine fibroblast L-929 and murine osteoblastic cell lines MC3T3-E1 are investigated by Trypan blue assay, Live/dead staining assay and MTT assay.

In **Chapter 3,** based on the results of cytotoxicity of Au NPs, new genipin-crosslinked chitosan-gold nanocomposite hydrogels are fabricated, which are applied in killing cancerous cells by using Au NPs with small size released from these nanocomposite hydrogels at acidic pH environment.

In **Chapter 4**, four different PEG-based hydrogels (i.e., 3BC-UV, PEG_{575}-UV, 8PEG-UV and 8PEG-VS-SH hydrogels) are utilized as substrate to immobilize Au NPs by transferring from silicon wafers to hydrogels. The transfer efficiency by this nano-contact transfer method is then compared.

In **Chapter 5**, a novel 8PEG-VS-SH hydrogel is selected as a substrate to immobilize Au NPs, owing to the strong Au-S bond between Au NPs and 8PEG-VS-SH hydrogel. Au NPs with different densities are immobilized on hydrogels to prepare nanocomposite hydrogels, which are further applied in controlling murine fibroblasts L-929 adhesion.

In **Chapter 6,** a "micro-contact deprinting method" is developed to pattern Au NPs on 8PEG-VS-SH hydrogels. Cell adhesion is controlled on these hydrogels by the patterned Au NPs lines in an ordered way.

Introduction

Nanomaterials have been categorized as those materials, which have structured components with at least one dimension between 1 and 100 nm.[1] Gold nanoparticles (Au NPs) as widely used and important nanomaterials have been utilized to combine with hydrogels to fabricate novel nanocomposite materials. Owing to unique physical, mechanical and chemical properties, these nanocomposite materials are applied in cell behavior studies. Thus, the background information about Au NPs and hydrogels is given in this chapter for further understanding and evaluating the experimental results obtained in the present thesis.

In this work, the following questions are tried to be answered. When Au NPs based composite hydrogels are incubated with cells, how do these novel composite hydrogels influence the cellular behavior? Would the cells directly interact with the surface of these composite hydrogels? In addition, would these nanocomposite hydrogels properly mimic Extracellular Matrix (ECM), which can adjust cell adhesion and tune the consequent responses such as spreading, proliferation and differentiation by tuning the physical and chemical properties of surface of the composite hydrogels?

1. Gold Nanoparticles

The rapid growth area in nanomaterials is to stimulate research concerning the impacts of manufactured nanomaterials, which are materials that have structural components smaller than 1 micrometer in at least one dimension.[2] Nowadays, numerous nanomaterials have been reported, including natural materials (*e.g.* protein, carbon and cellulose)[3] and inorganic nanomaterials (*e.g.* graphene, metal nanoparticles, quantum dots and nanogels).[4-10] Among these nanomaterials, Au NPs exhibit unique advantages such as inert, stable, optical and catalytic properties, which is the most important property in the present research of nanomaterials.[11,12] Au NPs have a rich history in chemistry. Dating back to ancient Roman times, Au NPs have already been used to stain glasses for decorative purposes.[13] The first information on colloidal gold can be found in tracts by Chinese and Indian scientists, who tried to attain colloidal gold as early as in the fifth-fourth centuries BC. They utilized it for medical

purposes (Indian "liquid gold", Chinese "gold solution") and other functions. In the middle ages in Europe, colloidal gold was studied and employed in alchemists' laboratories.[14] With the development of nanomaterials, Au NPs have been widely used in the field of chemistry, biology and medicine.[15,16]

1.1 Au NPs for chemical assay application

Au NPs with an appropriate size (d > 3.5 nm) can aggregate to induce inter-particle surface plasmon coupling, resulting in the solution color changing from red or purple to blue at even nanomolar concentration, which can be directly observed by eyes.[17] This provides a practical platform for absorption-based colorimetric assaying of any target analyte (*e.g.* metal irons or cancerous cells) that directly or indirectly triggers the Au NPs aggregation in a few seconds. For instance, Tan *et al.* used aptamer-conjugated Au NPs to sensitively detect acute leukemia cells CCRF-CEM via a simple colorimetric method (Figure 1), which combines with the selectivity and affinity of aptamers as well as the spectroscopic advantages of Au NPs.[18]

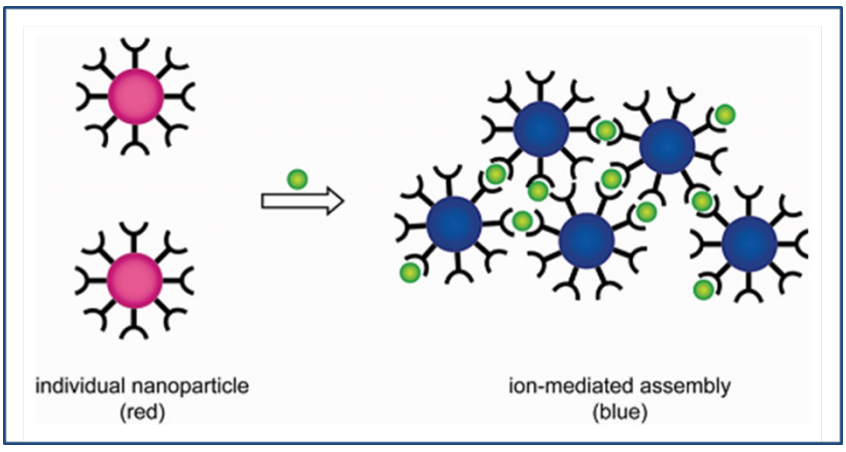

Figure 1: Schematic depiction of red-to-blue color colorimetric sensing of metal ions using the functionalized Au NPs. Image taken from reference [18].

1.2 Au NPs for biomedical applications

For biomedical applications, functionalization of Au NPs with specific ligands is essential in most case to specifically interact with cells or biomolecules. A summary of simplified scheme for the current biomedical applications of these functionalized Au NPs (GNPs) is shown in

Figure 2, which reveals the development of Au NPs in biomedical and medicine applications.[14] In general, Au NPs are an important class of nanomaterials which have already proven to be extensively useful in fundamental biological applications.

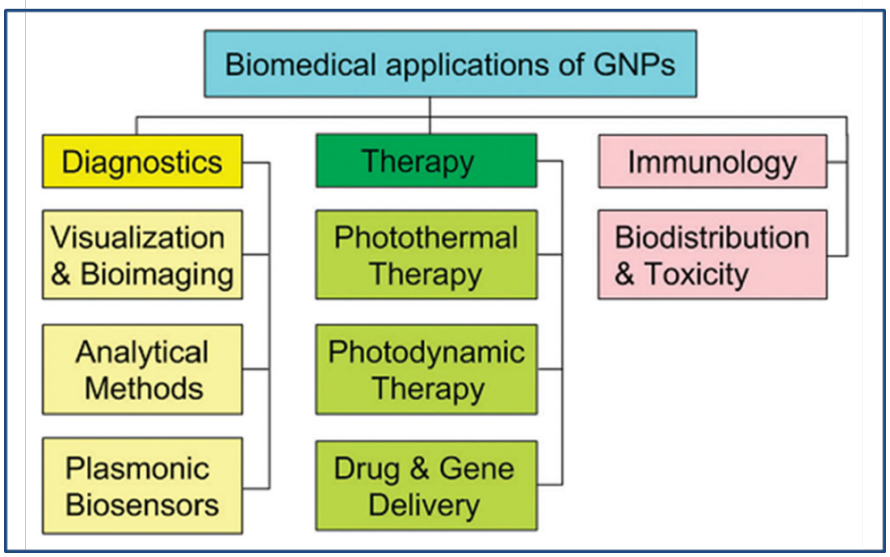

Figure 2: General scheme for the biomedical applications of Au NPs. Image taken from reference [14].

1.3 Au NPs for medicine application

Functionalized Au NPs have found their way from detection to therapeutics in today's medicine applications based on the functional moieties and their capabilities. An important demonstration of the potential of multifunctional Au NPs for drug delivery is the use of 5-fluorouracil functionalized Au NPs as a delivery vehicle and an active targeting agent for leukemic treatment as shown in Figure 3.[19,20] By means of the functionalized Au NPs, specific cellular targeting and therapy can be achieved in a way that the drug can be targetedly delivered and efficiently released. Moreover, Au NPs can be used for the co-administration of protein drugs to cure disease by virtue of their ability to cross specific cellular membranes. Various kinds of proteins, such as fluorescently labeled heparin, fluorophores, peptides, cell adhesion molecules, and antibodies, have been reported to functionalize Au NPs for targeting specific tissues, detecting biomolecules or DNA, and tumor imaging.[21 - 25]

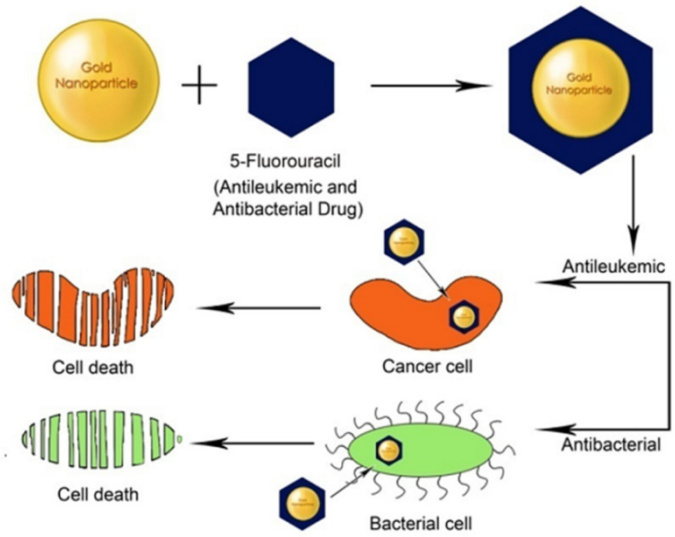

Figure 3: 5-fluorouracil functionalized Au NPs for targeting and killing leukemic cells and bacterial cells. Image taken from reference [19].

Generally, Au NPs can be considered as extraordinary molecular carriers for the targeting, intracellular trafficking and delivery of biomolecules, such as DNA, RNA, proteins, peptides, drugs, genes and other molecules of therapeutic significance.

1.4 Toxicity of Au NPs

In the past few years, the toxicity of nanomaterials, such as Au NPs, quantum dots (QDs), nanowires, and nanotubes has been reported.[26] Considering the wide usage of Au NPs in many fields, knowledge about Au NPs' potential toxicity and their health impact is essential before these nanomaterials are adopted in real clinical settings.[27] Simon *et al.* defined the interaction of Au NPs with biological materials *in vitro* and *in vivo* as "bioresponse", as well as the illustration of perspectives that arise for the application of Au NPs in biological environments.[28] Bioresponses of Au NPs are still in the debate, and the interactions between Au NPs and tissue at the cellular, intracellular and molecular levels are remaining poorly understood.[29,30] Until now, researchers found that Au NPs can enter into cells in a size,[31,32] shape,[33] agglomeration[34] and surface (ligand/charge/area)[35,36] independent manner, causing some effects to cells. For instance, Goodman *et al.* demonstrated that cationic Au NPs were moderately toxic, whereas anionic Au NPs were nontoxic.[37]

Nanoparticles could have many adverse effects on a cellular level by interacting with vital cell components such as the membrane, nucleus, or mitochondria.[38–40] Recently, many researchers have focused on the assessment of toxicity of Au NPs *in vitro*, which is defined as cytotoxicity.[40,41] Lin *et al.* showed that Au NPs can be directly adhered to lipid membranes by electrostatic interaction and induce structural defects, leading to the penetration of the particles into the cells. This open a path for intracellular delivery which bypasses the endocytic machinery, meanwhile, causing cytotoxic effects.[42] Cell toxicity can be determined by MTT/MTS assay, Trypan blue assay, LDH assay, neutral red assay and flow cytometry method, which indicate the cellular damage.[30,35,43,44] In this thesis, some methods are selected to study the cytotoxicity of Au NPs with different sizes, which will be introduced in **Chapter 2** with more details.

2. Biomaterials

Biomaterials are regarded as material that can be used to treat, enhance or replace any tissue, organ, or function in an organism and interact with biological system.[45] Most of them are polymeric materials.[46] Currently, natural and synthetic materials have been extensively explored in medical devices, drug delivery systems, and tissue engineering, intended to interact with biological systems.[45] Materials derived from the natural sources possess the biocompatibility, biodegradability, inherent properties of biological recognition properties for biomedical applications.[47,48] For instance, natural polymers including alginate, collagen, pectin,[49] hyaluronic acid,[50] chitin and chitosan,[51] keratin[52] and silk (fibrous proteins) from silkworms or spiders[53] are known to be used for tissue engineering. It should be noted that chitosan is the most widely used nontoxic, biocompatible and versatile natural polysaccharide after cellulose on earth.[54] Li *et al.* used chitosan-based hydrogel as scaffolds to culture the osteoblast cells, and the *in vivo* study showed that the scaffolds promoted rapid vascularization and deposited connective tissue in rats.[55] By contrast with natural polymers, synthetic polymers offer the potential for improved mechanical properties, repeatability, tunable structure, and degradability.[56] A broad variety of synthetic polymers, including poly ethylene glycol (PEG), poly vinyl alcohol (PVA), polyesters, polyacrylic acid (PAA) and poly N-

isopropylacrylamide (PNIPAAm), have been designed and synthesized into crosslinked networks with molecular-scale control over structure such as crosslinking density and with tailored properties (*e.g.* mechanical strength, and chemical and biological responses to stimuli).[48,57,58]

2.1 Hydrogels

Hydrogels comprise the mostly investigated three-dimensional (3D) networks of hydrophilic polymers.[48] For instance, linear, branched or star-shaped PEG macromonomers (multiarm structures) with functional groups, such as methyloxy, carboxyl, amine, thiol, vinyl sulfone, acetylene, and acrylate, are versatile for hydrogel formation. Thus, PEG based hydrogels arise as a promising tool for promoting tissue regeneration, bone and blood vessel engineering and drug delivery systems, due to the controlled mechanical properties, tunable structure and degradability, as well as the ability to mimic ECM of tissues.[59] In particular, functional PEG star polymers are regarded as a particularly interesting class of materials since they represent versatile building blocks for structured polymer hydrogels.[60] Anseth *et al.* synthesized a peptide- and protein-functionalized four-arm PEG hydrogel to locally influence and promote cartilage ECM production over a short period. This functionalized PEG hydrogel is useful in applications as a scaffold for *in vivo* cartilage regeneration.[61] In the present study, star-shaped PEG molecules (having 8 arms with acrylate end groups; 8PEG) are utilized for preparation of hydrogel.

In this thesis, more detailed information about the PEG hydrogels is presented in **Chapter 4** and **Chapter 5**.

2.2 Nanocomposite hydrogels

Recently, nanocomposite hydrogels, a new class of intelligent material used as biomaterials, which are defined as cross-linked polymer networks in the presence of nanoparticles or nanostructures, have attracted widespread interests.[62] The incorporation of nano-objects into hydrogel matrices may lead to extraordinary enhanced mechanical, thermal, electrical, optical

and biological properties. As shown in Figure 4, various types of nanostructured building blocks such as inorganic/ceramic nanoparticles (silica, silicates, calcium phosphate, hydroxyapatite), polymeric nanoparticles (hyper-branched polyesters, cyclodextrins, peptides), metal/metal-oxide nanoparticles (gold, silver, magnetic, iron-oxide) and carbon-based nanostructures (carbon nanotubes, graphene oxide) can be incorporated into the polymeric network to create the reinforced hydrogels.[62–67]

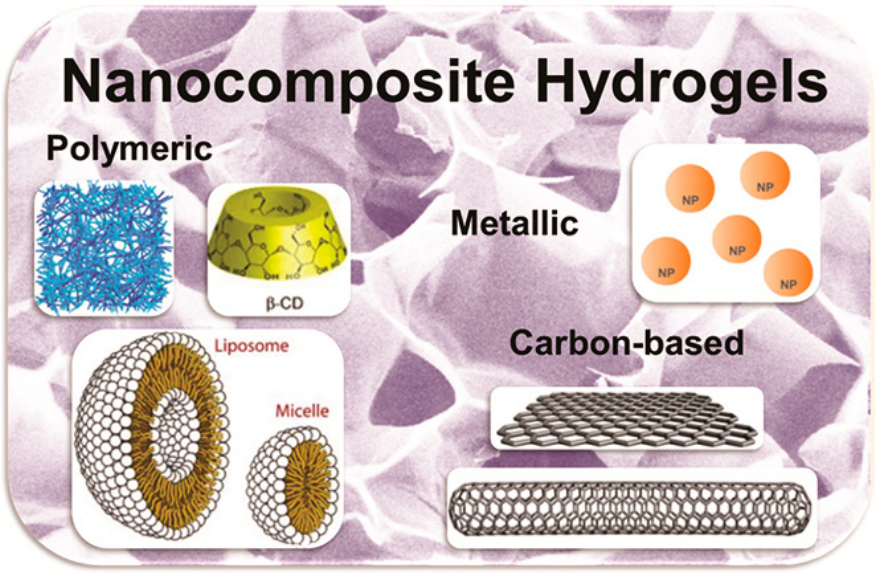

Figure 4: Nanocomposite hydrogels were created by nanoparticles such as metallic nanoparticles and carbon-based nanomaterials combined with the polymeric network. Image taken from reference [63].

The properties of the nanocomposite hydrogels can be easily tailored by manipulating the chemical and physical properties of the hydrogel and nanoparticles.[67,68] For example, Thomas *et al.* exploited that Ag NPs combined with hydrogels to form functional antibacterial nanocomposites, exhibiting excellent antibacterial activity against both Gram-positive and Gram-negative bacteria.[69] Researchers showed that incorporation of graphene oxide (GO) as a nanofiller in PVA hydrogels remarkably improved its tensile strength and thereby provided a promising candidate for tissue engineering.[70,71] Stegemann *et al.* reported the addition of carbon nanotubes (CNTs) to collagen increased the properties of electrical conductivity, and the resultant nanocomposite hydrogels promoted cell viability.[72] Volodkin *et al.* showed that after Au NPs incorporated into poly(L-lysine) (PLL) and hyaluronic acid (HA) architecture by a chemical crosslinked method, the elastic modulus of these highly swollen polyelectrolyte

architectures can be improved by more than 1 order of magnitude, afterwards the composite hydrogels have been used as the platform to promote murine fibroblasts L-929 adhesion as shown in Figure 5.[73]

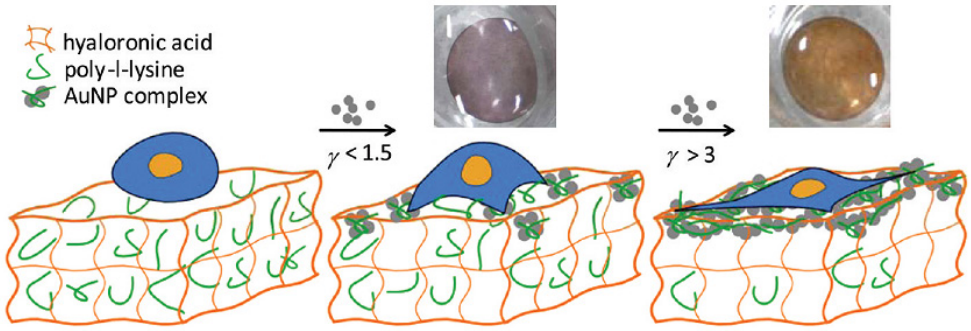

Figure 5: General scheme of the Au NPs HA/PLL hydrogel composites structure for controlling cell adhesion; Au NPs (spheres) bind by complexation with PLL (in green) with the film. (γ stands for surface concentration of Au NPs). Image taken from reference [73].

2.3 Methods for preparation of nanocomposite hydrogels

Several methods have been reported to prepare various kinds of nanocomposite hydrogels. The most common methods for preparation of the nanocomposite hydrogels are illustrated in the following part:

2.3.1 Solution mixing method

A simple technique to prepare polymer nanocomposites is "solution mixing method". A colloidal solution of initiator-functionalized NPs is mixed with aqueous polymer solution through mechanical stirring or sonication, followed by solvent evaporation, resulting in the entrapment of nanoparticles within the hydrogel networks.[74]

2.3.2 In situ method

Another efficient technique to prepare the nanocomposite hydrogel with uniformly distributed nanoparticles is the "in situ" method. After homogeneously mixing the precursor of hydrogels in presence of metal ions, the addition of curing agents or the UV free radical for

polymerization need to be performed to cure the hydrogel composite. Meanwhile, nearly uniformly distributed array of nanoparticles can be obtained within the polymer network.[69,75]

2.3.3 Physical or chemical cross-linking method

The incorporation of nanoparticles in the hydrogel networks can be achieved via physical or chemical interactions: the physical interactions are non-covalent in nature and often a result of hydrogen bonding, ionic and hydrophobic interactions; the chemical cross-linking is permanent due to covalent bonds.[76,77] It should be noticed that for this method, the hydrogels have to remain in the swollen state.[78]

2.3.4 Freeze–drying method

The polymer composite 3D scaffolds with variable porosity and pore size are usually prepared by "freeze-drying method". Freeze-drying works by freezing the hydrogel composite in the swollen state, and then reducing the surrounding pressure to allow the frozen water in the material to sublimate directly from the solid phase to the gas phase. During sublimating process, pores in the bulk of the gel can be fixed.[79,80]

In this thesis, more detailed information about the nanocomposite hydrogels is presented in **Chapter 3**.

3. Cell-substrate interaction

Biomaterials play key roles in modern strategies in tissue engineering and regenerative medicine by mimicking biochemical and biophysical ECM that can direct cellular behavior and functions. Especially, biomaterials can perform with an appropriate host response, playing an important role in the biomedical applications.[45,81] However, we need to know precisely how the interactions between biomaterials and cells take place. Thus, the present research work is carried out for studying the interactions of living cells with biomaterials (nanocomposite hydrogels) *in vitro*.

With the development of biomaterials, nanocomposite hydrogels can act as substrate, whose mechanical and chemical properties can be tuned on the time and length scales of cell development, to truly function as the ECM.[82,83] When cells are contacting with ECM, the most readily observable result of the interaction between cells and the ECM is the cell adhesion.[84] Subsequently, the cells display spreading, migration, proliferation and differentiation.[77,78] Nevertheless, all these activities are very complex. In this thesis, we focus on the initial activity (cell adhesion on nanocomposite hydrogels) of the cells when cultured with nanocomposites hydrogels. More details are shown in **Chapter 5** and **Chapter 6**.

3.1 Which factors will influence cell adhesion on substrate?

Cell adhesion to the ECM depends mainly on the activation of transmembrane receptors such as integrin. They are heterodimeric proteins with two membrane spanning subunits, which can form the assembly of specialized adhesion sites known as focal adhesions (FA).[84,87,88]

Recent studies indicated that, regardless of the chemical specificity of the adhesive receptors, many other physical features of the substrate surface, including its geometry, rigidity, and precise ligand spacing are critical for guiding receptor-mediated adhesion formation and signaling.[89,90]

3.3.1 Chemical features

As is well known, transmembrane adhesion receptors link with the ECM, as well as the cytoskeleton.[91] Integrins comprise the major receptors for ECM proteins, such as fibronectin, laminins, vitronectin and collagens, all of which are rich in the tripeptide arginine-glycine-aspartic acid (RGD). They can act as their cell recognition site to induce integrin-mediated adhesion of cells to ECM.[92,93] Thus, different functional groups can be modified on the nanomaterials surface, influencing the material protein or charge and the consequent material to cell interactions.[89] Kehr *et al.* used periodic mesoporous organosilica (PMO) nanoparticles functionalized with chiral-bioactive molecules in the alginate 3D hydrogel scaffold to provide simultaneously chemical and configurational information similar to native ECM, and then

modulated the affinity of cells with the hydrogel surfaces to control the enrichment of cells as well as simultaneous drug delivery in 3D network. [94]

3.3.2 Rigidity

Not only geometrically defined physical factors are known to influence cell adhesion behavior, but also rigidity has an impact on protein adsorption and cell adhesion.[95] Schmidt *et al.* demonstrated that due to Au NPs treatment, the HA/PLL film's stiffness and roughness increased, leading to the improved cell adhesion.[73] Depending on the shape of the applied proteins, in some cases stiffness of substrate surfaces are shown to cause an increase in the amount of adsorbed proteins and then to induce cell adhesion.[96,97] Although molecular pathways are still only partially known, muscle cells, neurons, and many other tissue cells have been shown to sense substrate stiffness. These cells cultured on tissue culture plastic or glass coverslips are attached to essentially rigid materials.[98,99]

The influence of substrate rigidity on adhesion behavior of cells will be further discussed in **Chapter 3** and **Chapter 6**.

3.3.3 Topography

Surface topography has been known to influence the attachment and orientation of neurons in cell culture.[100] Schulte *et al.* investigated the possibility of manipulating fibroblasts cellular behavior on an intrinsically non-adhesive material, star-shaped PEG (starPEG), by topographic patterning without additional surface chemistry modifications, and this imprinted topography enabled cell adhesion and spreading.[101] Not only geometrically defined micro- and nano-patterns are known to influence cell adhesion behavior, but also random surface roughness have an impact on protein adsorption and cell adhesion.[95,102–104]

4. References

(1) Lines, M. G. Nanomaterials for Practical Functional Uses. *J. Alloys Compd.* **2008**, *449* (1), 242–245.

(2) Buzea, C.; Pacheco, I. I.; Robbie, K. Nanomaterials and Nanoparticles: Sources and Toxicity. *Biointerphases* **2007**, *2* (4), MR17–R71.

(3) Klaine, S. J.; Koelmans, A. A.; Horne, N.; Carley, S.; Handy, R. D.; Kapustka, L.; Nowack, B.; von der Kammer, F. Paradigms to Assess the Environmental Impact of Manufactured Nanomaterials. *Environ. Toxicol. Chem.* **2012**, *31* (1), 3–14.

(4) Kotchey, G. P.; Hasan, S. A.; Kapralov, A. A.; Ha, S. H.; Kim, K.; Shvedova, A. A.; Kagan, V. E.; Star, A. A Natural Vanishing Act: The Enzyme-Catalyzed Degradation of Carbon Nanomaterials. *Acc. Chem. Res.* **2012**, *45* (10), 1770–1781.

(5) Dai, H.; Wong, E. W.; Liebert, C. M.; Lieber, C. M. Probing Electrical Transport in Nanomaterials: Conductivity of Individual Carbon Nanotubes. *Science* **1996**, *272* (5261), 523–526.

(6) Hoshino, A.; Fujioka, K.; Oku, T.; Suga, M.; Sasaki, Y. F.; Ohta, T.; Yasuhara, M.; Suzuki, K.; Yamamoto, K. Physicochemical Properties and Cellular Toxicity of Nanocrystal Quantum Dots Depend on Their Surface Modification. *Nano Lett.* **2004**, *4* (11), 2163–2169.

(7) Martel, R.; Schmidt, T.; Shea, H. R.; Hertel, T.; Avouris, P. Single- and Multi-Wall Carbon Nanotube Field-Effect Transistors. *Appl. Phys. Lett.* **1998**, *73* (17), 2447–2449.

(8) Sciences, M.; Barbara, S. Pyrolytically Grown BxCyNz Nanomaterials : Nanofibres and Nanotubes. *Chem. Phys. Lett.* **1996**, *4*, 0–6.

(9) Lee, J. S.; Park, K.; Kang, M. Il; Park, I. W.; Kim, S. W.; Cho, W. K.; Han, H. S.; Kim, S. ZnO Nanomaterials Synthesized from Thermal Evaporation of Ball-Milled ZnO Powders. *J. Cryst. Growth* **2003**, *254* (3-4), 423–431.

(10) Yan, M.; Ge, J.; Liu, Z.; Ouyang, P. Encapsulation of Single Enzyme in Nanogel with Enhanced Biocatalytic Activity and Stability. *J. Am. Chem. Soc.* **2006**, *128* (34), 11008–11009.

(11) Daniel, M. christine; Astruc, D. Gold Nanoparticles : Assembly , Supramolecular Chemistry , Quantum-Size-Related Properties , and Applications toward Biology , Catalysis , and Nanotechnology. *Chem. Rev.* **2004**, *104* (1), 293–346.

(12) Yao, X.; Li, X.; Toledo, F.; Zurita-Lopez, C.; Gutova, M.; Momand, J.; Zhou, F. Sub-Attomole Oligonucleotide and p53 cDNA Determinations via a High-Resolution Surface Plasmon Resonance Combined with Oligonucleotide-Capped Gold Nanoparticle Signal Amplification. *Anal. Biochem.* **2006**, *354* (2), 220–228.

(13) Giljohann, D. A.; Seferos, D. S.; Daniel, W. L.; Massich, M. D.; Patel, P. C.; Mirkin, C. A. Gold Nanoparticles for Biology and Medicine. *Angew. Chem. Int. Ed.* **2010**, *49* (19), 3280–3294.

(14) Dykman, L.; Khlebtsov, N. Gold Nanoparticles in Biomedical Applications: Recent Advances and Perspectives. *Chem. Soc. Rev.* **2012**, *41* (6), 2256.

(15) Tao, Y.; Ju, E.; Ren, J.; Qu, X. Bifunctionalized Mesoporous Silica-Supported Gold Nanoparticles: Intrinsic Oxidase and Peroxidase Catalytic Activities for Antibacterial Applications. *Adv. Mater.* **2015**, *27* (6), 1097–1104.

(16) Ralph A. Sperling, Pilar Rivera Gil, Feng Zhang, M. Z. and W. J. P. Bioligical Applications of Gold Nanoparticles. *Chem. Soc. Rev.* **2008**, *37* (9), 1896–1908.

(17) Medley, C. D.; Smith, J. E.; Tang, Z.; Wu, Y.; Bamrungsap, S.; Tan, W. Gold Nanoparticle-Based Colorimetric Assay for the Direct Detection of Cancerous Cells. *Anal. Chem.* **2008**, *80* (4), 1067–1072.

(18) Saha, K.; Agasti, S. S.; Kim, C.; Li, X.; Rotello, V. M. Gold Nanoparticles in Chemical and Biological Sensing. *Chem. Rev.* **2012**, *112* (5), 2739–2779.

(19) Duncan, B.; Kim, C.; Rotello, V. M. Gold Nanoparticle Platforms as Drug and Biomacromolecule Delivery Systems. *J. Control. Release* **2010**, *148* (1), 122–127.

(20) Tiwari, P. M.; Vig, K.; Dennis, V. a.; Singh, S. R. Functionalized Gold Nanoparticles and Their Biomedical Applications. *Nanomaterials* **2011**, *1* (1), 31–63.

(21) Chanda, N.; Kattumuri, V.; Shukla, R.; Zambre, A.; Katti, K.; Upendran, A.; Kulkarni, R. R.; Kan, P.; Fent, G. M.; Casteel, S. W.; et al. Bombesin Functionalized Gold Nanoparticles Show in Vitro and in Vivo Cancer Receptor Specificity. *Proc. Natl. Acad. Sci.* **2010**, *107* (19), 8760–8765.

(22) Chinen, A. B.; Guan, C. M.; Ferrer, J. R.; Barnaby, S. N.; Merkel, T. J.; Mirkin, C. A. Nanoparticle Probes for the Detection of Cancer Biomarkers, Cells, and Tissues by Fluorescence. *Chem. Rev.* **2015**, *115* (19), 10530–10574.

(23) Kim, C.; Agasti, S. S.; Zhu, Z.; Isaacs, L.; Rotello, V. M. Recognition-Mediated Activation of Therapeutic Gold Nanoparticles inside Living Cells. *Nat. Chem.* **2010**, *2* (11), 962–966.

(24) Osner, Z. R.; Holz, R. C.; Becker, D. P. An Analytical Method for Detecting Toxic Metal Cations Using Cyclotriveratrylene Derivative Capped Gold Nanoparticles. *Tetrahedron Lett.* **2015**, *56* (40), 5419–5423.

(25) Han, G.; Xing, Z.; Dong, Y.; Zhang, S.; Zhang, X. One-Step Homogeneous DNA Assay with Single-Nanoparticle Detection. *Angew. Chem. Int. Ed.* **2011**, *50* (15), 3462–3465.

(26) Nel, A.; Xia, T.; Mädler, L.; Li, N. Toxic Potential of Materials at the Nanolevel. *Science* **2006**, *311* (5761), 622–627.

(27) G, B.; Seog, J. H.; Graham, L. M.; Lee, S. B. Experimental Considerations on the Cytotoxicity of Nanoparticles. *Nanomedicine* **2011**, *6* (5), 929–941.

(28) Broda, J.; Schmid, G.; Simon, U. Size- and Ligand-Specific Bioresponse of Gold Clusters and Nanoparticles: Challenges and Perspectives. *Struct. Bond.* **2014**, *127* (430), 193–223.

(29) Colvin, V. L. The Potential Environmental Impact of Engineered Nanomaterials. *Nat.*

Biotechnol. **2003**, *21* (10), 1166–1170.

(30) Lewinski, N.; Colvin, V.; Drezek, R. Cytotoxicity of Nanopartides. *Small* **2008**, *4* (1), 26–49.

(31) Coradeghini, R.; Gioria, S.; García, C. P.; Nativo, P.; Franchini, F.; Gilliland, D.; Ponti, J.; Rossi, F. Size-Dependent Toxicity and Cell Interaction Mechanisms of Gold Nanoparticles on Mouse Fibroblasts. *Toxicol. Lett.* **2013**, *217* (3), 205–216.

(32) Deol, S.; Weerasuriya, N.; Shon, Y.-S. Stability, Cytotoxicity and Cell Uptake of Water-Soluble Dendron–conjugated Gold Nanoparticles with 3, 12 and 17 nm Cores. *J. Mater. Chem. B* **2015**, *3* (29), 6071–6080.

(33) Chithrani, B. D.; Ghazani, A. A.; Chan, W. C. W. Determining the Size and Shape Dependence of Gold Nanoparticle Uptake into Mammalian Cells. *Nano Lett.* **2006**, *6* (4), 662–668.

(34) Huang, D.; Zhou, H.; Liu, H.; Gao, J. The Cytotoxicity of Gold Nanoparticles Is Dispersity-Dependent. *Dalton Trans.* **2015**, *44* (41), 17911–17915.

(35) Love, S. a.; Maurer-Jones, M. a.; Thompson, J. W.; Lin, Y.-S.; Haynes, C. L. Assessing Nanoparticle Toxicity. *Annu. Rev. Anal. Chem.* **2012**, *5* (1), 181–205.

(36) Broda, J.; Setzler, J.; Leifert, A.; Steitz, J.; Benz, R.; Simon, U.; Wenzel, W. Ligand-Lipid and Ligand-Core Affinity Control the Interaction of Gold Nanoparticles with Artificial Lipid Bilayers and Cell Membranes. *Nanomedicine Nanotechnology, Biol. Med.* **2016**, *12*, 1–11.

(37) Goodman, C. M.; McCusker, C. D.; Yilmaz, T.; Rotello, V. M. Toxicity of Gold Nanoparticles Functionalzied with Cationic and Anionic Side Chians. *Bioconju. Chem.* **2004**, *15*, 897–900.

(38) Zhang, X. D.; Wu, H. Y.; Wu, D.; Wang, Y. Y.; Chang, J. H.; Zhai, Z. Bin; Meng, A. M.; Liu, P. X.; Zhang, L. A.; Fan, F. Y. Toxicologic Effects of Gold Nanoparticles in Vivo by Different Administration Routes. *Int. J. Nanomedicine* **2010**, *5* (1), 771–781.

(39) Zoroddu, M. A.; Medici, S.; Ledda, A.; Nurchi, V. M.; Lachowicz, J. I.; Peana, M. Toxicity of Nanoparticles. *Curr. Med. Chem.* **2014**, *21*, 3837–3853.

(40) Alkilany, A. M.; Murphy, C. J. Toxicity and Cellular Uptake of Gold Nanoparticles: What We Have Learned so Far? *J. Nanoparticle Res.* **2010**, *12* (7), 2313–2333.

(41) Cascone, M. G.; Tricoli, M.; Cerrai, P.; Del Guerra, R. S. Cell Cultures in the Biocompatibility Study of Synthetic Materials. *Cytotechnology* **1993**, *11*, 137–139.

(42) Soenen, S. J.; Rivera-Gil, P.; Montenegro, J. M.; Parak, W. J.; De Smedt, S. C.; Braeckmans, K. Cellular Toxicity of Inorganic Nanoparticles: Common Aspects and Guidelines for Improved Nanotoxicity Evaluation. *Nano Today* **2011**, *6* (5), 446–465.

(43) Fotakis, G.; Timbrell, J. A. In Vitro Cytotoxicity Assays: Comparison of LDH, Neutral Red, MTT and Protein Assay in Hepatoma Cell Lines Following Exposure to Cadmium Chloride. *Toxicol. Lett.* **2006**, *160* (2), 171–177.

(44) Dechsakulthorn, F.; Hayes, A.; Bakand, S.; Joeng, L.; Winder, C. In Vitro Cytotoxicity Assessment of Selected Nanoparticles Using Human Skin Fibroblasts. *Proceeding 6th World Congr. Altern. Anim. Use Life Sci.* **2007**, special issue, 397–400.

(45) D. F. Williams, Ed., E. Definitions in Biomaterials. *B. Rev.* **1999**, *36* (1), 111–124.

(46) Drury, J. L.; Mooney, D. J. Hydrogels for Tissue Engineering: Scaffold Design Variables and Applications. *Biomaterials* **2003**, *24* (24), 4337–4351.

(47) Khademhosseini, A.; Langer, R. Microengineered Hydrogels for Tissue Engineering. *Biomaterials* **2007**, *28* (34), 5087–5092.

(48) Lutolf, M. P.; Hubbell, J. a. Synthetic Biomaterials as Instructive Extracellular Microenvironments for Morphogenesis in Tissue Engineering. *Nat. Biotechnol.* **2005**, *23* (1), 47–55.

(49) Sun, J.; Tan, H. Alginate-Based Biomaterials for Regenerative Medicine Applications. *Materials.* **2013**, *6* (4), 1285–1309.

(50) O'Neill, H. S.; Gallagher, L. B.; O'Sullivan, J.; Whyte, W.; Curley, C.; Dolan, E.; Hameed, A.; O'Dwyer, J.; Payne, C.; O'Reilly, D.; et al. Biomaterial-Enhanced Cell and Drug Delivery: Lessons Learned in the Cardiac Field and Future Perspectives. *Adv. Mater.* **2016**, 1–14.

(51) Jayakumar, R.; Prabaharan, M.; Sudheesh Kumar, P. T.; Nair, S. V.; Tamura, H. Biomaterials Based on Chitin and Chitosan in Wound Dressing Applications. *Biotechnol. Adv.* **2011**, *29* (3), 322–337.

(52) Hill, P.; Brantley, H.; Van Dyke, M. Some Properties of Keratin Biomaterials: Kerateines. *Biomaterials* **2010**, *31* (4), 585–593.

(53) Vepari, C.; Kaplan, D. L. Silk as a Biomaterial. *Prog. Polym. Sci.* **2007**, *32* (8-9), 991–1007.

(54) Rinaudo, M.; Ã, M. R. Chitin and Chitosan: Properties and Applications. *Prog. Polym. Sci.* **2006**, *31* (7), 603–632.

(55) Li, Z.; Ramay, H. R.; Hauch, K. D.; Xiao, D.; Zhang, M. Chitosan-Alginate Hybrid Scaffolds for Bone Tissue Engineering. *Biomaterials* **2005**, *26* (18), 3919–3928.

(56) Saha, K.; Pollock, J. F.; Schaffer, D. V.; Healy, K. E. Designing Synthetic Materials to Control Stem Cell Phenotype. *Curr. Opin. Chem. Biol.* **2007**, *11* (4), 381–387.

(57) Gibas, I.; Janik, H. Review : Synthetic Polymer Hydrogels for Biomedical. *Chem. Technol.* **2010**, *4* (4), 297–304.

(58) Ward Muscatello, M. M.; Asher, S. A. Poly(vinyl Alcohol) Rehydratable Photonic Crystal Sensor Materials. *Adv. Funct. Mater.* **2008**, *18* (8), 1186–1193.

(59) Ratner, B. D.; Bryant, S. J. Biomaterials: Where We Have Been and Where We Are Going. *Annu. Rev. Biomed. Eng.* **2004**, *6* (1), 41–75.

(60) Keys, K. B.; Andreopoulos, F. M.; Peppas, N. A. Poly (Ethylene Glycol) Star Polymer Hydrogels. *Macromolecules* **1998**, *31* (23), 8149–8156.

(61) Sridhar, B. V.; Brock, J. L.; Silver, J. S.; Leight, J. L.; Randolph, M. A.; Anseth, K. S. Development of a Cellularly Degradable PEG Hydrogel to Promote Articular Cartilage Extracellular Matrix Deposition. *Adv. Healthc. Mater.* **2015**, *4* (5), 702–713.

(62) Satarkar, N. S.; Hilt, J. Z. Magnetic Hydrogel Nanocomposites for Remote Controlled Pulsatile Drug Release. *J. Control. Release* **2008**, *130* (3), 246–251.

(63) Merino, S.; Martín, C.; Kostarelos, K.; Prato, M.; Vázquez, E. Nanocomposite Hydrogels: 3D Polymer–Nanoparticle Synergies for On-Demand Drug Delivery. *ACS Nano* **2015**, *9* (5), 4686–4697.

(64) Sudheesh Kumar, P. T.; Lakshmanan, V. K.; Anilkumar, T. V.; Ramya, C.; Reshmi, P.; Unnikrishnan, A. G.; Nair, S. V.; Jayakumar, R. Flexible and Microporous Chitosan Hydrogel/nano ZnO Composite Bandages for Wound Dressing: In Vitro and in Vivo Evaluation. *ACS Appl. Mater. Interfaces* **2012**, *4* (5), 2618–2629.

(65) Meenach, S. A.; Hilt, J. Z.; Anderson, K. W. Poly(ethylene Glycol)-Based Magnetic Hydrogel Nanocomposites for Hyperthermia Cancer Therapy. *Acta Biomater.* **2010**, *6* (3), 1039–1046.

(66) Ding, L.; Hao, C.; Xue, Y.; Ju, H. A Bio-Inspired Support of Gold Nanopaticles - Chitosan Nanocomposites Gel for Immobilization and Electrochemical Study of K562 Leukemia Cells. *Biomacromolecules* **2007**, *8* (4), 1341–1346.

(67) Kabiri, K.; Omidian, H.; Zohuriaan-Mehr, M. J.; Doroudiani, S. Superabsorbent Hydrogel Composites and Nanocomposites: A Review. *Polym. Compos.* **2011**, *16* (2), 277–290.

(68) Haraguchi, K. Nanocomposite Hydrogels. *Curr. Opin. Solid State Mater. Sci.* **2007**, *11* (3-4), 47–54.

(69) Thomas, V.; Yallapu, M. M.; Sreedhar, B.; Bajpai, S. K. A Versatile Strategy to Fabricate Hydrogel-Silver Nanocomposites and Investigation of Their Antimicrobial Activity. *J. Colloid Interface Sci.* **2007**, *315* (1), 389–395.

(70) Xu, Y.; Wu, Q.; Sun, Y.; Bai, H.; Shi, G. Three-Dimensional Self-Assembly of Graphene Oxide and DNA into Multifunctional Hydrogels. *ACS Nano* **2010**, *4* (12), 7358–7362.

(71) Zhang, L.; Wang, Z.; Xu, C.; Li, Y.; Gao, J.; Wang, W.; Liu, Y. High Strength Graphene Oxide/polyvinyl Alcohol Composite Hydrogels. *J. Mater. Chem.* **2011**, *21* (28), 10399.

(72) MacDonald, R. A.; Voge, C. M.; Kariolis, M.; Stegemann, J. P. Carbon Nanotubes Increase the Electrical Conductivity of Fibroblast-Seeded Collagen Hydrogels. *Acta Biomater.* **2008**, *4* (6), 1583–1592.

(73) Schmidt, S.; Madaboosi, N.; Uhlig, K.; Köhler, D.; Skirtach, A.; Duschl, C.; Möhwald, H.; Volodkin, D. V. Control of Cell Adhesion by Mechanical Reinforcement of Soft Polyelectrolyte Films with Nanoparticles. *Langmuir* **2012**, *28* (18), 7249–7257.

(74) Zare, Y.; Shabani, I. Polymer/metal Nanocomposites for Biomedical Applications. *Mater. Sci. Eng. C* **2016**, *60* (28), 195–203.

(75) Jeong, S.-H.; Koh, Y.-H.; Kim, S.-W.; Park, J.-U.; Kim, H.-E.; Song, J. Strong and Biostable Hyaluronic Acid–Calcium Phosphate Nanocomposite Hydrogel via in Situ Precipitation Process. *Biomacromolecules* **2016**, *17* (3), 841–851.

(76) Schexnailder, P.; Schmidt, G. Nanocomposite Polymer Hydrogels. *Colloid Polym. Sci.* **2009**,

287 (1), 1–11.

(77) Dutta, P. K. Chitin and Chitosan for Regenerative Medicine. *Springer* **2015**, 1–389.

(78) Regiel-Futyra, A.; Kus-Liskiewicz, M.; Sebastian, V.; Irusta, S.; Arruebo, M.; Stochel, G.; Kyzio, A. Development of Noncytotoxic Chitosan-Gold Nanocomposites as Efficient Antibacterial Materials. *ACS Appl. Mater. Interfaces* **2015**, *7* (2), 1087–1099.

(79) Liu, M.; Wu, C.; Jiao, Y.; Xiong, S.; Zhou, C. Chitosan–halloysite Nanotubes Nanocomposite Scaffolds for Tissue Engineering. *J. Mater. Chem. B* **2013**, *1*, 2078.

(80) Qian, L.; Zhang, H. Controlled Freezing and Freeze Drying: A Versatile Route for Porous and Micro-/nano-Structured Materials. *J. Chem. Technol. Biotechnol.* **2011**, *86* (2), 172–184.

(81) Williams, D. F. On the Nature of Biomaterials. *Biomaterials* **2009**, *30* (30), 5897–5909.

(82) Cushing, M. C.; Anseth, K. S. Materials Science. Hydrogel Cell Cultures. *Science* **2007**, *316* (5828), 1133–1134.

(83) Tibbitt, M. W.; Anseth, K. S. Hydrogels as Extracellular Matrix Mimics for 3D Cell Culture. *Biotechnol. Bioeng.* **2009**, *103* (4), 655–663.

(84) Ruoslahti, E.; Pierschbacher, M. D. New Perspectives in Cell Adhesion: RGD and Integrins. *Science* **1987**, *238* (4826), 491–497.

(85) Seda Kehr, N.; Riehemann, K. Controlled Cell Growth and Cell Migration in Periodic Mesoporous Organosilica/Alginate Nanocomposite Hydrogels. *Adv. Healthc. Mater.* **2015**, *5* (2) 193–197.

(86) Tay, C. Y.; Irvine, S. A.; Boey, F. Y. C.; Tan, L. P.; Venkatraman, S. Micro-/nano-Engineered Cellular Responses for Soft Tissue Engineering and Biomedical Applications. *Small* **2011**, *7* (10), 1361–1378.

(87) Hynes, R. O. Cell Adhesion: Old and New Questions. *Trends Cell Biol.* **1999**, *9* (12), M33–M37.

(88) Hynes, R. O. Integrins: Versatility, Modulation, and Signaling in Cell Adhesion. *Cell* **1992**, *69* (1), 11–25.

(89) Arnold, M.; Hirschfeld-Warneken, V. C.; Lohmuller, T.; Heil, P.; Blummel, J.; Cavalcanti-Adam, E. A.; Walther, Paul, Kessler, H.; Geiger, B.; Spatz, J. P. Induction of Cell Polarization and Migration by a Gradient of Nanoscale Variations in Adhesive Ligand Spacing. *Nano Lett.* **2008**, *8* (7), 2063–2069.

(90) Amschler, K.; Erpenbeck, L.; Kruss, S.; Schön, M. P. Nanoscale Integrin Ligand Patterns Determine Melanoma Cell Behavior. *ACS Nano* **2014**, *8* (9), 9113–9125.

(91) Calderwood, D. A; Ginsberg, M. H. M. H. Talin Forges the Links between Integrins and Actin. *Nat. Cell Biol.* **2003**, *5* (8), 694–697.

(92) Verma, A.; Stellacci, F. Effect of Surface Properties on Nanoparticle-Cell Interactions. *Small* **2010**, *6* (1), 12–21.

(93) Huang, J.; Grater, S. V; Corbellini, F.; Rinck, S.; Bock, E.; Kemkemer, R.; Kessler, H.; Ding, J.; Spatz, J. P. Impact of Order and Disorder in RGD Nanopatterns on Cell Adhesion. *Nano Lett.* **2009**, *9* (3), 1111–1116.

(94) Kehr, N. S. Enantiomorphous Periodic Mesoporous Organosilica-Based Nanocomposite Hydrogel Scaffolds for Cell Adhesion and Cell Enrichment. *Biomacromolecules* **2016**, *17* (10), 1117–1122.

(95) Roach, P.; Parker, T.; Gadegaard, N.; Alexander, M. R. Surface Strategies for Control of Neuronal Cell Adhesion: A Review. *Surf. Sci. Rep.* **2010**, *65* (6), 145–173.

(96) Murphy-Ullrich, J. E. The de-Adhesive Activity of Matricellular Proteins: Is Intermediate Cell Adhesion an Adaptive State? *J. Clin. Invest.* **2001**, *107* (7), 785–790.

(97) Yap, F. L.; Zhang, Y. Protein and Cell Micropatterning and Its Integration with Micro/nanoparticles Assembly. *Biosens. Bioelectron.* **2007**, *22* (6), 775–788.

(98) Discher, D. E. Tissue Cells Feel and Respond to the Stiffness of Their Substrate. *Science* **2005**, *310* (5751), 1139–1143.

(99) Cavalcanti-Adam, E. A.; Spatz, J. P. Receptor Clustering Control and Associated Force Sensing by Surface Patterning : When Force Matters. *Nanomedicine* **2015**, *10* (5), 681–684.

(100) Craighead, H. G.; Turner, S. W.; Davis, R. C.; James, C.; Perez, A. M.; St. John, P. M.; Isaacson, M. S.; Kam, L.; Shain, W.; Turner, J. N.; et al. Chemical and Topographical Surface Modification for Control of Central Nervous System Cell Adhesion. *Biomed. Microdevices* **1998**, *1* (1), 49–64.

(101) Schulte, V. A.; Díez, M.; Möller, M.; Lensen, M. C. Surface Topography Induces Fibroblast Adhesion on Intrinsically Nonadhesive Poly(ethylene Glycol) Substrates. *Biomacromolecules* **2009**, *10* (10), 2795–2801.

(102) Mrksich, M.; Huang, S.; Whitesides, G. M.; Ingber, D. E. Geometric Control of Cell Life and Death. Science **1997**, *276* (5317), 1425–1428.

(103) Arnold, M.; Cavalcanti-Adam, E. A.; Glass, R.; Bl??mmel, J.; Eck, W.; Kantlehner, M.; Kessler, H.; Spatz, J. P. Activation of Integrin Function by Nanopatterned Adhesive Interfaces. *ChemPhysChem* **2004**, *5* (3), 383–388.

(104) Bettinger, C. J.; Langer, R.; Borenstein, J. T. Engineering Substrate Topography at the Micro- and Nanoscale to Control Cell Function. *Angew. Chem. Int. Ed.* **2009**, *48* (30), 5406–5415.

Chapter 2

Synthesis of Au NPs with Different Sizes and Their Cytotoxicity Effects

Abstract

Gold nanoparticles (Au NPs) have potential applications in drug delivery, gene diagnosing and biomedical imaging, but one of the important concerns is about their safety. This chapter describes safety issues by evaluating the cytotoxicity of Au NPs with different sizes. Firstly, we have successfully synthesized Au NPs with different sizes from 4.5 nm to 60 nm, and then it is demonstrated that these Au NPs have different cytotoxicity to two cell lines murine fibroblasts L-929 and murine osteoblasts MC3T3-E1 under the same experimental conditions (i.e. treatment time and surface chemistry) by using Try blue assay, Live/dead assay and MTT test, which are *in vitro* assay methods. The results indicate that 4.5 nm Au NPs show the highest toxicity to the L-929 cells, and the viability of L-929 cells is only 10%. The main cause is due to the fact that 4.5 nm Au NPs can impair the cell membrane integrity. With the increase of the sizes, the Au NPs are less toxic to cells. Au NPs with a diameter of 60 nm are found to be non-cytotoxic to L-929 and MC3T3-E1 cells.

1. Introduction

Gold nanoparticles (Au NPs) are key materials in nanoscience and nanotechnology due to their unique optical,[1] electrical[2] and catalytic properties,[3,4] and have been widely applied in the areas of optoelectronics, biosensing application, catalysis, drug delivery, gene diagnose and biomedical imaging.[5–7] Due to the similarity of size with certain cellular components or proteins, Au NPs therefore may pass through natural mechanical barriers, then possibly lead to adverse tissue reaction.[8] For instance, Pernodet *et al.* found that with the presence of intracellular 13 nm Au NPs, actin stress fibers disappeared and adverse effects on cell viability were induced.[9] Nevertheless, functionalization of Au NPs with biomolecules can decrease cytotoxicity. It was demonstrated that Au NPs with 3.5 nm in diameter capped by lysine and poly-L-lysine were biocompatible and non-immunogenic.[10]

To the best of our knowledge, few systematic studies have been undertaken to clarify the cytotoxicity of nanoparticles concerning their size, shape, agglomeration and stability in medium and chemistry.[11,12] The parameters mentioned above have different trajectory and molecular targets when they are incubated with cells.[8,13] Considering that Au NPs have already been widely used in researches, the knowledge about Au NPs' potential toxicity and health impact is essential before these nanomaterials are applied in the real clinical settings.[14,15]

In this work, Au NPs with the sizes ranged from 4.5 nm to 60 nm were firstly synthesized and characterized, and then the cytotoxicity of these as-obtained Au NPs were studied. The cytotoxicity tests were conducted with murine fibroblasts L-929 and murine osteoblasts MC3T3-E1 by using the Trypan blue assay, Live/dead staining assay and MTT test *in vitro*.

2. Experimental Section

2.1 Materials

$HAuCl_4 \cdot 3H_2O$, trisodium citrate (99%), sodium borohydride, MTT (3-(4,5-dimethylthiazol-2-yl)-2,5-diphenyltetrazolium bromide), fluorescein diacetate (FDA) and Trypan blue solution (0.4%) were purchased from Sigma-Aldrich. RPMI 1640, fetal bovine serum (FBS), 1% penicillin/streptomycin and Trypsin-EDTA were purchased from PAA Laboratories GmbH. Propidium iodide (PI ≥ 94%) and phosphated buffer saline (PBS) containing K_2HPO_4 and KH_2PO_4 were purchased from Fluka. Ultrapure deionized water was used for all solution preparations. All glassware was cleaned with Aqua Regia (V_{HNO3}: V_{HCl} = 1:3).

2.2 Apparatus

UV-vis spectra were recorded on a Shimadzu UV-2400 spectrophotometer by Agilent Technologies compony with a 1 cm optical path quartz cuvette. The size of Au NPs was determined by transmission electron microscope (TEM) JEOL 2100. Optical images were obtained using a Carl Zeiss fluorescence microscope (Göttingen Company). Fluorescence microscopy Axio Observer Z1 was used to achieve optical sectioning through the fluorescent samples. Pictures were taken using an AxioCam MRm digital camera and analyzed using the AxioVisionV4.8.1 software package (Carl Zeiss, Göttingen, Germany). Tecan plate reader was bought from Tecan Company (Switzerland).

2.3 Synthesis of Au NPs

The Au NPs with 4.5 nm in diameter were synthesized according to the method reported previously.[16] Typically it involved the preparation of a 10 mL aqueous solution containing 2.5×10^{-4} M $HAuCl_4$ and 2.5×10^{-4} M trisodium citrate. To this solution was added with 0.3 mL of ice-cold 0.1 M $NaBH_4$ under vigorous stirring. The mixture immediately turned red, indicating the formation of Au NPs.

The Au NPs with larger sizes were synthesized according to another procedure.[17] Briefly, a solution of 2.2 mM trisodium citrate in water (15 mL) was heated with a silicone oil bath in a 25 mL three-neck round-bottom flask for 20 min under vigorous stirring. A condenser was utilized to prevent the evaporation of the solvent. After boiling had commenced, 1 mL of 25 mM $HAuCl_4$ was injected. The color of the solution changed in 10 min. The resulting particles were 20 nm Au NPs. Once synthesis was finished, the temperature cooled down to 90 °C and 2 mL of aliquots was extracted for the further experiments. In order to get next generation of Au NPs, 1 mL 60 mM sodium citrate and 1 mL of a 25 mM $HAuCl_4$ solution were sequentially injected (time delay 2 min) to the rest of solution, another 2 mL of aliquots was extracted out after 30 min. By repeating this process (sequential addition of 0.1 mL of 60 mM sodium citrate and 1 mL of 25 mM $HAuCl_4$), up to 5, 9 and 13 generations of Au NPs with the sizes of 20, 40 and 60 nm, respectively, were progressively obtained.

2.4 Characterization of Au NPs

2.4.1 Transmission Electron Microscopy

Au NPs were visualized using TEM at 80 keV. 10 μL of the dispersion was casted onto a piece of ultrathin formvar-coated 200-mesh copper grid (Ted-pella, Inc.) and left to dry at room temperature.

2.4.2 UV-vis spectroscopy

UV-vis spectra were acquired with a Shimadzu UV-2400 spectrophotometer. 1 mL of Au NPs solution was placed in a cell, and spectral analysis was performed in the 200 to 800 nm range at room temperature.

2.4.3 Zeta-sizer Nano ZS, Malvern

500 μL of Au NPs solution was placed in a cell, and then the measurement was performed at room temperature.

2.5 Stability of Au NPs in cell culture medium

For Au NPs stability tests, 500 µL of Au NPs was added to the 500 µL of medium and the mixture was incubated for 6 h. Afterwards the mixture was placed in a cell and analyzed by the UV-vis spectroscopy.

2.6 Cell culture

Two cell lines, murine fibroblasts L-929 were kindly provided by Dr. J. Lehmann (Fraunhofer Institute for Cell Therapy and Immunology IZI, Leipzig) and murine osteoblasts MC3T3-E1 were kindly provided by Prof. Z. Su (Beijing University of Chemical Technology, China). L-929 cell lines were cultured in 75 cm^2 cell culture flasks containing RPMI 1640 supplemented with 10% fetal bovine serum (FBS) and 1% penicillin/streptomycin (PS, 100×, all PAA Laboratories GmbH). MC3T3-cells were grown in 75 cm^2 cell culture flasks containing minimum essential medium (Sigma-Aldrich) supplemented with 10% FBS and 1% PS at 37 °C and 5% CO_2 in a humidified incubator. The cells were grown until confluence, and washed with Dulbecco's phosphate buffered saline solution and treated with Trypsin-EDTA (PAA Laboratories GmbH). After incubation for 2 min for L-929 and 4 min for MC3T3-E1 at 37 °C, the detached cells were suspended in cell culture medium. The cell suspension was transferred into a falcon tube (VWR International GmbH) and centrifuged for 3 min at 1300 rpm, 4 °C. Finally, the cell pellet was resuspended in fresh medium and cells were counted using a hemocytometer (Paul Marienfeld GmbH & Co. KG). During the incubation, cell culture medium was refreshed every second day.

2.7 Cytotoxicity assays

2.7.1 Trypan blue assay

For Trypan blue assay, 450 µL of a cell suspension containing 40.000 cells/mL L-929 and 50.000 cells/mL MC3T3-E1 cells were seeded onto each 24-well plates separately and incubated at 37 °C, 5 % CO_2 atmosphere and 100% humidity. After 24 h, the medium was

sucked out carefully in order to clean up metabolite. Then a mixture of fresh medium with a certain of Au NPs was added to each well and the cells were incubated for another 24 h. Following incubation, cells were washed with Dulbecco's phosphate buffered saline solution and treated with Trypsin-EDTA (PAA Laboratories GmbH). After incubation for 3 min at 37 °C, the detached cells were suspended in 450 μL of fresh medium, and transferred into a tube. 50 μL of trypan blue solution was added into the cell suspension. After being mixed well for 8 min, the cells were counted by a hemocytometer. The data shown in the thesis is an average of three experiments.

2.7.2 Live/dead staining assay

For Live/dead assay, 300 μL of a cell suspension containing 40.000 cells/mL L-929 and 50.000 cells/mL MC3T3-E1 cells were seeded onto each 6-well plates separately and incubated at 37 °C, 5% CO_2 atmosphere and 100% humidity. After 24 h, the medium was sucked out carefully in order to clean up metabolite. Then a mixture of fresh medium with a certain amount of Au NPs was added to each well, and the cells were incubated for another 24 h. Following incubation, cells were washed with Dulbecco's PBS and then stained with 100 μL of a vitality staining solution that contains fluorescein diacetate (FDA stock solution 0.5 mg/mL in acetone, Sigma-Aldrich) and propidium iodide (PI stock solution 0.5 mg/mL in DPBS, Fluka). Live and dead cells were analyzed by fluorescence microscope (Carl Zeiss, Goettingen, Germany).

2.7.3 MTT test

For MTT test, cells were plated in 96-well flat bottom plates at initial densities of 4000 cells/mL L-929 and 5000 cells/mL MC3T3-E1 cells per well. After allowing 18 h of incubation for cell attachment, Au NPs solutions were diluted appropriately in a fresh medium and 150 μL of the as-prepared solution was added to wells. After two days of incubation, cell viability was determined by MTT assay. After the addition of MTT solution (20 μL, 5 mg/mL MTT in sterile PBS), the plate was incubated for an additional 4 h at 37 °C and 5% CO_2, allowing viable cells to convert the yellowish water-soluble tetrazolium salt to a water-

insoluble purple formazan product within viable breathing cells as a proxy of cell number and viability. Absorption of each sample was measured by a spectrophotometer (Tecan Plate Reader, Tecan Company, Switzerland) at 490 nm. The amount of formazan produced is directly proportional to the number of living cells in the well. This experiment was carried out in triplicate.[18]

With regard to the cytotoxicity test, each sample had the same order of magnitudes of Au NPs to the cells.

3. Results and Discussion

3.1 Characterization of Au NPs by TEM

The size and morphology of the as-synthesized Au NPs have been verified by TEM. TEM images of five samples used in the present work are shown in Figure 2, as it can be observed that all the as-synthesized Au NPs exhibit uniformly spherical shapes. Average size of these Au NPs has been measured to be 4.5, 12, 30, 50 and 60 nm in diameter, respectively.

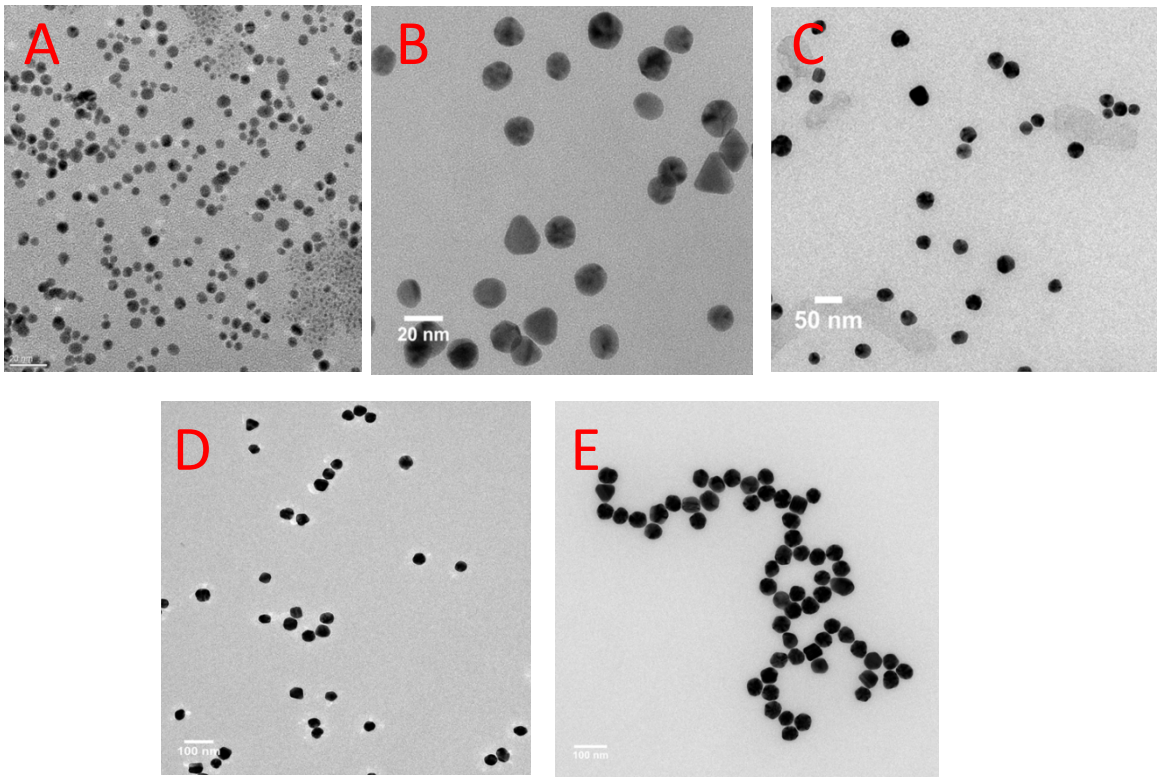

Figure 1: Representative TEM images of the as-synthesized Au NPs with a diameter of 4.5 nm(A), (B) 12 nm, (C) 30 nm, (D) 50 nm and (E) 60 nm.

3.2 Characterization of Au NPs by UV-vis spectroscopy

The optical properties of Au NPs with different sizes depicted in Figure 1 are measured by UV-vis spectroscopy, where the observed trend agrees well with the expected changes in the optical behavior when increasing the particle size. As Au NPs increase in size, the characteristic absorption peaks are red-shifted, which attributes to the dipolar surface plasmon

resonance (SPR) of the isolated nanoparticles.[19] The initial peak red shifts from 515 to 532 nm as the size of the Au NPs increases from 4.5 to 60 nm, indicating that Au NPs with the different sizes have been successfully synthesized.

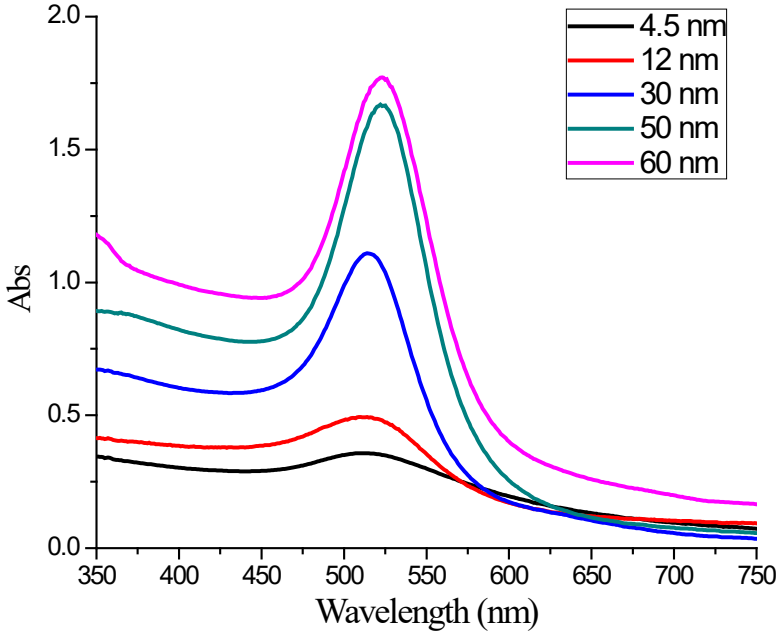

Figure 2: UV-vis spectra of Au NPs with different sizes.

3.3 Characterization of Au NPs by Zeta-sizer

Zeta-potential measurements of the as-synthesized Au NPs have been performed by Malvern Zeta-sizer. As shown in Figure 3, the surface potential of Au NPs with 4.5 nm, 12 nm, 30 nm, 50 nm and 60 nm in diameter have been determined to be -60.5 mV, -10.2 mV, -17.8 mV, -38.8 mV and -54.6 mV, respectively. Au NPs have been prepared by reducing chloroauric acid with citrate. The reduction of $HAuCl_4$ occurrs through the transfer of electrons from the citrate to the Au^{3+} ion leading to the formation of Au^0, this metallic gold then nucleates and grows to form Au NPs. Citrate is the reducing agent and the stabilizer, thus generating negative potential on the surface of citrate-capped Au NPs.

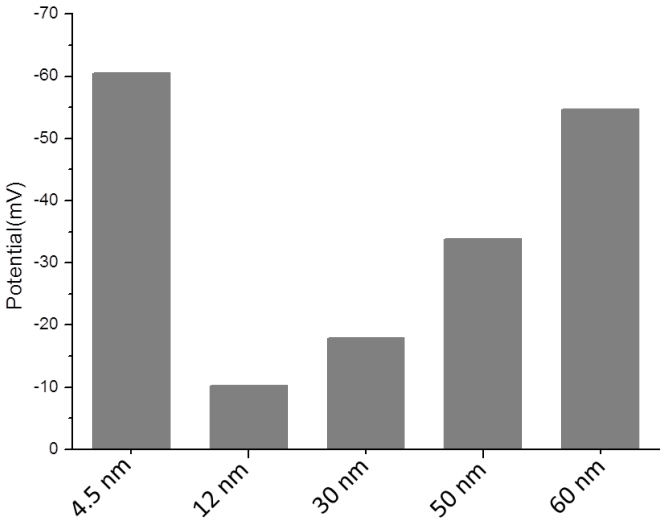

Figure 3: Surface potential of Au NPs with different sizes.

3.4 Stability of Au NPs in cell culture medium

The stability of Au NPs in cell culture medium is monitored by UV-vis spectrophotometry, which is very sensitive to the aggregation state of Au NPs.[20] As shown in Figure 4, the characteristic absorption peak of Au NPs with a diameter of 60 nm is around 532 nm when they are dispersed in water. After incubation with cell culture medium, no red or blue shift of the SPR peak can be observed, indicating that no aggregates are formed. Similar results have been obtained when Au NPs with other sizes are exposed to the culture medium. This indicates that the as-synthesized Au NPs show excellent stability in the medium composition, avoiding the formation of Au NPs aggregates, which influence the endocytic pathway of cells during the incubation.

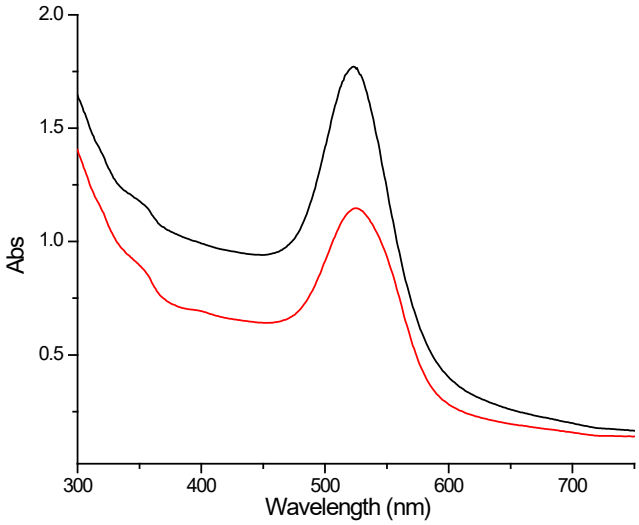

Figure 4: UV-vis absorption spectra of Au NPs with a diameter of 60 nm dispersed in water (black line) and in cell medium (red line).

3.5 Trypan blue assay

The cytotoxicity of the as-synthesized Au NPs has been firstly tested by Trypan blue assay. Logarithmic-phase L-929 and MC3T3-E1 cells have been selected for viability test. After incubation with Au NPs, dead cells are distinctively blue in color under the microscope and counted using a hemocytometer.[21] As shown in Figure 5A, livability of L-929 cells is 15% after incubation with 4.5 nm Au NPs, and the livability of L-929 cells increases with the increasing of sizes. For 60 nm Au NPs, the livability of L-929 cells can reach as high as 78%. This indicates Au NPs with the diameter of 4.5 nm are most toxic to L-929 cells, and the cytotoxicity to L-929 decreases as the sizes increase. Au NPs with 60 nm in diameter are less toxic to L-929 cells. Figure 5B shows that 12 nm Au NPs are the most toxic to MC3T3-E1 cells compared to Au NPs with other sizes. When incubated with 60 nm Au NPs, the livability of MC3T3-E1 cells can reach as high as 80%, indicating that most of cells are survived and 60 nm Au NPs show the lowest cytotoxicity. Generally, Au NPs with the same size show different cytotoxicity to different cell types. Small-sized Au NPs can destroy cell membrane by endocytic way. Au NPs have less damage to the cell membrane with the increase of the size.

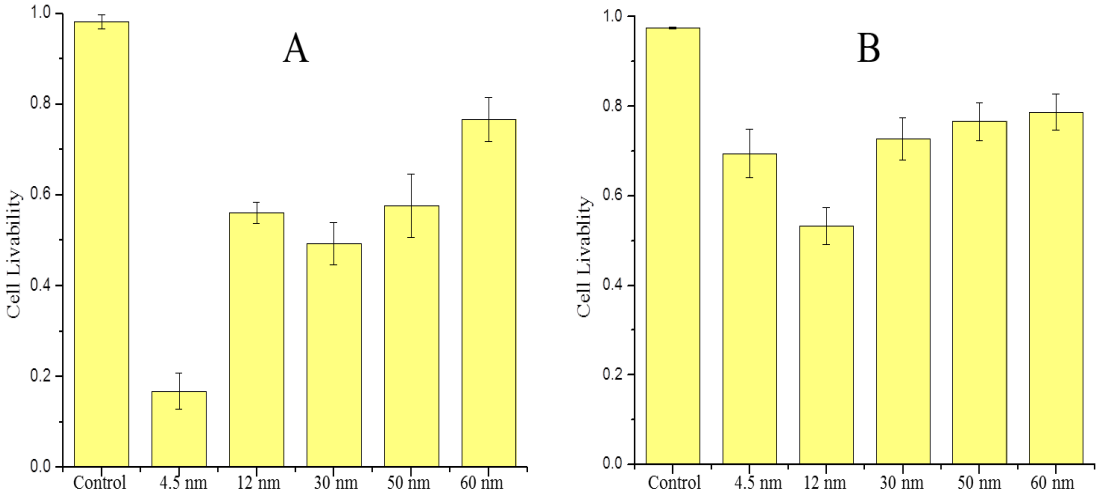

Figure 5: Viability of cell lines exposed to Au NPs with different sizes tested by Trypan blue assay. (A) L-929 cells, (B) MC3T3-E1 cells. (Control means cells cultured on TCPs). Data are combined from at least three independent experiments. Results are presented as average ± standard deviation. $P < 0.05$.

3.6 Live/dead staining assay

To further investigate the cytotoxicity of Au NPs, a Live/dead staining assay has been performed via direct contact of cells (L-929 and MC3T3-E1 cells) with different-sized Au NPs after 24 h of incubation. In this assay, the live cells are able to convert the non-fluorescent FDA into the green fluorescent metabolite fluorescein, and the dead cells with a non-integer cell membrane show a red fluorescence due to the incorporation of a second dye PI at DNA when observed with a fluorescence microscope.[22] Figure 6A shows that the livability of L-929 after cultured with 4.5 nm Au NPs is 5 %, and the livability of L-929 increases as the sizes increase. Au NPs with 12 and 30 nm in diameter also show cytotoxicity to L-929 cells. Figure 6B shows that Au NPs are less cytotoxic to MC3T3-E1 compared to L-929 cells. It can be seen that Au NPs with the smallest size show the highest toxicity to the L-929 and MC3T3-E1cells. With the increase of the size, the Au NPs are less toxic to cells especially for MC3T3-E1cells.

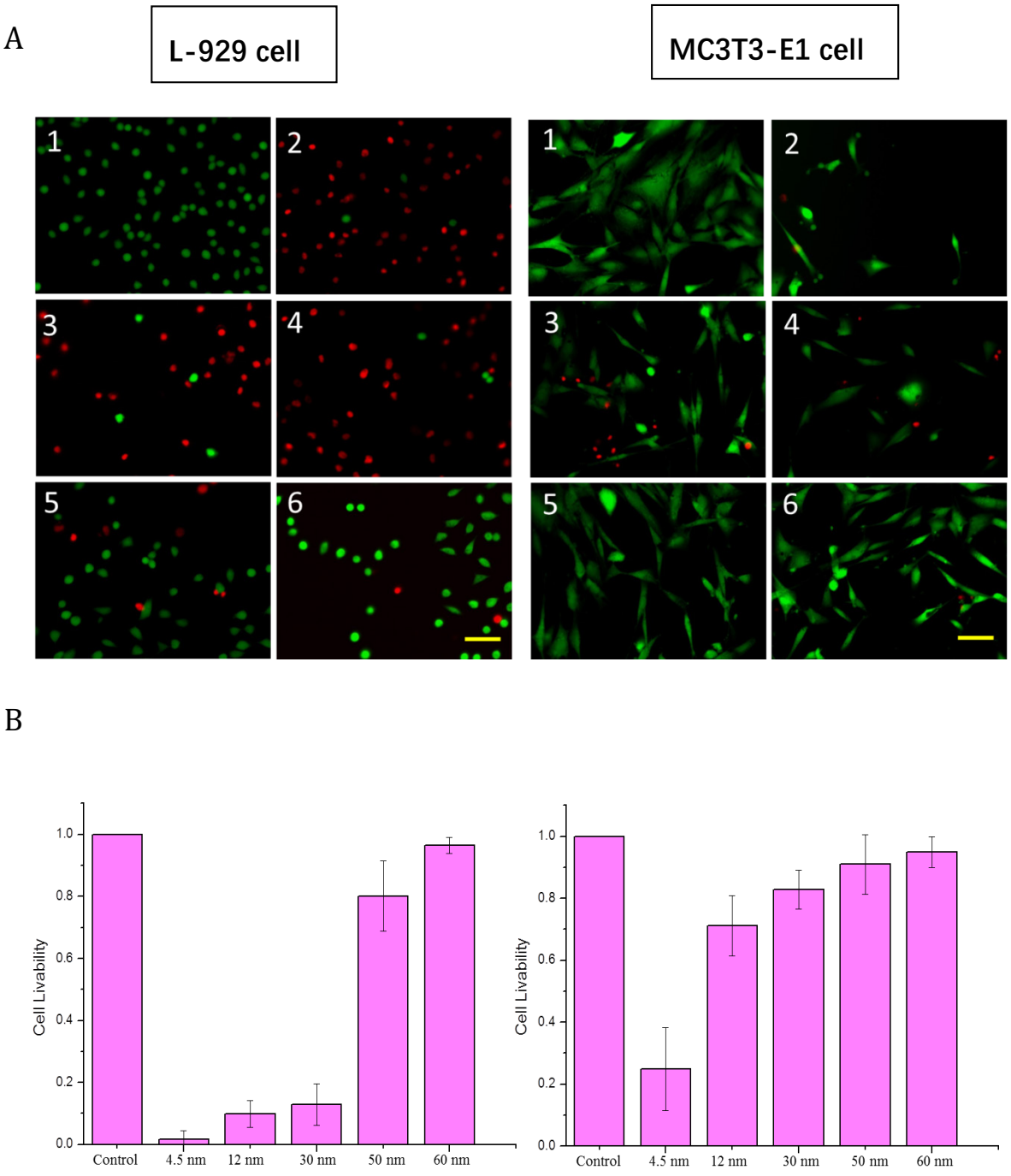

Figure 6: Fluorescent images of viability of cells exposed to Au NPs with different sizes by Live/dead staining assay (A). Statistical chart of viability of cells according to results of Live/dead staining assay (B). (1) untreated cells on TCPs, (2) 4.5 nm Au NPs, (3) 12 nm Au NPs, (4) 30 nm Au NPs, (5) 50 nm Au NPs, (6) 60 nm Au NPs. Data are combined from at least three independent experiments. Results are presented as average ± standard deviation. $P < 0.1$.

3.7 MTT assay

MTT assay measures the conversion of the yellowish water-soluble tetrazolium salt to a water-insoluble purple formazan product within viable cells as a proxy of cell viability.[23,24] In Figure 7, the livability of two kinds of cells is 42% and 52% when cultured with 4.5 nm Au NPs, respectively. 60 nm Au NPs induce less cell viability compared to 50 nm Au NPs in the MTT assay. This difference indicates that 50 nm Au NPs is prone to affect the mitochondrial activity of L-929 and MC3T3-E1 cells but show less effect on cell membrane integrity.

In the present work, as-synthesized Au NPs especially with diameter of 4.5 nm can enter into L-929 cells, causing cytotoxicity. The possible explanation is that Au NPs with small size damage organelles such as lipids of the cell membrane, proteins and DNA, inducing cell death.[25,26]

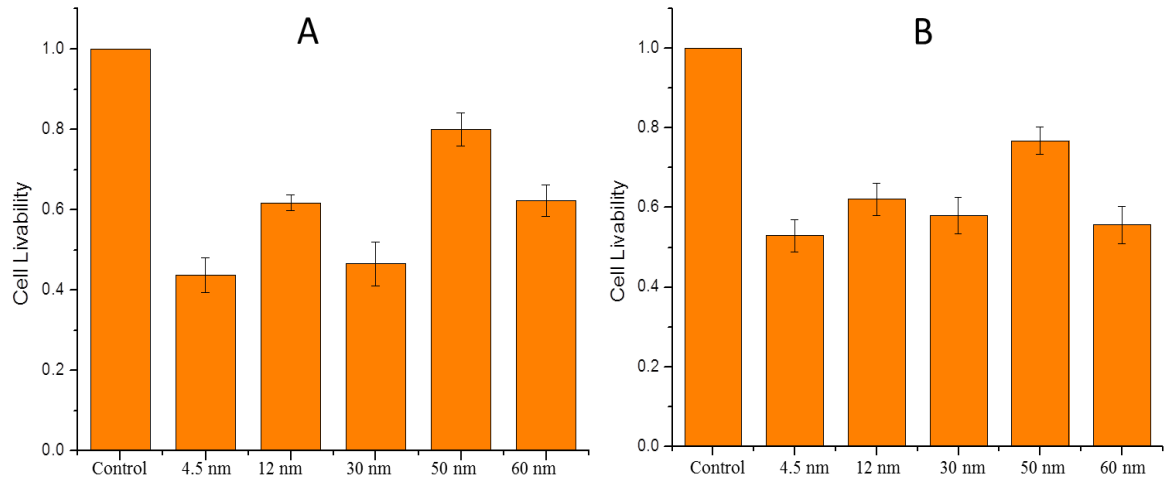

Figure 7: Viability of cells exposed to Au NPs with different sizes by MTT assay. (A) L-929 cell lines, (B) MC3T3-E1 cell lines. (Control means cells cultured on TCPs). Data are combined from at least three independent experiments. Results are presented as average ± standard deviation. $P < 0.05$.

4. Conclusions

In this chapter, Au NPs with different diameters from 4.5 nm to 60 nm have been synthesized. The as-synthesized Au NPs dispersion shows good stability in cell culture medium, which is verified UV-vis adsorption test. Two cell lines (L-929 and MC3T3-E1 cells) have been selected to determine the cytotoxicity of Au NPs with different sizes by using Trypan blue assay, Live/dead staining and MTT assay. It has been demonstrated that compared with L-929, Au NPs are cyto-compatibile to MC3T3-E1 cells. Further, the size of Au NPs shows a great impact on cell viability. 4.5 nm Au NPs have been proved to be highly toxic. As the size increases, Au NPs are less toxic to L-929 and MC3T3-E1 cells, and 60 nm Au NPs are comparatively nontoxic. In comparison with 60 nm Au NPs, 50 nm Au NPs are prone to affect the mitochondrial activity of cell but show less effect on L-929 cells membrane integrity. This finding suggests that small-sized Au NPs not only interact with cell membrane, but also damage mitochondria following endocytosis. These Au NPs could be applied to the biomedical applications.

5. References

(1) Daniel, M. christine; Astruc, D. Gold Nanoparticles : Assembly , Supramolecular Chemistry, Quantum-Size-Related Properties, and Applications toward Biology, Catalysis, and Nanotechnology. *Chem. Rev.* **2004**, *104* (1), 293–346.

(2) Ozin, G. A. Nanochemistry : Synthesis in Diminishing Dimensions. *Adv. Mater.* **1992**, *4* (10), 612–649.

(3) Nurgaziyeva, E. K.; Tatykhanova, G. S.; Mun, G. A.; Khutoryanskiy, V. V; Kudaibergenov, S. E. Catalytic Properties of Gel-Immobilized Gold Nanoparticles in Decomposition of Hydrogen Peroxide. *Proc. Int. Conf.* **2015**, *4* (2), 1–4.

(4) Li, N.; Zhao, P.; Astruc, D. Anisotropic Gold Nanoparticles: Synthesis, Properties, Applications, and Toxicity. *Angew. Chem. Int. Ed.* **2014**, *53* (7), 1756–1789.

(5) Chinen, A. B.; Guan, C. M.; Ferrer, J. R.; Barnaby, S. N.; Merkel, T. J.; Mirkin, C. A. Nanoparticle Probes for the Detection of Cancer Biomarkers, Cells, and Tissues by Fluorescence. *Chem. Rev.* **2015**, *115* (19), 10530–10574.

(6) Osner, Z. R.; Holz, R. C.; Becker, D. P. An Analytical Method for Detecting Toxic Metal Cations Using Cyclotriveratrylene Derivative Capped Gold Nanoparticles. *Tetrahedron Lett.* **2015**, *56* (40), 5419–5423.

(7) Han, G.; Xing, Z.; Dong, Y.; Zhang, S.; Zhang, X. One-Step Homogeneous DNA Assay with Single-Nanoparticle Detection. *Angew. Chem. Int. Ed.* **2011**, *50* (15), 3462–3465.

(8) Coradeghini, R.; Gioria, S.; García, C. P.; Nativo, P.; Franchini, F.; Gilliland, D.; Ponti, J.; Rossi, F. Size-Dependent Toxicity and Cell Interaction Mechanisms of Gold Nanoparticles on Mouse Fibroblasts. *Toxicol. Lett.* **2013**, *217* (3), 205–216.

(9) Pernodet, N.; Fang, X.; Sun, Y.; Bakhtina, A.; Ramakrishnan, A.; Sokolov, J.; Ulman, A.; Rafailovich, M. Adverse Effects of Citrate/gold Nanoparticles on Human Dermal Fibroblasts. *Small* **2006**, *2* (6), 766–773.

(10) Yen, H.-J.; Hsu, S.-H.; Tsai, C.-L. Cytotoxicity and Immunological Response of Gold and Silver Nanoparticles of Different Sizes. *Small* **2009**, *5* (13), 1553–1561.

(11) G, B.; Seog, J. H.; Graham, L. M.; Lee, S. B. Experimental Considerations on the Cytotoxicity of Nanoparticles. *Nanomedicine* **2011**, *6* (5), 929–941.

(12) Huang, D.; Zhou, H.; Liu, H.; Gao, J. The Cytotoxicity of Gold Nanoparticles Is Dispersity-Dependent. *Dalton Trans.* **2015**, *44* (41), 17911–17915.

(13) Chen, Y. S.; Hung, Y. C.; Liau, I.; Huang, G. S. Assessment of the in Vivo Toxicity of Gold Nanoparticles. *Nanoscale Res. Lett.* **2009**, *4* (8), 858–864.

(14) Goodman, C. M.; McCusker, C. D.; Yilmaz, T.; Rotello, V. M. Toxicity of Gold Nanoparticles Functionalzied with Cationic and Anionic Side Chians. *Bioconju. Chem.* **2004**, *15*, 897–900.

(15) Klekotko, M.; Matczyszyn, K.; Siednienko, J.; Olesiak-Banska, J.; Pawlik, K.; Samoc, M. Bio-Mediated Synthesis, Characterization and Cytotoxicity of Gold Nanoparticles. *Phys. Chem. Chem. Phys.* **2015**, *17*, 1–2.

(16) Jana, N. R.; Gearheart, L.; Murphy, C. J. Wet Chemical Synthesis of High Aspect Ratio Cylindrical Gold Nanorods. *Phys Chem B.* **2001**, *105*, 4065–4067.

(17) Bastus, N. G.; Comenge, J.; Puntes, V. Kinetically Controlled Seeded Growth Synthesis of Citrate-Stabilized Gold Nanoparticles of up to 200 Nm: Size Focusing versus Ostwald Ripening. *Langmuir* **2011**, *27* (17), 11098–11105.

(18) Duncan, B.; Kim, C.; Rotello, V. M. Gold Nanoparticle Platforms as Drug and Biomacromolecule Delivery Systems. *J. Control. Release* **2010**, *148* (1), 122–127.

(19) Haiss, W.; Thanh, N. T. K.; Aveyard, J.; Fernig, D. G. Determination of Size and Concentration of Gold Nanoparticles from UV−Vis Spectra. *Anal. Chem.* **2007**, *79* (11), 4215–4221.

(20) Zhou, J.; Beattie, D. A.; Ralston, J.; Sedev, R. Colloid Stability of Thymine-Functionalized Gold Nanoparticles. *Langmuir* **2007**, *23* (24), 12096–12103.

(21) Zhang, X. D.; Wu, H. Y.; Wu, D.; Wang, Y. Y.; Chang, J. H.; Zhai, Z. Bin; Meng, A. M.; Liu, P. X.; Zhang, L. A.; Fan, F. Y. Toxicologic Effects of Gold Nanoparticles in Vivo by Different Administration Routes. *Int. J. Nanomedicine* **2010**, *5* (1), 771–781.

(22) Zoroddu, M. A.; Medici, S.; Ledda, A.; Nurchi, V. M.; Lachowicz, J. I.; Peana, M. Toxicity of Nanoparticles. *Curr. Med. Chem.* **2014**, *21*, 3837–3853.

(23) Wang, S.; Lu, W.; Tovmachenko, O.; Rai, U. S.; Yu, H.; Ray, P. C. Challenge in Understanding Size and Shape Dependent Toxicity of Gold Nanomaterials in Human Skin Keratinocytes. *Chem. Phys. Lett.* **2008**, *463* (1-3), 145–149.

(24) Connor, E. E.; Mwamuka, J.; Gole, A.; Murphy, C. J.; Wyatt, M. D. Gold Nanoparticles Are Taken up by Human Cells but Do Not Cause Acute Cytotoxicity. *Small* **2005**, *1* (3), 325–327.

(25) Pan, Y.; Leifert, A.; Ruau, D.; Neuss, S.; Bornemann, J.; Schmid, G.; Brandau, W.; Simon, U.; Jahnen-Dechent, W. Gold Nanoparticles of Diameter 1.4 Nm Trigger Necrosis by Oxidative Stress and Mitochondrial Damage. *Small* **2009**, *5* (18), 2067–2076.

(26) Lin, J.; Zhang, H.; Chen, Z.; Zheng, Y. Penetration of Lipid Membranes by Gold Nanoparticles : Insights into Cellular. *ACS Nano* **2010**, *4* (9), 5421–5429.

Chapter

3

Genipin Cross-linked Chitosan-Gold Nanocomposite Hydrogels for Cancer Treatment Applications

Abstract

The objective of the present study is to develop and investigate novel pH-responsive genipin-crosslinked chitosan-gold composite hydrogels. Due to their high toxicity to murine fibroblasts L-929, Au NPs with a diameter of 4.5 nm have been selected to prepare genipin cross-linked chitosan-gold composite hydrogels. The obtained composite hydrogels exhibit pH responsivity. Swelling ratio of the chitosan-gold composite hydrogels is as high as 365% at acidic pH of 6.4, which is higher than that of the hydrogels at neutral pH of 7.4. Most importantly, the obtained composite hydrogels can work as substrate for cell culture. Genipin cross-linked chitosan-gold composite hydrogels do not only show good cytocompatibility, but also promote adhesion and proliferation of murine fibroblasts L-929. In contrast, the viability of human hepatocellular carcinoma Hep G2 (cancerous cell line) has been deeply affected by the Au NPs released from the composite hydrogels in the weakly acidic environment, inducing the death Hep G2 cells.

1. Introduction

Over the past decades, significant progresses have been made in synthesis of composite biomaterials for cancer treatment.[1] The unique physicochemical properties of composite biomaterials have offered an opportunity to integrate different nanomaterials into a single platform for cancer treatment, which can improve the therapeutic efficacy to tumor cells and meanwhile avoid toxicity to normal cells.[2,3] To achieve such a goal, two prerequisites should be met, i.e., controlled release of therapeutic systems and biocompatibility of the composite biomaterials.[4] Despite extensive efforts launched in this area, the construction of such a material that fulfills both requirements, however, remains a challenging task.

Recently, research on composite biomaterials for cancer treatment has been greatly advanced, not only in inorganic materials-based systems, but also in novel polymer-based systems. Composite hydrogels have emerged as a promising option in this regard. Hydrogels highly hydrated crosslinked polymer networks have emerged as powerful synthetic analogues for promising biomaterials in biomedical application.[5] For instance, they can serve as scaffolds that provide structural integrity to tissue engineering, and can be used to control drug delivery.[10,11] However, the major determinant factor for its successful functioning is biocompatibility,[8] as non-compatible materials can elicit inflammatory responses *in vivo* and thus limit their use in living systems.[9]

Various natural and synthetic polymers have been used for hydrogels, chitosan is a natural cationic copolymer that presents well deal of interests for hydrogel structures.[10] Owing to its intriguing biological properties, excellent gel-forming ability and the numerous reactive amino groups for chemical modifications, chitosan has long been known and used in drug delivery and cell culture.[11] However, it often needs to be crosslinked in order to modulate their general properties and get a material with potential applications.[12,13] Genipin, extracted from the fruits of *Gardenia Jasminoides*, exhibits remarkable effects as an anti-inflammatory and anti-angiogenesis agent, and inhibits lipid peroxidation.[14] It reacts with compounds containing primary amine groups, such as chitosan to form covalently cross-linked networks.[15] Therefore, using genipin as a biological cross-linker on the one hand will lead to no adverse effects to

hydrogels, and on the other hand will give rise to improvements in the mechanical properties and stability of hydrogel films in water.[16–18]

Due to the similar size to certain cellular components or proteins, Au NPs may go through natural mechanical barriers, then possibly leading to adverse tissue reaction and immunogenicity.[19,20] Based on our results of cytotoxicity of Au NPs, by controlled release of Au NPs in acidic cell environment, the cytotoxicity of Au NPs will open up opportunities for applications in cancer treatment.[21,22,23]

In this chapter, novel genipin-crosslinked chitosan-gold nanocomposite hydrogels have been developed for biomedical applications. Au NPs with 4.5 nm in diameter have been selected, owing to their high cytotoxicity to L-929 cells as demonstrated in Chapter 2. pH-responsive crosslinked composite hydrogels have been prepared by using chitosan as the base matrix and genipin as the cross-linker via a cross-linking method as shown in Scheme 1. Genipin reacts with chitosan containing primary amine groups to form covalently crosslinked networks.[25,25] During the gelation, Au NPs are physically entrapped within the hydrogel networks. The swelling tests of the chitosan-gold nanocomposite hydrogels have been carried out under different pH solution. At pH = 6.4, the Au NPs are released from the nanocomposite hydrogels, due to the protonation of chitosan chain at acidic medium, which results from electrostatic repulsions between chitosan chains, repelling each other and favoring penetration of the hydrogel by water as shown in Scheme 2. At pH = 7.4, most of Au NPs are kept in the nanocomposite hydrogels. The influence of the chitosan-gold nanocomposite hydrogels on the viability of murine fibroblasts cells L-929 and human hepatocellular carcinoma Hep G2 has been investigated, respectively. The present approach combines the advantage of Au NPs and pH-responsive hydrogels, providing a platform for applications in sensing, imaging, delivery and biomedicine.

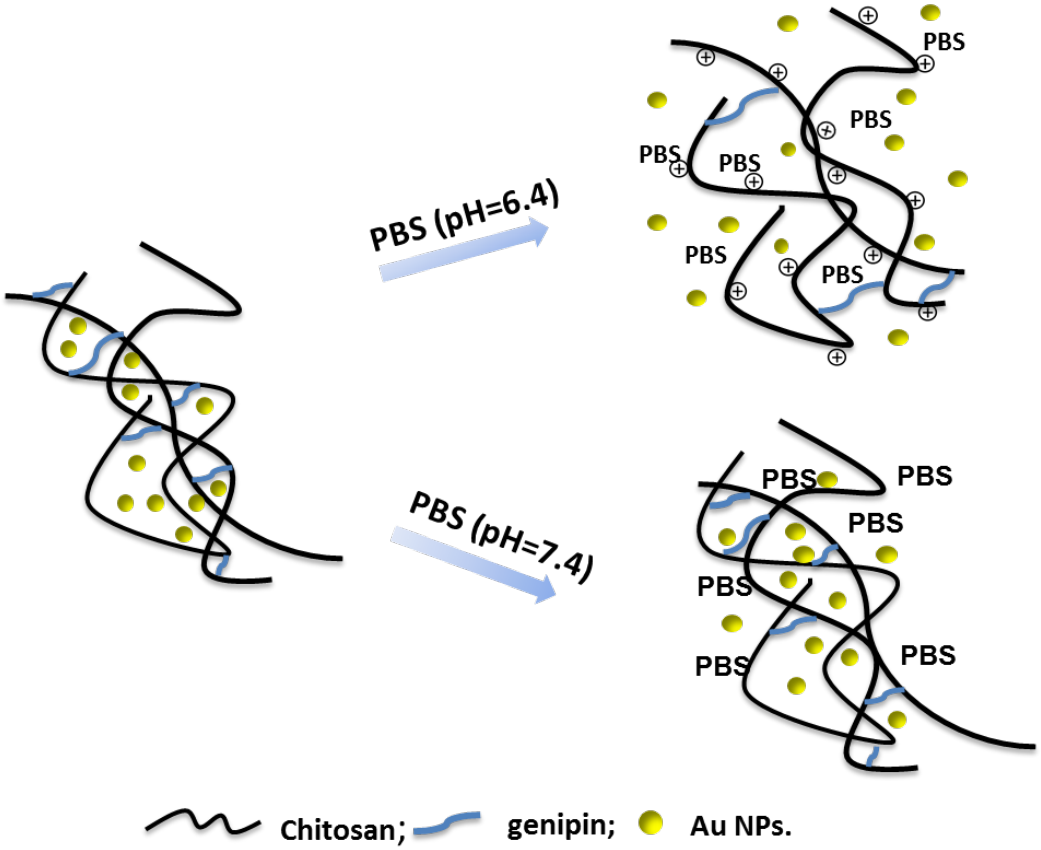

Scheme 1: Chitosan-gold nanocomposite hydrogels under different pH solution.

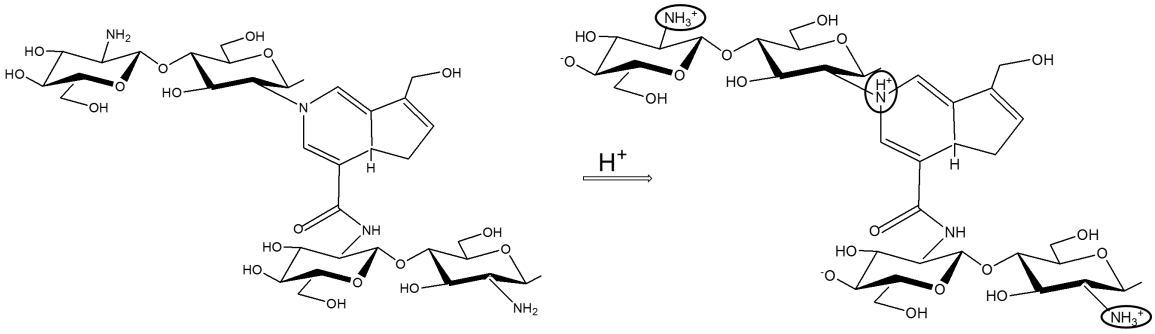

Scheme 2: Scheme of protonation of genipin crosslinked chitosan chains at acidic pH.

2. Experimental section

2.1 Materials

$HAuCl_4 \cdot 3H_2O$, trisodium citrate (99%), sodium borohydride, chitosan (medium weight, were originally obtained from chitin of crab shells), genipin, acetic acid (≥ 99%), Dulbecco's modified eagle medium (DMEM), 3-(4,5-dimethylthiazol-2-yl)-2,5-diphenyltetrazolium bromide (MTT), fluorescein diacetate (FDA) and Trypan blue solution (0.4%) were purchased from Sigma-Aldrich. RPMI 1640, fetal bovine serum (FBS), 1% penicillin/streptomycin and Trypsin-EDTA were purchased from PAA Laboratories GmbH. Propidium iodide (PI ≥ 94%), phosphate buffer saline (PBS) containing K_2HPO_4 and KH_2PO_4 was purchased from Fluka.

All chemicals were used as received unless stated otherwise. Solvents were at least analytical grade quality. Ultrapure deionized water was used for all solution preparations.

2.2 Apparatus

UV spectra were taken using a Shimadzu UV-2400 spectrophotometer. The sizes of Au NPs were measured by Transmission Electron Microscope (TEM) JEOL 2100. Fluorescent images were obtained using Axio Observer Z1 microscope (Carl Zeiss, Germany). The Fourier transform infrared attenuated total reflectance spectroscope was used by a Bruker Optics GmbH Equinox 55 in order to qualitatively examine the presence of functional groups. The fluorescent images were analyzed using the AxioVisionV4.8.1 software package.

2.3 Synthesis and characterization of Au NPs

The preparation of 4.5 nm Au NPs was performed according to the procedure described in detail in Chapter 2, section 2.3. The characterization of Au NPs was performed by TEM according to the procedure described in detail in Chapter 2, section 2.4.

2.4 Cell culture

For cell culture experiments, two cell lines were used. Murine fibroblasts L-929 were kindly provided by Dr. J. Lehmann, Fraunhofer Institute for Cell Therapy and Immunology IZI, Leipzig) and hepatoma cell line (Hep G2) were kindly provided by Prof. Dr. Roderich Süssmuth, Technical University of Berlin. L-929 cells were cultured in 75 cm^2 cell culture flasks (VWR Company) containing RPMI 1640 supplemented with 10% fetal bovine serum (FBS) and 1% penicillin/streptomycin (PS, 100X, all PAA Laboratories GmbH). Hep G2 cells were grown in 25 cm^2 cell culture flasks containing Dulbecco's modified eagle medium supplemented with 10% FBS and 1% PS at 37 °C and 5% CO_2 in a humidified incubator. Both cell lines were grown until confluence, and washed with Dulbecco's phosphate buffered saline solution and treated with Trypsin-EDTA (PAA Laboratories GmbH). After incubation for 3 min (L-929) or 5 min (Hep G2) at 37 °C, the detached cells were suspended in cell culture medium. The cell suspension was transferred into a falcon tube and centrifuged for 3 min at 1300 rpm, 4 °C. Finally, the cell pellet was resuspended in a fresh medium and cells were counted using a hemocytometer (Paul Marienfeld GmbH & Co. KG). Cells culture medium was refreshed every second day.

2.5 Cytotoxicity assays of Au NPs by Live/dead staining assay

Cytotoxicity tests of 4.5 nm Au NPs were carried out as the procedures described in **detail in Chapter 2, section 2.7.**

2.6 Preparation of genipin cross-linked chitosan-gold nanocomposite hydrogels

A 1.5% (W/V) aqueous chitosan solution was prepared by dissolving 1 g chitosan powder in 6.7 mL H_2O with 20 µL of aqueous acetic acid. Genipin solution (0.4 wt%) was prepared by dissolving 5 g genipin powder into 12.5 ml of water. All prepared solutions were stored in a fridge at 4 °C. Chitosan-gold nanocomposite solution was prepared by mixing chitosan solution with various amounts Au NPs. 20 µL of 0.4 wt% genipin solution was added into this glass vial while stirring for 12 h at room temperature to obtain a uniformly distributed and

viscous solution. Chitosan-gold nanocomposite films were prepared by casting 3 mL of solution into a plastic vial. They were dried at a drying oven at 40 °C for 24 h. The as-obtained nanocomposite hydrogels were stored in a desiccator at room temperature for further experiments. All the chitosan films and chitosan-gold nanocomposite films were neutralized in a 0.1 M NaOH solution for about 5 min, washed thoroughly with deionized water for 3 times, and dried again for the future experiments.

2.7 Characterization of chitosan-gold nanocomposite hydrogels

2.7.1 UV-vis spectroscopy analysis

UV-vis spectra were recorded on a Cary 4000 (Agilent Technologies) UV-visible spectrophotometer over the 300-800 nm range with 1 nm resolution and background correction using a glass slide. Chitosan-gold nanocomposite hydrogels in the swollen state were placed on the glass slide.

2.7.2 FT-IR analysis

The Fourier transform infrared attenuated total reflectance spectroscopy (FT-IR) spectra of chitosan solution, chitosan film, chitosan-gold nanocomposite films were recorded at room temperature in the range of 500 to 4000 cm^{-1}.

2.7.3 Swelling test

The swelling tests of the chitosan-gold nanocomposite hydrogels were carried out by the following method.[26] The hydrogel films were cut into 1×1 cm length and measured the dried weight (W_0). Then, the hydrogel films were immersed in various phosphate buffered saline (PBS, pH 6.4 and pH 7.4) at room temperature. After 24 h, 48 h and 96 h, the samples were taken out and after blotting with a filter paper to remove the surface water, followed by immediate weighing (W_1). The swelling ratio (R) was calculated using the following equation:

$$\text{Swelling ratio (R)} = \frac{W_1 - W_0}{W_0} \times 100\%$$

Each swelling experiment was repeated for three times and the average values were reported.

2.8 Chitosan-gold nanocomposite hydrogels culturing with Hep G2 cells

First, the as-synthesized chitosan and chitosan-gold nanocomposite films were cut into a 0.6×0.6 cm square film. After spraying ethanol (70 % V/V) on both sides of films, the cut hydrogels were washed carefully by deionized water and waited for drying in the sterile bench. Afterwards, they were put into each 8-well plates with 300 μL of a cell suspension containing 40 000 cells/mL L-929 and 40.000 cells/mL Hep G2 cells separately and incubated at 37 °C, 5% CO_2 atmosphere and 100% humidity. Followed by incubation for 48 h, cells were washed with Dulbecco's PBS and then stained with 100 μL of a vitality staining solution containing FDA (stock solution 0.5 mg/mL in acetone) and PI (stock solution 0.5 mg/mL in DPBS). Live and dead cells were detected by fluorescence microscope.

3. Results and Discussion

3.1 Cytotoxicity of Au NPs

Size and cytotoxicity of Au NPs results (TEM images and Live/dead staining assay results) can be found in Chapter 2, section 3.7.

3.2 Preparation of genipin cross-linked chitosan-gold nanocomposite hydrogels

Genipin is known to cross-link only chemically the amino groups of the chitosan chains[25,25] and in this case, Au NPs can be physically entrapped into the chitosan networks during the gelation. It can be seen from Figure 1 that the precursor solution is transparent, while the precursor solution turns red after the addition of Au NPs, indicating that Au NPs are stable and uniformly distributed in precursor solution and no aggregates form, which can be used for hydrogel formation.

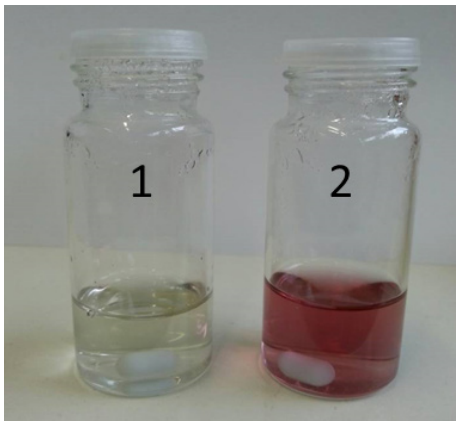

Figure 1: Optical images of precursor solution of hydrogel (1) before and (2) after addition of Au NPs.

3.2.1 FT-IR analysis

The successful synthesis of composite hydrogels had been proved by FT-IR spectra shown in Figure 2. In the IR spectra of chitosan hydrogel film and chitosan-gold nanocomposite hydrogel films, strong adsorption peak appears at 1536 cm^{-1} (Figure 2a,2b,2c) that is absent

from the spectrum of chitosan hydrogel, which can be attributed to vibration of amide N-H, verifying the formation of the chitosan hydrogel. The FT-IR spectra of composite hydrogels (a and b) are the same as that of pure chitosan hydrogel (c), indicating that the structure of chitosan hydrogel is maintained after "in situ" incorporation of Au NPs into chitosan.

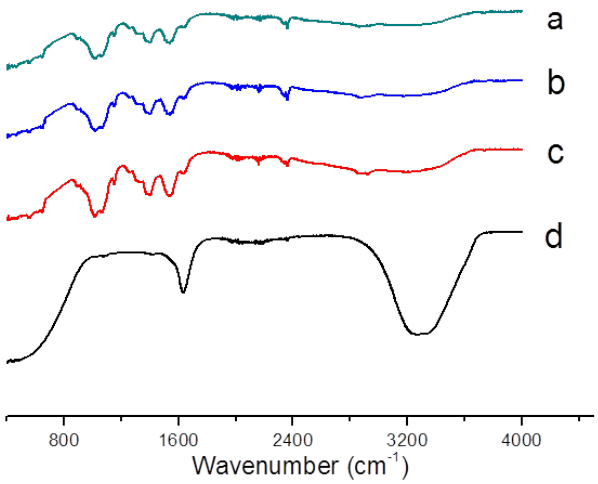

Figure 2: FT-IR spectra of genipin-crosslinked chitosan with 3600 µL colloidal gold nanocomposite hydrogel film (a), genipin-crosslinked chitosan with 1800 µL colloidal gold nanocomposite hydrogel film (b), genipin-crosslinked chitosan hydrogel film (c), chitosan and genipin solution (d).

3.2.2 UV-vis analysis

Since Au NPs absorb light at characteristic wavelengths in the UV-vis region, this technique is applied to identify the presence of Au NPs in nanocomposite hydrogel film. Figure 3a exhibits a UV-vis absorption peak centered at 519 nm, a typical surface plasmon resonance (SPR) band for Au NPs on chitosan-gold nanocomposite hydrogel film, while no absorption is observed for pure chitosan hydrogel film (Figure 3b), indicating the formation of chitosan-gold nanocomposite hydrogel film. The chitosan-gold nanocomposite hydrogel film appears deep-red because of the incorporation of Au NPs, while pure chitosan hydrogel film is transparent. This indicates that the Au NPs have been homogeneously incorporated in the hydrogels.

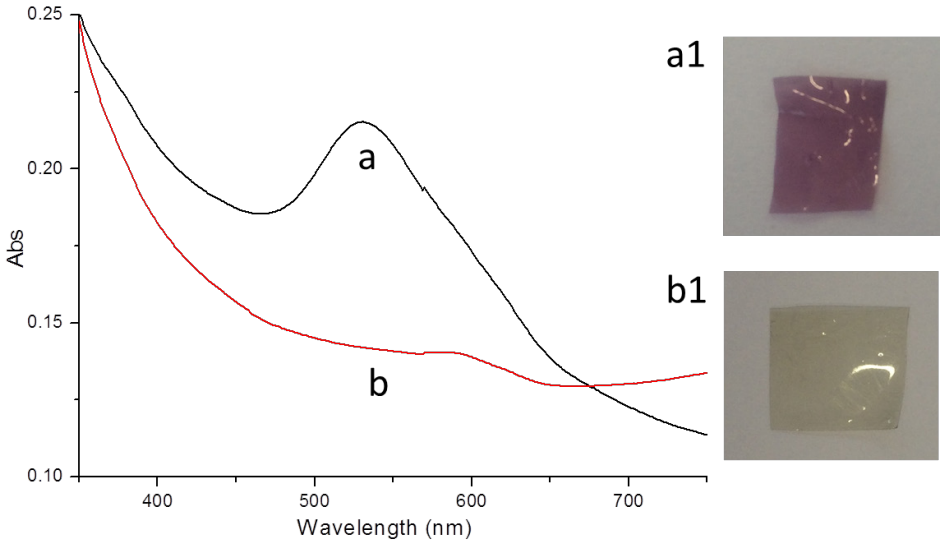

Figure 3: UV-vis absorption spectra of chitosan-gold nanocomposite hydrogel film (a) and chitosan film (b); optical images of chitosan-gold nanocomposite hydrogel film (a1) and chitosan film (b1).

3.3 Swelling test

To investigate the swelling ratio of chitosan and chitosan-gold nanocomposite hydrogel films in aqueous solution, swelling tests have been performed by immersing the as-prepared hydrogels in PBS solution of pH 6.4 and pH 7.4 at different time intervals, respectively. Swelling behaviors of the hydrogels are presented in Figure 5. As can be observed, the swelling ratio of both hydrogels increases with the increase of immersion time and the swelling become constant at 72 h. The swell ratio of the hydrogels at pH 6.4 is higher than that at pH 7.4 at the same time interval. For instance, the swelling ratio of nanocomposite hydrogels is as high as 365% of their original weight at pH 6.4 after 72 h of immersion; while at pH 7.4, the swelling ratio is only 240%. Similarly, the swelling ratio of the pure hydrogel in the acidic solution is higher than that in the neutral one, which can be explained by the protonation of chitosan chains at a low pH 6.4, resulting in repelling them from each other and favoring penetration of the hydrogel by water. The Au NPs immobilized in hydrogels can promote the swelling ratio, benefiting the release of Au NPs from the gel matrix to the PBS when the hydrogels are in the swollen state.

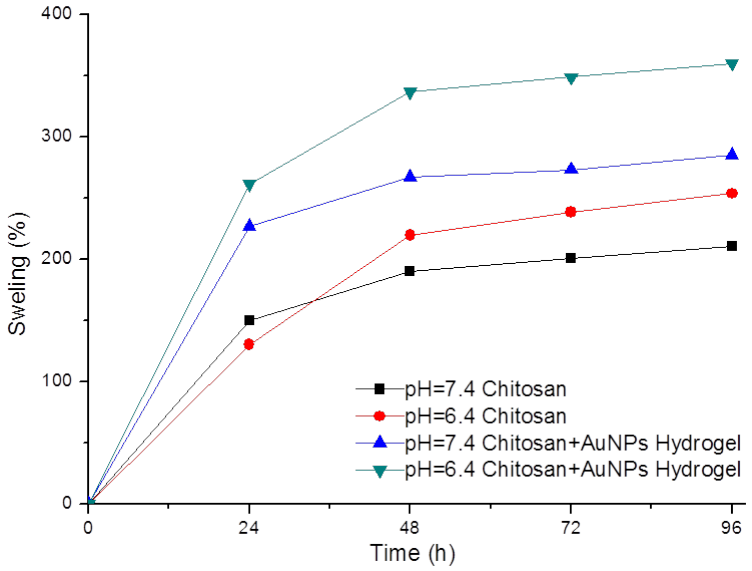

Figure 4: Swelling tests of genipin-crosslinked chitosan hydrogels and genipin-crosslinked chitosan-gold nanocomposite hydrogels in buffer solution at different pH values.

3.4 Chitosan-gold nanocomposite hydrogels cultured with Hep G2 cells

Fluorescence-based Live/dead assays have been used to evaluate the viability of the cancerous and normal cells after incubation with the as-synthesized pH-responsive nanocomposite hydrogels.[27] Fluorescein diacetate (FDA) and propidium iodide (PI) have been used to stain viable and dead cells, respectively. Simultaneous use of two fluorescent dyes allows a two-color discrimination of the population of living cells from the dead-cell population. Live cells are able to convert the non-fluorescent FDA into the green fluorescent metabolite fluorescein. The measured signal serves as indicator for viable cells, as the conversion is esterase dependent. In contrast, the nuclei staining dye PI cannot pass through a viable cell membrane. It reaches the nucleus by passing through disordered areas of dead cell membranes, and intercalates with the DNA double helix of the cell. Thus, dead cells show a red fluorescence when observed with a fluorescence microscope.

As shown in Figure 5A, L-929 cells grow very well on TCPS. In Figure 5B, fewer L-929 cells are able to adhere to the chitosan hydrogels, but dead cells were not detected, indicating chitosan hydrogels have good cytocompatibility but limited cell attachment property. In Figure 5C, more green live L-929 cells with a spindle-shaped morphology can be observed on the

chitosan-gold nanocomposite hydrogels. This indicates that the nanocomposite hydrogels can promote L-929 cellular adhesion and growth. As mentioned above, the chitosan-gold nanocomposite hydrogel is pH-responsive. And the extracellular pH of tumorous tissues is often acidic (pH = 6.4) while that of normal tissue is neutral (pH = 7.4).[28] Therefore, all the Au NPs are trapped in the hydrogels at neutral environment created by L-929 cells. The existence of Au NPs in nanocomposite hydrogels increases the stiffness of the surface, which can benefit cellular adhesion and growth. In addition, the swelling behavior of the hydrogel is reported to be crucial for bio-adhesive behavior.[29,30] The cell adhesion increases with the degree of hydration. Therefore, the high swelling ratio of the nanocomposite hydrogel promotes cell adhesion.

As can be seen from Figure 5D, Hep G2 cells are polygon-shaped and grown on TCPS. In Figure 5E, fewer cells adhere to the chitosan hydrogels, which show poor ability to adhere Hep G2 cells. In Figure 5F, no qualitative difference in Hep G2 shape can be observed, and many Hep G2 cells appear to be red after incubation with the chitosan-gold nanocomposite hydrogels, indicating that tumorous Hep G2 cells are dead. The weakly acid environment generated by Hep G2 cells during cancer cells growth and proliferation leads to the release of 4.5 nm Au NPs from pH-responsive nanocomposite hydrogel matrix. Hep G2 cells are thereby killed by the released Au NPs with 4.5 nm in diameter, which shows high toxicity to cells as already demonstrated in Chapter 2. Because Au NPs with small size can damage the membrane, penetrate into Hep G2 cells and then induce cell death. In this case, Au NPs can be employed instead of traditional drugs to kill cancerous cells.

In conclusion, due to the pH responsiveness of the chitosan-gold nanocomposite hydrogels, the acidic environment of cancerous cells can be used to modulate the release of Au NPs from chitosan-gold nanocomposite hydrogels, selectively killing the cancerous cells or promoting growth of fibroblast cells. Au NPs with 4.5 nm in diameter are released from the chitosan-gold nanocomposite network in the weakly acid environment created by cancerous Hep G2 cells. The death of cancerous cells is caused by Au NPs, which show promising potential to replace traditional drugs to kill cancerous cells. Moreover, at neutral environment chitosan-gold

nanocomposite hydrogels can promote cell adhesion and growth of normal tissue cells. Therefore, these nanocomposite hydrogels are a promising candidate for tissue-engineering applications.

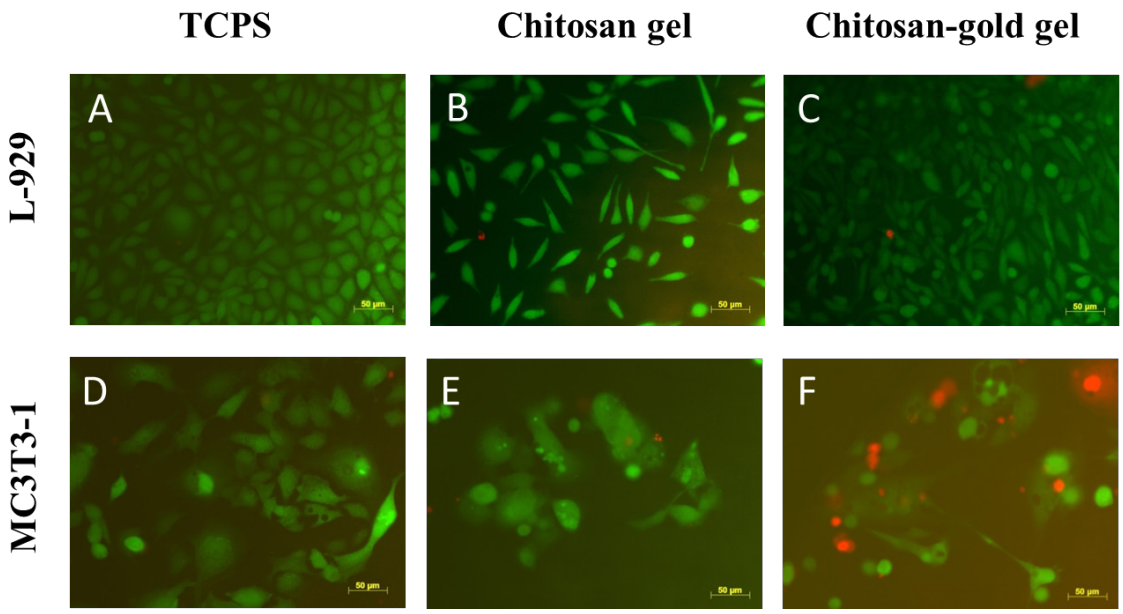

Figure 5: Fluorescent images of cells tested by fluorescence-based live-dead staining assays after incubation with nanocomposite hydrogels for 48 h. (A) L-929 cells on TCPS, (B) L-929 cells on chitosan hydrogels, (C) L-929 cells on chitosan-gold nanocomposite hydrogels; (D) Hep G2 cells on TCPS, (E) Hep G2 cells on chitosan hydrogels, (F) Hep G2 cells on chitosan-gold nanocomposite hydrogels.

4. Conclusion

In this chapter, 4.5 nm Au NPs with high cycotoxicity have been selected to prepare genipin crosslinked chitosan-gold nanocomposite hydrogels. We present herein the potential application of these novel nanocomposite hydrogels in cancer treatment by being cultured with murine fibroblasts L-929 and human hepatocellular carcinoma Hep G2. It has been proved that Au NPs with 4.5 nm in diameter can be released from the nanocomposite hydrogels due to a higher swelling degree of the hydrogel at acidic pH environment, which is generated by Hep G2 cells. The released Au NPs are able to kill cancerous Hep G2 cells. In contrast, the Au NPs are not expected to be released at the neutral pH environment surrounding normal tissue cells. The chitosan-gold nanocomposite hydrogels can thereby act as substrate to promote the cell growth and proliferation of normal cells. These novel chitosan-gold nanocomposite hydrogels not only provide a platform to promote proliferation of normal cells, but also can be used in biomedical applications for selectively attacking cancer tissues.

5. References

(1) Satarkar, N. S.; Zach Hilt, J. Hydrogel Nanocomposites as Remote-Controlled Biomaterials. *Acta Biomater.* **2008**, *4* (1), 11–16.

(2) Ruoslahti, E.; Pierschbacher, M. D. New Perspectives in Cell Adhesion: RGD and Integrins. *Science* **1987**, *238* (4826), 491–497.

(3) Satarkar, N. S.; Biswal, D.; Hilt, J. Z. Hydrogel Nanocomposites: A Review of Applications as Remote Controlled Biomaterials. *Soft Matter* **2010**, *6* (11), 2364.

(4) Ratner, B. D.; Bryant, S. J. Biomaterials: Where We Have Been and Where We Are Going. *Annu. Rev. Biomed. Eng.* **2004**, *6* (1), 41–75.

(5) Hoffman, a S. Hydrogels for Biomedical Applications. *Ann. N. Y. Acad. Sci.* **2001**, *944*, 62–73.

(6) Chung, B. G.; Lee, K.-H.; Khademhosseini, A.; Lee, S.-H. Microfluidic Fabrication of Microengineered Hydrogels and Their Application in Tissue Engineering. *Lab Chip* **2012**, *12* (1), 45.

(7) Tibbitt, M. W.; Anseth, K. S. Hydrogels as Extracellular Matrix Mimics for 3D Cell Culture. *Biotechnol. Bioeng.* **2009**, *103* (4), 655–663.

(8) Seda Kehr, N.; Riehemann, K. Controlled Cell Growth and Cell Migration in Periodic Mesoporous Organosilica/Alginate Nanocomposite Hydrogels. *Adv. Healthc. Mater.* **2015**, 193–197.

(9) Liu, M.; Wu, C.; Jiao, Y.; Xiong, S.; Zhou, C. Chitosan–halloysite Nanotubes Nanocomposite Scaffolds for Tissue Engineering. *J. Mater. Chem. B* **2013**, *1*, 2078.

(10) Liu, Z.; Wang, H.; Wang, Y.; Lin, Q.; Yao, A.; Cao, F.; Li, D.; Zhou, J.; Duan, C.; Du, Z.; et al. The Influence of Chitosan Hydrogel on Stem Cell Engraftment, Survival and Homing in the Ischemic Myocardial Microenvironment. *Biomaterials* **2012**, *33* (11), 3093–3106.

(11) Dehnavi, A. S.; Aroujalian, A.; Raisi, A.; Fazel, S. Preparation and Characterization of Polyethylene/silver Nanocomposite Films with Antibacterial Activity. *J. Appl. Polym. Sci.* **2013**, *127* (2), 1180–1190.

(12) Dash, M.; Chiellini, F.; Ottenbrite, R. M.; Chiellini, E. Chitosan - A Versatile Semi-Synthetic Polymer in Biomedical Applications. *Prog. Polym. Sci.* **2011**, *36* (8), 981–1014.

(13) Mi, F. L.; Sung, H. W.; Shyu, S. S. Synthesis and Characterization of a Novel Chitosan-Based Network Prepared Using Naturally Occurring Crosslinker. *J. Polym. Sci. Part A Polym. Chem.* **2000**, *38* (15), 2804–2814.

(14) Muzzarelli, R. A. Genipin-Crosslinked Chitosan Hydrogels as Biomedical and Pharmaceutical

Aids. *Carbohydr. Polym.* **2009**, *77* (1), 1–9.

(15) Guo, C.; Zhou, L.; Lv, J. Effects of Expandable Graphite and Modified Ammonium Polyphosphate on the Flame-Retardant and Mechanical Properties of Wood Flour-Polypropylene Composites. *Polym. Polym. Compos.* **2013**, *21* (7), 449–456.

(16) Das, D.; Kar, T.; Das, P. K. Gel-Nanocomposites: Materials with Promising Applications. *Soft Matter* **2012**, *8* (8), 2348.

(17) Ding, L.; Hao, C.; Xue, Y.; Ju, H. A Bio-Inspired Support of Gold Nanopaticles - Chitosan Nanocomposites Gel for Immobilization and Electrochemical Study of K562 Leukemia Cells. *Biomacromolecules* **2007**, *8* (4), 1341–1346.

(18) Merino, S.; Martín, C.; Kostarelos, K.; Prato, M.; Vázquez, E. Nanocomposite Hydrogels: 3D Polymer–Nanoparticle Synergies for On-Demand Drug Delivery. *ACS Nano* **2015**, *9* (5), 4686–4697.

(19) Pan, Y.; Neuss, S.; Leifert, A.; Fischler, M.; Wen, F.; Simon, U.; Schmid, G.; Brandau, W.; Jahnen-Dechent, W. Size-Dependent Cytotoxicity of Gold Nanoparticles. *Small* **2007**, *3* (11), 1941–1949.

(20) Lee, U.; Yoo, C.-J.; Kim, Y.-J.; Yoo, Y.-M. Cytotoxicity of Gold Nanoparticles in Human Neural Precursor Cells and Rat Cerebral Cortex. *J. Biosci. Bioeng.* **2015**, *121* (3), 341–344.

(21) Uygur, B.; Craig, G.; Mason, M. D.; Ng, A. K. Cytotoxicity and Genotoxicity of Silver Nanomaterials. *NSTI-Nanotech.* **2009**, *2* (2), 383–386.

(22) Dykman, L.; Khlebtsov, N. Gold Nanoparticles in Biomedical Applications: Recent Advances and Perspectives. *Chem. Soc. Rev.* **2012**, *41* (6), 2256.

(23) Kong, B.; Seog, J. H.; Graham, L. M.; Lee, S. B. Experimental Considerations on the Cytotoxicity of Nanoparticles. *Nanomedicine* **2011**, *6* (5), 929–941.

(24) Harris, R.; Lecumberri, E.; Heras, A. Chitosan-Genipin Microspheres for the Controlled Release of Drugs: Clarithromycin, Tramadol and Heparin. *Mar. Drugs* **2010**, *8* (6), 1750–1762.

(25) Kamiński, K.; Zazakowny, K.; Szczubiałka, K.; Nowakowska, M. pH-Sensitive Genipin-Cross-Linked Chitosan Microspheres for Heparin Removal. *Biomacromolecules* **2008**, *9* (11), 3127–3132.

(26) Hortigüela, M. J.; Aranaz, I.; Gutiérrez, M. C.; Ferrer, M. L.; Del Monte, F. Chitosan Gelation Induced by the in Situ Formation of Gold Nanoparticles and Its Processing into Macroporous Scaffolds. *Biomacromolecules* **2011**, *12* (1), 179–186.

(27) Lewinski, N.; Colvin, V.; Drezek, R. Cytotoxicity of Nanopartides. *Small* **2008**, *4* (1), 26–49.

(28) Rofstad, E. K.; Mathiesen, B.; Kindem, K.; Galappathi, K. Acidic Extracellular pH Promotes

Experimental Metastasis of Human Melanoma Cells in Athymic Nude Mice. *Cancer Res.* **2006**, *66* (13), 6699–6707.

(29) González, A.; Strumia, M. C.; Alvarez Igarzabal, C. I. Cross-Linked Soy Protein as Material for Biodegradable Films: Synthesis, Characterization and Biodegradation. *J. Food Eng.* **2011**, *106* (4), 331–338.

(30) Peh, K. K.; Wong, C. F. Polymeric Films as Vehicle for Buccal Delivery : Swelling , Mechanical , and Bioadhesive Properties . *J Pharm Pharm. Sci* **1999**, *2* (2), 53–61.

Chapter

4

Surface Immobilization of Au NPs onto Different type of PEG-based Hydrogels

Abstract

Immobilization of nanomaterials *e.g.* gold nanoparticles (Au NPs) onto hydrogel supports is very useful for biosensor and biomedical applications. In the present work, four kinds of poly (ethylene glycol) (PEG)-based hydrogels, i.e. PEG-PPG-PEG-UV (3BC-UV), PEG_{575}-UV, 8PEG-UV and 8PEG-VS-SH, act as soft support for immobilizing Au NPs by transferring Au NPs from the surface of silicon wafers to the hydrogel surface. The transfer efficiency of Au NPs was determined from UV-vis spectroscopy and SEM measurements. The amount and distribution of Au NPs on hydrogels was studied. It was found that 3BC-UV and 8PEG-VS-SH hydrogels can serve as efficient supports for immobilizing Au NPs, and the Au NPs transferring efficiency can be up to 99.8%. On the contrary, PEG_{575}-UV and 8PEG-UV hydrogels were unsuitable to transfer and immobilize Au NPs. Moreover, the stability of Au NPs fixed onto hydrogels has been tested. For PEG-PPG-UV and 8PEG-VS-SH hydrogels immobilized Au NPs, the Au NPs still remain on the hydrogels after 15 min of ultrasonication.

1. Introduction

Immobilization of nanomaterials is crucial for many important applications including biosensor development,[1] biological detection, catalysis,[2] biomaterials design[3] and nanotechnology.[4] Gold nanoparticles (Au NPs) are a leading platform as the core structure of nano-constructs because they are stable, easy to synthesize, and readily functionalized with biomolecules such as DNA or RNA.[5,6] Recently, they have been used in sensing applications,[7] and other researchers immobilized Au NPs on the surface of electrospun nanofiber scaffolds to encourage a longer outgrowth of neurites.[8]

However, the issues of aggregation and non-dispersibility of Au NPs in the desired solvent or film need to be solved, and the best way is to immobilize them onto a support.[4] In the past two decades, many supports have been employed for nanoparticle immobilization, such as gold electrode,[9] glass,[10] carbon,[10,11] lipids[12] and paper.[13] But the problem is that the surface of these material has a low porosity with limited surface areas.

Hydrogels are crosslinked hydrophilic polymer networks. The presence of water in gel matrix provide hydrogels with a high porosity, a large surface area, softness, flexibility and biocompatibility.[14–16] PEG hydrogels are among the most widely studied and extensively used polymers as matrix for controlling drug delivery, as well as cell delivery vehicles for promoting tissue regeneration. The network properties, swelling and the elasticity of the gels can be controlled by tuning the length of polymers and their functionalities. In addition, PEG hydrogels are optically transparent, allowing effectively optical detection with minimal background.[17,18] In the meantime, the properties of preventing unspecific protein adsorption and undesired cell attachment also make it as the perfect cell-resistant substrate for biomaterial investigation.[19] In this chapter, PEG hydrogels have been chosen as the templates for the immobilization of Au NPs.

Au NPs can be immobilized onto hydrogels by entrapment, chemical adsorption or physical adsorption.[3] Physical adsorption method is one of the most common methods for synthesis of nanocomposite hydrogels by mixing nanoparticles with precursors of hydrogels or modifying

Au NPs on the surface of hydrogel surface.[20,21] As the development of bio-conjugate chemistry and nanotechnology progresses, immobilization of Au NPs can be achieved via highly specific biomolecular interactions. In this study, both physical adsorption and covalent linkages have been adopted to immobilize Au NPs onto hydrogel surfaces. Au NPs were firstly deposited on (3-Aminopropyl) triethoxysilane (APTES), which is rich in amino groups, modified silicon wafer through the interaction between positive charge from amino groups of APTES and negative charge from Au NPs surface. Secondly, the hydrogels were brought into conformal contact with the surface of the Au NPs decorated silicon wafers. Lastly, the immobilization of Au NPs on the hydrogels was achieved by peeling off the hydrogels from silicon wafers. Au NPs are effectively transferred from the silicon wafers to the PEG-hydrogel surface.

2. Experimental section

2.1 Materials

Silicon wafers (polished on one side) were purchased from Microchemicals. Isopropanol, acetone, (3-Aminopropyl) triethoxysilane (APTES), ammonia (25%), hydrogen peroxide (H_2O_2 30%) and concentrated sulfuric acid (H_2SO_4 98%) were purchased from Carl Roth. Acryloyl chloride, 2-iminothiolane hydrochloride, vinyl sulfone, DL-Dithiothreitol (DTT), 2-hydroxy-4′-(2-hydroxyethoxy)-2-methylpropiophenone, photoinitiator (PI) Irgacure 2959, PEG-b-PPG-b-PEG diacrylate and PEG_{575} diacrylate were purchased from Sigma-Aldrich; 8arm PEG acrylate was purchased from Jenkem technology. Information of the corresponding block copolymers can be found in Table 1. All chemicals were used as received unless stated otherwise. Solvents were at least analytical grade quality.

Table 1: Physicochemical properties of PEG-based precursors: PEG-PPG-PEG (3BC), PEG Diacrylate (PEG), 8arm PEG acrylate (8PEG) and 8arm PEG Vinyl Sulfone (8PEG-VS). Values are obtained from the manufacturer. R: hexaglycerin core structure, r.t: room temperature.

Material	**PEG-b-PPG-b-PEG Diacrylate (3BC)**	**PEG Diacrylate (PEG)**	**8-arm PEG Acrylate (8PEG)**	**8-arm PEG Vinyl Sulfone (8PEG-VS)**
Structure	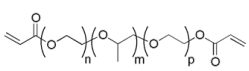	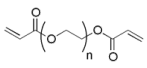	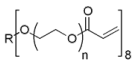	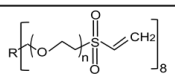
M_w [Da]	4400	575	15000	15000
Chain Length	n+p ~ 12; m ~ 57	n ~ 13	n ~ 40	n ~ 40
PEG [%]	30 (70 % PPG)	100	100	100
State at r.t.	Liquid	Liquid	Solid	Liquid
Gel formation	UV	UV	UV	Michael addition reaction

2.2 Preparation of hydrogels

2.2.1 3BC-UV hydrogel

The liquid precursor of block copolymer (3BC with molecular weight 4400) containing 1% of PI (1 wt% with respect to the amount of the precursor) were firstly mixed in a vial. Then the vial was put into oven at 60 °C for about 5 min until the mixture became clear. Subsequently, 80 μL precursor mixtures were deposited on a clean glass slide, capped with a cover glass (18 mm × 18 mm Carl Roth GmbH & Co KG) and exposed to UV light (λ = 366 nm Vilber Lourmat GmbH) for 15 min using a working distance of 10 cm in a nitrogen-filled glovebox. The cured transparent hydrogels were peeled off with tweezers, and then the samples were kept in water in a petri dish.

2.2.2 PEG_{575} hydrogel

PEG (with molecular weight 575) liquid precursors containing 1% of PI (1 wt% with respect to the amount of the precursor) were mixed in a vial. Then the vial was put into oven at 60 °C about 5 min until the mixture became clear. Subsequently, 80 μL of the as-prepared mixtures were deposited on a clean glass slide, capped with a cover glass (18 mm × 18 mm Carl Roth GmbH & Co KG) and exposed to UV light (λ = 366 nm Vilber Lourmat GmbH) for 30 min using a working distance of 10 cm in a nitrogen-filled glovebox. The cured transparent hydrogels were peeled off with tweezers, and then the samples were kept in water in a petri dish.

2.2.3 8PEG-UV hydrogel

8PEG-UV hydrogel was synthesized by Dr. Zhenfang Zhang.[22] 8-PEG, aqueous solutions (50 wt%) containing 1% of PI (1 wt% with respect to the amount of the precursor) were mixed in a vial. Then the vial was put into oven at 60 °C about 5 min until the mixture became clear. Subsequently, 80 μL of the as-prepared mixtures were deposited on a clean glass slide, capped with a cover glass (18 mm × 18 mm Carl Roth GmbH & Co KG) and exposed to UV light (λ = 366 nm Vilber Lourmat GmbH) for 30 min using a working distance of 10 cm in a nitrogen-

filled glovebox. The cured transparent hydrogels were peeled off with tweezers. And then the samples were kept in water in a petri dish.

2.2.4 8PEG-VS-SH hydrogel

A certain volume of ammonium solution (30% NH_3 in H_2O) was added to the powder of 8-arm PEG with vinyl sulfone (8PEG-VS) with 50% water content at room temperature under vigorous magnetic stirring until the solution turned to a viscous liquid. Then the viscous liquid was deposited on the glass slide, covered with a thin glass coverslip and left curing for 60 min. After gel formation, the transparent polymeric film with an inverse relief to that on the glass slide was peeled off mechanically. The stand-alone films (250−300 μm in thickness) were handled with tweezers. These hydrogels were immersed in DTT solution (5 mg/mL) for 60 min. Afterwards, these hydrogels were washed thoroughly with water for several times and kept in water overnight before use.

2.3 Silanization of silicon wafer surfaces by Chemical Vapor Deposition (CVD)

After ultrasonication in a mixture of acetone and water (V/V = 1:1) for 20 min, the silicon wafers were immersed in piranha solution (mixture of H_2SO_4 and H_2O_2 with V/V = 7:3) for 30 min. They were thoroughly washed with Milli-Q water and isopropanol, and then dried under a stream of pure nitrogen gas. Afterwards, the silicon wafers were placed inside a small Teflon chamber filled with a solution of APTES (100 μL). The aminosilane APTES was then introduced into the sealed chamber with raising the pressure of the deposition chamber. The reaction time of the surface with the gas phase adsorbate was 2 h, and then wafers were washed with anhydrous toluene (3×), isopropanol immediately and dried with nitrogen followed by evacuation. In order to measure silicon wafers, an atomic force microscopy (AFM) Nanowizard II (JPK instruments, Germany) was used. Imaging was done in contact mode using silicon nitride cantilevers (PNP TR, k ≈ 0.08 N/m, f0 ≈ 17 kHz; Nano world Innovative technologies) with a chromium-gold coating. Images were edited with Nano Wizard IP Version 3.3a (JPK instruments).

2.4 Deposition of Au NPs onto silicon wafers

A drop of 100 μL homogeneously dispersed Au NPs with diameter 42 nm was placed on APTES modified silicon wafers. After 60 min of incubation, the silicon wafers were washed thoroughly with deionized water for 8 times, and then dried under the flow of nitrogen to obtain Au NPs modified silicon wafers.

2.5 Transfer of Au NPs from silicon wafer to hydrogels

The as-prepared hydrogels were brought to firmly contact with the Au NPs modified silicon wafers for about 15 s before they were withdrawn from their surface. At last, the hydrogels were washed for 3 times with deionized water gently in order to remove the residual adsorbent Au NPs. They were kept in water as a swollen state for further experiments, and other samples were kept at room temperature for 12 h as a dried state for SEM measurements.

2.6 Characterization of Au NPs by UV-vis spectroscopy

Au NPs nanocomposite hydrogels in hydrated state were placed on a glass slide. Spectra were recorded on a Cary 4000 (Agilent Technologies) UV-vis spectrophotometer over the 300-800 nm range with 1 nm resolution. For the stability tests of Au NPs adhered to the surface of hydrogels were analyzed by UV-vis spectroscopy after the same hydrogels were ultrasonicated for 15 min by a ultrasonic cleaner (VWR Company).

2.7 Characterization of Au NPs by scanning electron microscopy (SEM)

Scanning electron microscopy (SEM) was performed on LEO 982 from Zeiss Company, the optical parts of the microscope from GEMINI Optics. The samples were firstly coated by carbon to improve the contrast prior to measurements, and the measurements were performed using Inlens detector operating at 20 kV.

3. Results and Discussion

3.1 Characterization of silicon wafer after deposition of APTES through CVD method

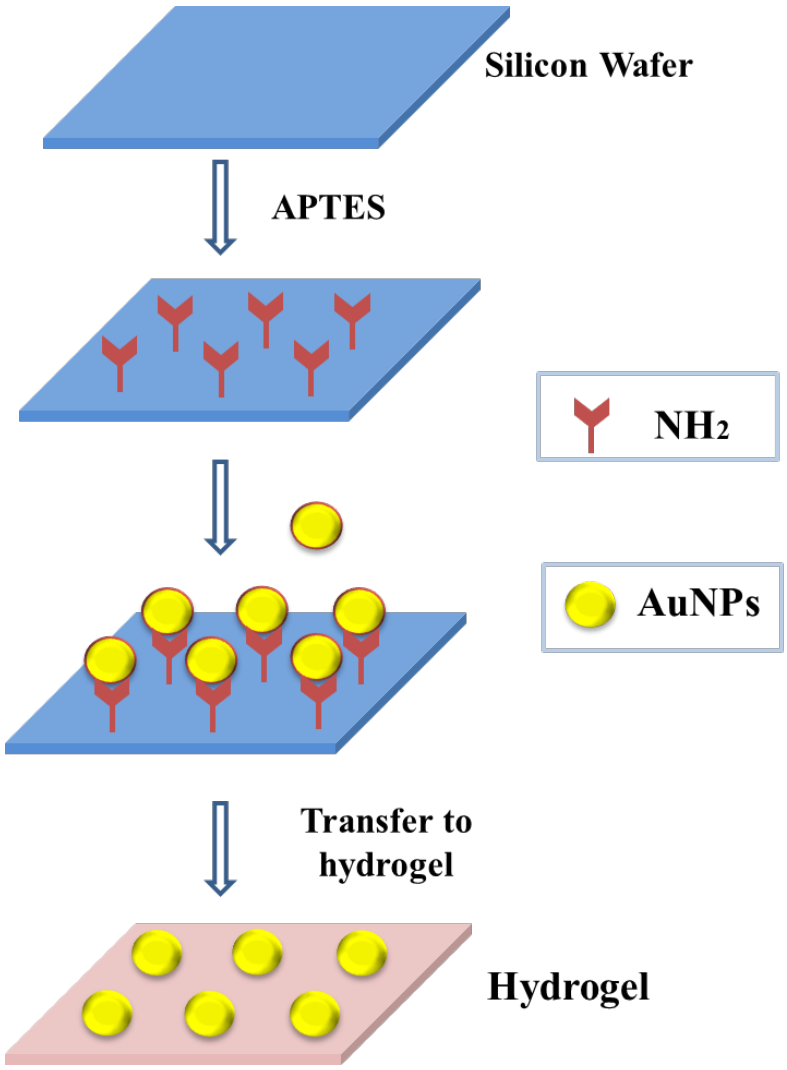

Scheme 1: General scheme of the immobilization of Au NPs on the hydrogels.

APTES with hydrolysable ethoxy groups to ensure a robust anchoring of the silane deposited on the surface of silicon wafer, whereas the amino groups remain available for further reaction, as shown in Figure 1A.[23] Chemical Vapor Deposition (CVD) is the most potentially reproducible method for producing high density, homogeneously functionalized silane assemblies on silicon substrate surfaces.[24] They can be uniformly modified on the silicon surface, and introduce the primary amino groups on the silicon by silanization. It is a well-

developed method employed to decorate the silicon substrate, yielding amino groups. In Figure 1B, AFM images reveal that no interfacial roughness for the silicon wafers can be observed before and after deposition of APTES. The surface of the treated silicon wafer is very smooth, because APTES is uniformly modified onto the silicon wafer.

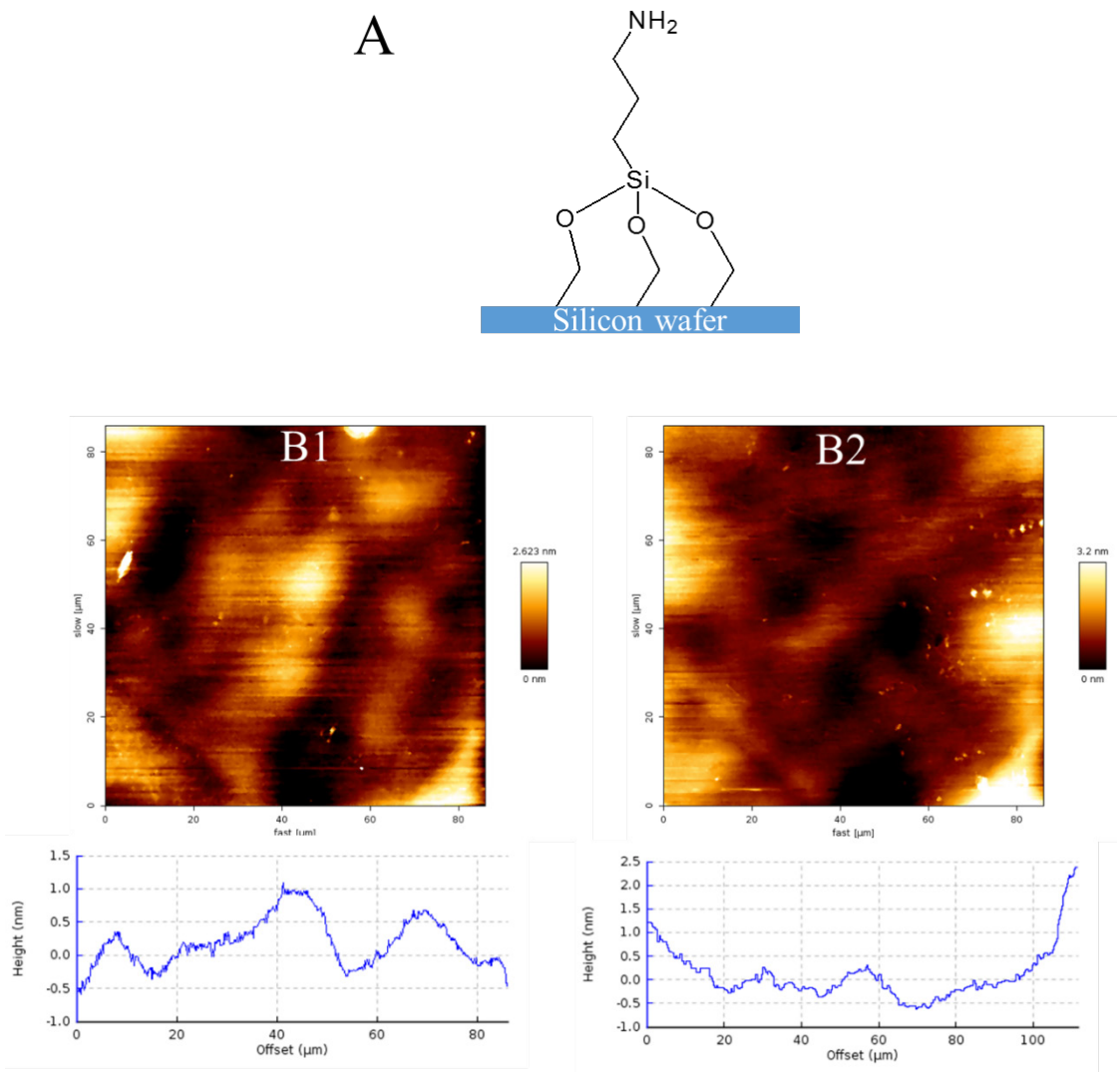

Figure 1: Reaction between APTES and the silicon wafer (A). AFM topography images and corresponding cross sections of the surface of silicon wafers before (B1) and after (B2) functionalization with APTES.

3.2 Characterization of Au NPs deposited on silicon wafers by SEM

Figure 2 shows SEM images recorded after the deposition of Au NPs on APTES modified silicon surfaces. It can be seen that Au NPs are uniformly distributed on the surface of silicon

substrate. The electrostatic interactions between the citrate-stabilization of negatively charged Au NPs and the positively charged APTES self-assembled monolayers (SAMs) result in the adsorption of Au NPs onto the surface silicon wafer.[25] It can be used as the transfer substrate for further experiments.

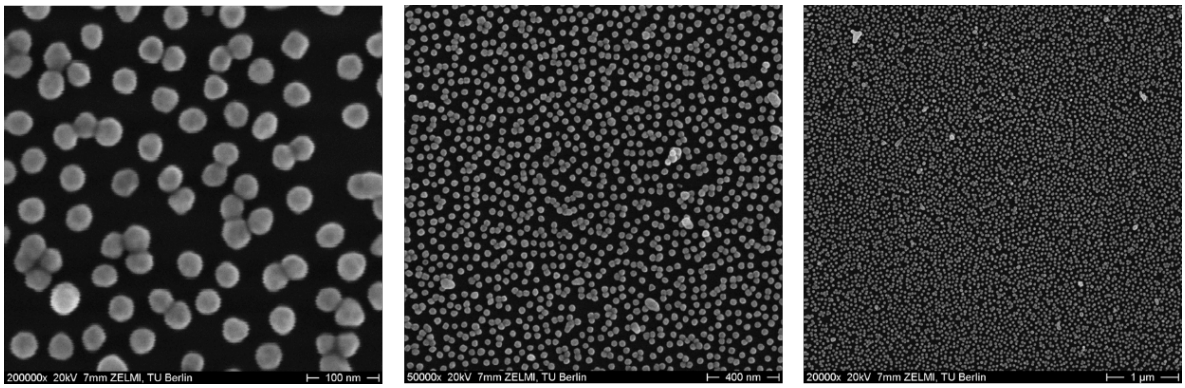

Figure 2: SEM images of Au NPs on the surface of silicon wafers.

3.3 Characterization of Au NPs immobilized on the surface of hydrogels by UV-vis spectroscopy

After being transferred the Au NPs to the four different hydrogels, the as-obtained nanocomposite hydrogels have been characterized by UV-vis spectroscopy as shown in Figure 3. Absorption peaks at 530 nm can be observed for the 3BC-UV and 8PEG-VS-SH hydrogels immobilized Au NPs, which is the characteristic peak of Au NPs.[26] This indicates that the Au NPs have been successfully immobilized on the hydrogel surface, corresponding to the color change of the hydrogels from colorless to red color before and after Au NPs are transferred to the surface of 3BC-UV and 8PEG-VS-SH hydrogels. Whereas the absence of absorption peak at 530 nm in the spectra of PEG_{575}-UV and 8PEG-UV hydrogels indicates that Au NPs are not successfully transferred to these two hydrogels.

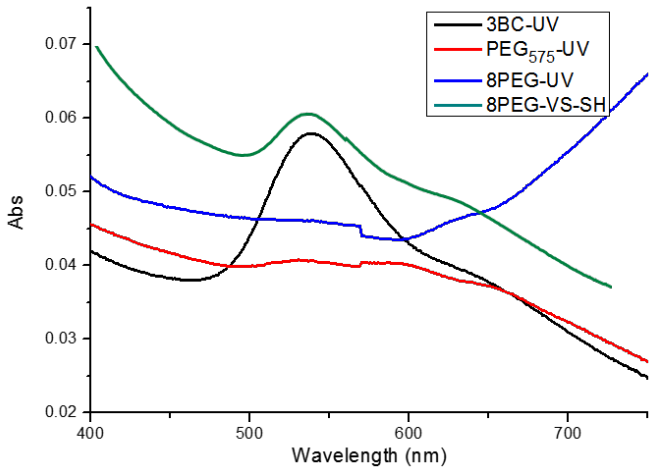

Figure 3: UV-vis spectra of the as-synthesized gold nanocomposite hydrogels.

3.4 Characterization of immobilized Au NPs on the surface of hydrogels by SEM

In order to investigate the transfer efficiency of Au NPs from silicon wafers to hydrogels via this novel method, SEM is utilized to characterize and count the number of Au NPs on the silicon before and after transferring procedure. Please note that the area of hydrogel in SEM images is actually more than 4 times larger than the silicon wafer, since they are in dried state for SEM measurements, therefore there are many more Au NPs on surface of hydrogel than on silicon wafer under the same view with same magnification. SEM images shown in Figure 4 provide a direct observation for the distribution of Au NPs on the hydrogels. As can be observed from Figure 4a1 and Figure 4d1, a monolayer of Au NPs is deposited on the surface of 3BC-UV and 8PEG-VS-SH hydrogels after the hydrogels were peeled off from silicon wafers. Only few Au NPs are left on the silicon wafers shown in Figure 4a2 and 4d2. The transfer efficiency of Au NPs from silicon wafers to these hydrogels is 99.8% and 98% (Table 2), respectively, indicating that almost all the Au NPs are transferred from silicon wafers onto the surface of 3BC-UV and 8PEG-VS-SH hydrogels. In contrast, Au NPs can hardly be found on the PEG_{575}-UV and 8PEG-UV hydrogels shown in Figure 4b1 and Figure 4c1. The transfer efficiency of Au NPs from silicon wafers to these hydrogels is less than 1 % (Table 2).

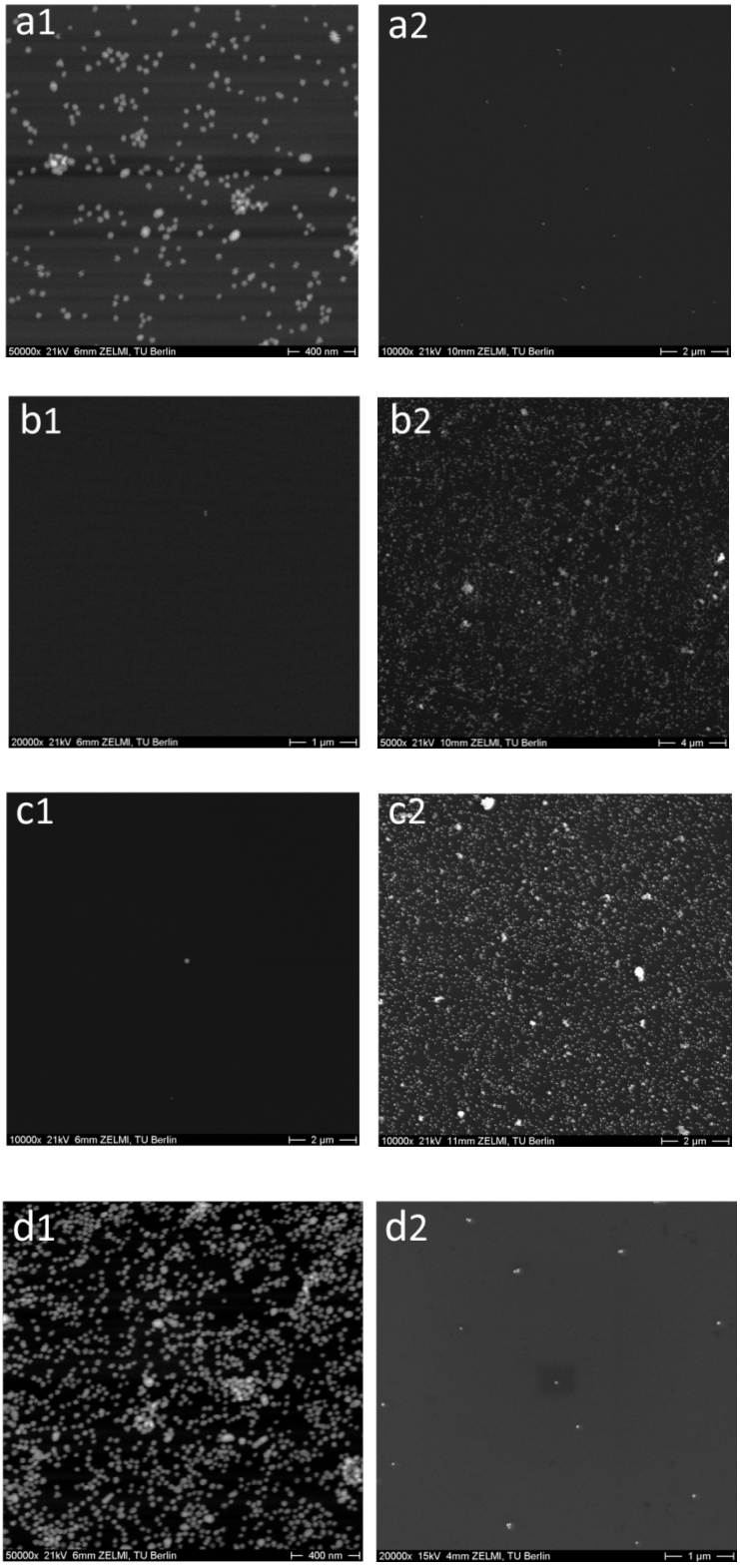

Figure 4: SEM images of Au NPs on the surface of (a1) 3BC-UV hydrogels, (b1) PEG_{575}-UV hydrogels, (c1) 8PEG-UV hydrogels, (d1) 8PEG-VS-SH hydrogels and silicon wafers (a2-d2).

Table 2: Transfer efficiency of Au NPs from silicon wafers to 4 different hydrogels

Hydrogels	Transfer efficiency (%)
3BC-UV	99.8 ± 0.1
PEG_{575}-UV	0
8PEG-UV	0
8PEG-VS-SH	98 ± 1.8

The huge difference between the transfer efficiency of the different gels is very remarkable. In order to understand this, we have to consider several physicochemical properties that differ between the 4 different hydrogels.

We hypothesize that the difference in the transfer efficiency could be due to the different porosity of these hydrogels. As can be observed from Table 1, 3BC-UV, PEG_{575}-UV and 8PEG-UV hydrogels are formed through the same crosslinking method, but the chemical structure of 3BC is different with PEG_{575} and 8PEG. 3BC is found to be more hydrophobic in comparison to PEG_{575}-UV and 8PEG-UV hydrogels,[27] which may result in the porosity difference of the hydrogels.

The flexibility of hydrogels might also influence the transfer efficiency. In comparison with PEG_{575}-UV and 8PEG-UV hydrogels, 3BC-UV hydrogels are more flexible. Thus, the contact area between 3BC-UV hydrogels and Au NPs modified silicon is therefore larger due to the ease of deformation of 3BC-UV hydrogels, leading to higher adhesive force between Au NPs and hydrogels, thereby guaranteeing the Au NPs transfer to the hydrogels. For 8PEG-VS-SH hydrogels, both physical interaction and covalent bonding are responsible for immobilization of Au NPs. The -SH linker molecules, which covalently attached to the Au NPs by Au-S bond, and the interaction between Au NPs and relatively flexible PEG polymer chains, can couple the Au NPs to the hydrated PEG-VS-SH hydrogels. Au NPs are therefore supposed to be transferred from silicon wafers to the surface of 8PEG-VS-SH hydrogels.

Surface elasticity could be another factor to induce the difference in transfer efficiency. As can be seen from Table 1, the elastic modulus of 3BC-UV, PEG_{575}-UV and 8PEG-UV hydrogels is 1.20 ± 0.03 MPa, 0.44 ± 0.05 MPa and 0.27 ± 0.05 MPa, respectively. No big difference in elasticity can be found among these hydrogels. Thus, the difference in transfer efficiency might be not affected by surface elasticity.

More experiments need to be performed in future to prove these hypotheses.

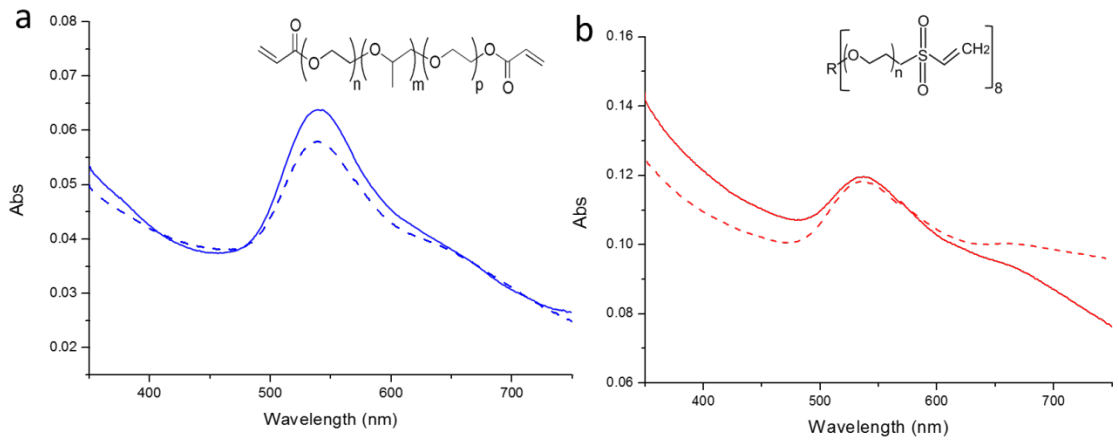

Figure 5: UV-vis spectra of Au NPs on (A) 3BC-UV hydrogels and (B) 8PEG-VS-SH hydrogels. (solid lines represent Au NPs on the hydrogels before ultrasonication treatment; dashed lines represent Au NPs on the hydrogels after 15 min of ultrasonication treatment.)

UV-vis spectroscopy has been used to characterize the stability of Au NPs bound on the 3BC-UV and 8PEG-VS-SH hydrogels. As shown in Figure 5a and b, an obvious absorption peak at ~530 nm can be observed before and after ultrasonication treatment of Au NPs immobilized on the 3BC-UV and 8PEG-VS-SH hydrogels, which is the characteristic peak of Au NPs. This indicates that Au NPs are firmly immobilized on the hydrogels.

4. Conclusions

In this study, after uniform deposition of Au NPs on the surface of silicon wafers 3BC-UV, PEG_{575}-UV, 8PEG-UV and 8PEG-VS-SH hydrogels have been employed to immobilize Au NPs by transferring them from silicon wafers to the surface of the hydrogels. UV-vis spectroscopy and SEM analysis have revealed that that 3BC-UV and 8PEG-VS-SH hydrogels can efficiently immobilize Au NPs, and the transfer efficiency is as high as 98%. In contrary, PEG_{575}-UV and 8PEG-UV hydrogels cannot immobilize any Au NPs.

Considering that the 8PEG-VS-SH hydrogel is cell-repellent, and the Au NPs can be efficiently immobilized on the hydrogel surface, these composite hydrogels can be applied as substrate for cell culture, and for the investigation of the interactions between Au NPs and cells. Therefore, we develop a soft and stable substrate for efficient immobilization of Au NPs, which is a useful material for next part of my research work.

5. References

(1) Xu, H.; Hong, R.; Lu, T.; Uzun, O.; Rotello, V. M. Recognition-Directed Orthogonal Self-Assembly of Polymers and Nanoparticles on Patterned Surfaces. *J. Am. Chem. Soc.* **2006**, *128* (10), 3162–3163.

(2) Park, H.-Y.; Schadt, M. J.; Wang, L.; Lim, I.-I. S.; Njoki, P. N.; Kim, S. H.; Jang, M.-Y.; Luo, J.; Zhong, C.-J. Fabrication of Magnetic Core@shell Fe oxide@Au Nanoparticles for Interfacial Bioactivity and Bio-Separation. *Langmuir* **2007**, *23* (17), 9050–9056.

(3) Nurgaziyeva, E. K.; Tatykhanova, G. S.; Mun, G. A.; Khutoryanskiy, V. V; Kudaibergenov, S. E. Catalytic Properties of Gel-Immobilized Gold Nanoparticles in Decomposition of Hydrogen Peroxide. *Proc. Int. Conf.* **2015**, *4* (2), 1–4.

(4) Baeissa, A.; Moghimi, N.; Liu, J. Hydrogel Porosity Controlling DNA-Directed Immobilization of Gold Nanoparticles Revealed by DNA Melting and Scanning Helium Ion Microscopy. *RSC Adv.* **2012**, *2* (7), 2981.

(5) Dam, D. H. M.; Lee, H.; Lee, R. C.; Kim, K. H.; Kelleher, N. L.; Odom, T. W. Tunable Loading of Oligonucleotides with Secondary Structure on Gold Nanoparticles through a pH-Driven Method. *Bioconjug. Chem.* **2015**, *26* (2), 279–285.

(6) Hu, M.; Chen, J.; Li, Z.-Y.; Au, L.; Hartland, G. V; Li, X.; Marquez, M.; Xia, Y. Gold Nanostructures: Engineering Their Plasmonic Properties for Biomedical Applications. *Chem. Soc. Rev.* **2006**, *35* (11), 1084–1094.

(7) Li, Z.; Mao, W.; Devadas, M. S.; Hartland, G. V. Absorption Spectroscopy of Single Optically Trapped Gold Nanorods. *Nano Lett.* **2015**, *15* (11), 7731–7735.

(8) Baranes, K.; Shevach, M.; Shefi, O.; Dvir, T. Gold Nanoparticle-Decorated Scaffolds Promote Neuronal Differentiation and Maturation. *Nano Lett.* **2015**, A – E.

(9) Su, J.; He, X.; Wang, Y.; Wang, K.; Chen, Z.; Yan, G. A Sensitive Signal-on Assay for MTase Activity Based on Methylation-Responsive Hairpin-Capture DNA Probe. *Biosens. Bioelectron.* **2012**, *36* (1), 123–128.

(10) Kumar, P.; Choithani, J.; Gupta, K. C. Construction of Oligonucleotide Arrays on a Glass Surface Using a Heterobifunctional Reagent, N-(2-Trifluoroethanesulfonatoethyl)-N-(Methyl)-Triethoxysilylpropyl-3-Amine (NTMTA). *Nucleic Acids Res.* **2004**, *32* (10), 80.

(11) Tang, L.; Wang, Y.; Liu, Y.; Li, J. DNA-Directed Self-Assembly of Graphene Oxide with Applications to Ultrasensitive Oligonucleotide Assay. *ACS Nano* **2011**, *5* (5), 3817–3822.

(12) Dave, N.; Liu, J. Protection and Promotion of UV Radiation-Induced Liposome Leakage via DNA-Directed Assembly with Gold Nanoparticles. *Adv. Mater.* **2011**, *23* (28), 3182–3186.

(13) Zhao, W.; Ali, M. M.; Aguirre, S. D.; Brook, M. a; Li, Y. Paper-Based Bioassays Using Gold Nanoparticle Colorimetric Probes. *Anal. Chem.* **2008**, *80* (22), 8431–8437.

(14) Hennink, W. E.; van Nostrum, C. F. Novel Crosslinking Methods to Design Hydrogels. *Adv. Drug Deliver. Rev.* **2012**, *64*, 223–236.

(15) Hoffman, A. S. Hydrogels for Biomedical Applications. *Adv. Drug Delivr. Rev.* **2012**, *64*, 18–23.

(16) Seliktar, D. Designing Cell-Compatible Hydrogels. *Science* **2012**, *336*, 1124–1129.

(17) Chung, B. G.; Lee, K.-H.; Khademhosseini, A.; Lee, S.-H. Microfluidic Fabrication of Microengineered Hydrogels and Their Application in Tissue Engineering. *Lab Chip* **2012**, *12* (1), 45.

(18) Nuttelman, C. R.; Rice, M. A.; Rydholm, A. E.; Salinas, C. N.; Shah, D. N.; Anseth, K. S. Macromolecular Monomers for the Synthesis of Hydrogel Niches and Their Application in Cell Encapsulation and Tissue Engineering. *Prog. Polym. Sci.* **2008**, *33* (2), 167–179.

(19) Lee, T. T.; García, J. R.; Paez, J. I.; Singh, A.; Phelps, E. A.; Weis, S.; Shafiq, Z.; Shekaran, A.; Del Campo, A.; García, A. J. Light-Triggered in Vivo Activation of Adhesive Peptides Regulates Cell Adhesion, Inflammation and Vascularization of Biomaterials. *Nat. Mater.* **2015**, *14* (3), 352–360.

(20) Thoniyot, P.; Tan, M. J.; Karim, A. A.; Young, D. J.; Loh, X. J. Nanoparticle-Hydrogel Composites: Concept, Design, and Applications of These Promising, Multi-Functional Materials. *Adv. Sci.* **2015**, *2* (1-2), 1400010.

(21) Schmidt, S.; Madaboosi, N.; Uhlig, K.; Köhler, D.; Skirtach, A.; Duschl, C.; Möhwald, H.; Volodkin, D. V. Control of Cell Adhesion by Mechanical Reinforcement of Soft Polyelectrolyte Films with Nanoparticles. *Langmuir* **2012**, *28* (18), 7249–7257.

(22) Zhang, Z. Synthesis and Characterization of 8 Arm-Poly(ethylene Glycol) Based Hydrogels via Michael Addition or Click Chemistry for Biomedical Applications, 2015. PhD Thesis, Technical University Berlin

(23) Haddada, M. Ben; Blanchard, J.; Casale, S.; Krafft, J.; Vallée, A. Optimizing the Immobilization of Gold Nanoparticles on Functionalized Silicon Surfaces : Amine- vs Thiol-Terminated Silane. *Gold Bull.* **2013**, *46*, 335–341.

(24) Zhang, F.; Sautter, K.; Larsen, A. M.; Findley, D. a.; Davis, R. C.; Samha, H.; Linford, M. R. Chemical Vapor Deposition of Three Aminosilanes on Silicon Dioxide: Surface Characterization, Stability, Effects of Silane Concentration, and Cyanine Dye Adsorption. *Langmuir* **2010**, *26* (18), 14648–14654.

(25) Kumar, A.; Mandal, S.; Selvakannan, P. R.; Pasricha, R.; Mandale, a. B.; Sastry, M. Investigation into the Interaction between Surface-Bound Alkylamines and Gold Nanoparticles. *Langmuir* **2003**, *19* (16), 6277–6282.

(26) Tokarev, I.; Tokareva, I.; Minko, S. Gold-Nanoparticle-Enhanced Plasmonic Effects in a Responsive Polymer Gel. *Adv. Mater.* **2008**, *20* (14), 2730–2734.

(27) Strehmel, C.; Zhang, Z.; Strehmel, N.; Lensen, M. C. Cell Phenotypic Changes of Mouse Connective Tissue Fibroblasts (L-929) to Poly(ethylene Glycol)-Based Gels. *Biomater. Sci.* **2013**, *1*, 850–859.

Chapter 5

Facile Transfer of Gold Nanoparticles to Functional Hydrogels and the Effect on Cell Adhesion

Abstract

Cell adhesion is a crucial process for the assembly of individual cells into functional tissues, which depends on the environmental parameters, such as rigidity, topography, chemistry and porosity of the substrate or scaffold. Herein, we show that a novel poly(ethylene glycol) (PEG)-based hydrogel (**8PEG-VS-SH**) can be synthesized and further functionalized by amine Michael-type addition reactions – first with ammonia and then with Dithiothreitol (DTT) – to yield hydrogels with high affinity for gold. Consequently, gold nanoparticles (Au NPs) can be firmly bound and immobilized on the surface. This nanoparticle-hydrogel architecture has a great potential as a substrate for advanced cell engineering. In this chapter, Au NPs (20 nm and 42 nm, respectively) with different densities are transferred from silicon wafers to the surface of hydrogels, with a transfer efficiency of up to 98 or even 100%. Electron microscopy was employed to analyze the novel nanocomposite gel surfaces and the silicon wafers before and after the transfer process. Optical microscopy studies of cell culture reveal that the amount of murine fibroblasts L-929 adhering to the substrate increases with the increase of the density of Au NPs, with no cell adhesion on the hydrogels with the lowest density of Au NPs. Apparently, the Au NPs on an anti-adhesive PEG-background serve as anchoring points for cell adhesion. We propose that protein adsorption is enabled and this in turn results in the cell adhesion.

1. Introduction

Functionalized nanostructured materials, such as self-assembled monolayers (SAMs) of nanoparticles (NPs), play an increasingly important role in many applications, such as biosensor development,[1] biological detection, catalysis,[2] biomaterials design[3] and nanotechnology.[4,5] Due to the chemical stability as well as facility to synthesize and functionalize their surface with biomolecules (*e.g.* proteins), gold nanoparticles (Au NPs) have become a leading platform as the core structure of nano-constructs.[6,7] However, the issues of aggregation and non-dispersibility of Au NPs in the desired solvent or film need to be solved, which can be achieved via immobilization of Au NPs onto a support in a controlled manner.[8]

In the last two decades, many hard inorganic supports, such as gold electrodes,[9] glass,[10] carbon[11] and silicon[12] have been employed for nanoparticle immobilization. Nevertheless, polymer-based supports are significantly more advantageous than inorganic supports in certain hindsights. Usually, polymeric substrates are more flexible, yet offering a wider range of rigidity, can be stretched dynamically, and may adopt different shapes. Moreover, the properties of polymer materials may be tailored to specific purposes, either by chemically modifying the polymers or by varying the polymerization and/or crosslinking conditions.[13] Polymeric supports, especially those consisting of a highly hydrated material such as poly(ethylene glycol) (PEG)-based hydrogels, exhibit a number of advantageous properties such as being transparent, deformable, cytocompatible, and permeable to nutrients, solutes and gases.[14]

The initial nonspecific adsorption of proteins and cells usually need to be avoided in tissue engineering, biosensor systems and other biomedical applications.[15] PEG hydrogels, which possess an inert and protein-repellent surface, have demonstrated to be especially useful as a background platform for the *in vitro* investigation of cell behavior. In addition, the network properties, the swelling and the elasticity of the gels can be controlled by tuning the length of the polymer chains and their functionalities.[16–18] In our work, multivalent, 8-arm star shaped PEG macromonomers (having a hexaglycerol core and a molecular weight of ~ 15,000 Da; 8PEG) have been utilized for hydrogel preparation, offering some significant advantages over

their linear counter-parts, specifically 1) increased functionality (i.e. 8 instead of only 2 functional end-groups), and 2) more variable physicochemical properties.

UV radiation and sulfur-type Michael-type addition crosslinking polymerization are two typical methods to crosslink PEG with functional C=C double bonds to prepare hydrogels. However, all functional groups of PEG precursors are usually consumed through these methods.[19,20] Considering that the remaining functional C=C double bonds can be further used for photoinitiated crosslinking and/or chemical functionalization with other functional groups, a new class of PEG-NH_3 hydrogels formed by a modified amine Michael-type addition reaction between acrylate and amine functional groups has been developed in the Lensen Lab.[21] This crosslinking reaction of acrylate terminated 8PEG-macromonomers with NH_3 allows the formation of hydrogels with mechanical properties and up to 70% of residual acrylate end-groups for further (bio)chemical functionalization of the partly crosslinked gels.[21] These unreacted functional groups provide the sites for biomolecule modification. However, due to the hydrolysis of ester groups, it was found that such hydrogels formed via crosslinking reaction between acrylate and amine groups may degrade within one day during incubation, making them not suitable for cell adhesion tests.

In the present work, in order to avoid the degradability of hydrogels that are crosslinked by acrylate and amine groups, and to provide stable substrates for further cell tests, instead of acrylate groups, vinyl sulfone groups have been utilized to form hydrogels, and after gelation, the residual functional groups can be converted to thiol groups with the ability of binding with Au NPs. By a soft lithographic procedure, coined “nano-contact transfer”, Au NPs with diameters of 20 nm and 42 nm are transferred from silicon to 8PEG-VS-SH hydrogels, displaying variable densities (surface coverage).

To mimic the cellular environment of the soft tissue analogs, a transfer technique was utilized to convey gold nanostructures from a solid substrate to PEG-based hydrogels, which is considered to be the platform for investigating *in vitro* cellular responses, such as cell adhesion.[22] Cell adhesion is crucial for the assembly of individual cells into three-dimensional tissues, which are regulated by the extracellular matrix (ECM).[22–24] Many other cell

parameters, such as migration, proliferation and morphogenesis, are initiated by cell adhesion.[25–27] The most commonly used method to control cell adhesion is fabricating functional substrates linked with arginine-glycine-aspartate (RGD) or fibronectin.[28–30] Therefore, PEG-based hydrogels decorated with Au NPs assemblies functionalized with biomolecules, are excellent substitutes of natural ECM with hierarchically organized nanostructures for cell adhesion. SEM and UV-vis spectroscopy confirm that the Au NPs are immobilized on the surface of hydrogels. These materials as substrate are cultured with cells, and the influence of different densities and diameters of Au NPs on fibroblasts adhesion and cytocompatibility has been investigated.

2. Experimental Section

2.1 Materials

Silicon wafers (polished on one side) were obtained from Microchemicals. Isopropanol, acetone, (3-Aminopropyl) triethoxysilane (APTES), ammonia (25 %), hydrogen peroxide (H_2O_2 30%), concentrated sulfuric acid (H_2SO_4 98%) and toluene were purchased from Carl Roth. Acryloyl chloride, sodium hydride (NaH), 2-iminothiolane hydrochloride, vinyl sulfone, DL-Dithiothreitol (DTT) and fluorescein diacetate (FDA) were purchased from Sigma-Aldrich. RPMI 1640, fetal bovine serum (FBS), 1% penicillin/streptomycin and Trypsin-EDTA were purchased from PAA Laboratories GmbH. Propidium iodide (PI ≥94%) and phosphate-buffered saline (PBS) containing K_2HPO_4 and KH_2PO_4 were purchased from Fluka. Ultrapure deionized water was used for all solution preparations. All glassware was cleaned with Aqua Regia (V_{HNO3}:V_{HCl} = 1:3).

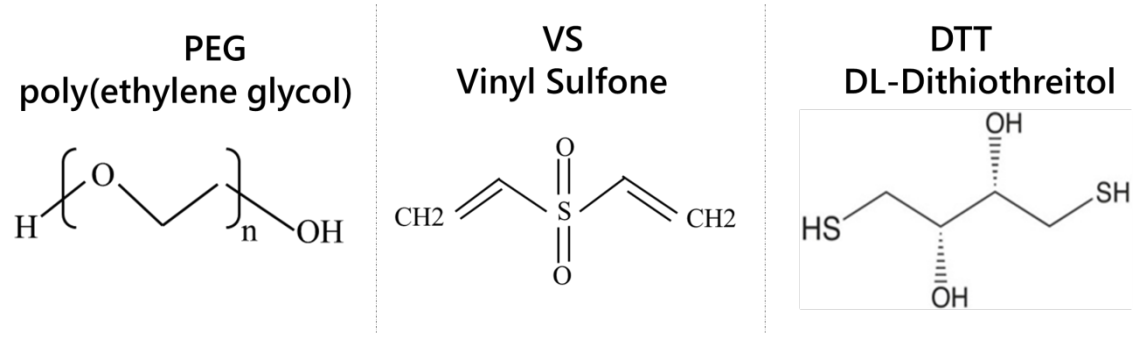

2.2 Apparatus

Silicon wafers (polished on one side) were purchased from Microchemicals. Raman spectra were measured using a confocal Raman spectrometer (LabRam HR 800, Jobin Yvon) coupled to a liquid nitrogen-cooled CCD detector. The spectral resolution was 1 cm^{-1} with an increment per data point of 0.28 and 0.15 cm^{-1} using 512, 597 and 649nm laser excitation line, respectively. The laser power on the sample was 1.0 mW. The laser beam was focused onto the sample by a Nikon 20× objective with a numeric aperture of 0.35. Accumulation times of the SERR spectra were between 1 and 12 s. For SEM observation, the hydrogels were carbon-

coated prior to the measurements, which were performed using an Inlens detector operating at 15.0 KV. UV spectra were recorded on a Cary 4000 by Agilent Technologies spectrophotometer with a 1 cm optical path quartz cuvette. Optical images were obtained using a Carl Zeiss fluorescence microscope (Göttingen Company). For fluorescence microscopy Axio Observer Z1 was used to achieve optical sectioning through the fluorescent sample. Pictures were taken using an AxioCam MRm digital camera and analysed using the Axio Vision V4.8.1 software package (Carl Zeiss, Goettingen, Germany).

2.3 Synthesis of 8arm PEG-vinyl sulfone (8PEG-VS) macromonomers

8arm PEG-vinyl sulfone (8PEG-VS) hydrogel was synthesized by Dr. Zhenfang Zhang of Lensen Lab following the method developed by Lutolf *et al.*[31] PEG-OH (ca. 5 g) was used as received and dissolved directly in 300 mL of anhydrous dichloromethane (previously dried over molecular sieves). To the PEG dissolved in dichloromethane, NaH was added under nitrogen, at a 5-fold molar excess over -OH groups. After hydrogen evolution, divinyl sulfone was added very quickly at 50- to 100-fold molar excess over -OH groups. The reaction was carried out at room temperature for 3 days under nitrogen atmosphere with constant stirring. Afterwards the reaction solution was neutralized with concentrated acetic acid, filtered through paper until clear, and reduced to a small volume (ca. 10 mL) by rotary evaporation. PEG was precipitated by adding the remaining solution dropwise into ice-cold diethyl ether. The polymer was recovered by filtration, washed with diethyl ether, and dried under vacuum. The dried polymer was then dissolved in 200 mL of deionized water containing ca. 5 g of sodium chloride and extracted three times with 200 mL of dichloromethane. This solution was dried with sodium carbonate, and the volume was again reduced by rotary evaporation. Finally, the product was reprecipitated and thoroughly washed with diethyl ether to remove all remaining vinyl sulfone. The final product was dried under vacuum and stored under argon at -20 °C. Derivatization was confirmed with ^{1}H NMR ($CDCl_3$): 3.6 ppm (PEG backbone), 6.1 ppm (d, 1H, $=CH_2$), 6.4 ppm (d, 1H, $=CH_2$), and 6.8 ppm (q, 1H, $-SO_2CH=$). The degree of end group conversion, as shown by NMR, was found to be at least 95%.

2.4 synthesis of 20 nm and 40 nm Au NPs

The different-sized spherical Au NPs were synthesized following the protocol of Bastús *et. al*.[32] First of all, Au NPs seeds were synthesized. In the next step, the seeds were continuously grown to bigger particles; hereby spherical particles from 25 nm to 200 nm were obtained. For the seed synthesis 150 ml of aqueous solution of sodium citrate (2.2 mM) were boiled for 15 min. Then 1 ml of $HAuCl_4$ solution (25 mM) was injected immediately. The color of the solution was changed from yellow to bluish-grey and then finally to soft pink within 10 min. For growing of bigger-sized particles (up to 200 nm) the solution was cooled down to a temperature of 90 °C. Into that solution 1 ml sodium citrate (60 mM) and 1 ml $HAuCl_4$ solution (25 mM) were injected. After 30 min the reaction was completed and again $HAuCl_4$ solution (25 mM) was added. After another 30 min the solution was diluted via taking out 27.7 ml of the Au NPs solution (20 nm) and adding 27.6 ml water. By repeating this process (sequential addition of 1 mL of 60 mM sodium citrate and 1 mL of 25 mM $HAuCl_4$), up to 4 generations of Au NPs were progressively performed. The Au NPs with diameter of 20 nm and 42 nm were obtained.

2.5 Synthesis and characterization of 8PEG-VS-SH hydrogel

Different amounts of ammonium solution (30% NH_3 in H_2O) were added to the precursor solution of 8-arm poly(ethylene glycol) vinyl sulfone (8PEG-VS) with 50% water content at room-temperature under vigorous magnetic stirring until the solution turned to a viscous liquid. Compositions were set in order to receive 20%, 10%, 5% and 2.5 wt% NH_3-8PEG by weight. The resulting liquids were deposited on a glass slide and covered with a glass cover slip. After 30 min, the 8PEG-VS hydrogel were formed. After gel formation, the colorless polymeric films formed with 5% NH_3 were peeled off mechanically. The stand-alone films (250−300 μm in thickness) were handled with tweezers. These hydrogels were immersed in DTT solution (5 mg/mL) for 60 min. Afterwards, these hydrogels were washed thoroughly with water for several times and stored in water before use.

2.6 Preparation of triethoxysilane (APTES) modified silicon wafer by Chemical Vapor Deposition (CVD) method

After ultrasonication in a mixture of acetone and water (V/V = 1:1) for 20 min, the silicon wafers were immersed in Piranha solution (mixture of H_2SO_4 and H_2O_2 with V/V = 7:3) for 30 min. They were thoroughly washed with Milli-Q water and isopropanol, and then dried under a stream of pure nitrogen gas. Afterwards, the as-prepared silicon wafers were placed inside a small Teflon chamber filled with a solution of APTES (100 μL). APTES was then introduced into the sealed chamber as raising the pressure of the deposition chamber. The surface reacted with the gas phase adsorbate for 2 h, then the wafers were washed with anhydrous toluene (3 times), isopropanol immediately and dried with nitrogen followed by evacuation.

2.7 Deposition of Au NPs onto silicon wafers

The concentration of Au NPs was tuned by diluting original dispersion of 20 nm Au NPs 2×, 4×, 8× and 16× with water, and 42 nm Au NPs with 2×, 4×, 8 ×, 16 ×, and 32× of water, respectively. A drop of 100 μL homogeneously dispersed Au NPs was placed on APTES modified silicon wafer. After incubation for 60 min, the silicon wafers were washed thoroughly with deionized water for 8 times and then dried with nitrogen gas. They were kept in a glove box to avoid oxidization before use.

2.8 Transfer of Au NPs in different densities from silicon wafers to hydrogels

The as-prepared 8PEG-VS-SH hydrogels were firmly contacted with the silicon wafers for about 30 s before they were withdrawn from their surface. At last, they were washed gently for 3 times with deionized water in order to remove the residual adsorbent Au NPs. They were kept in water in swollen state for cell culture, and other samples were kept at room temperature for 12 h in dried state before measurements. The Au NPs density (D) on sample is given by:

$$D = N \cdot A_{cs} = N \cdot \pi \cdot r^2$$

where N is the number of Au NPs on 1 μm^2 area of sample, which is counted from 6 randomly selected regions. A_{cs} stands for the maximum cross-sectional area of spherical Au NPs and r is given by the radius of Au NPs which has been estimated by SEM observation.

2.9 Incubation hydrogels with fibroblasts L-929

After spraying ethanol (70 % V/V) on both sides of hydrogels, they were washed carefully by deionized water and waited for drying in the sterile bench. Afterwards, they were put into each 8-well plates with 300 µL of a cell suspension containing 30 000 cells/mL L-929 cells separately and incubated at 37 °C, 5% CO_2 atmosphere and 100% humidity. After following incubation for 24 h, the adhered cells were observed by microscopy. Viability staining of the cells was carried out according to protocol with a LIVE/DEAD® staining kit, cells were washed with Dulbecco's PBS and then stained with 100 µL of a vitality staining solution containing FDA (stock solution 0.5 mg/mL in acetone) and PI (stock solution 0.5 mg/mL in DPBS). Live and dead cells were detected by fluorescence microscope (Carl Zeiss, Goettingen, Germany).

3. Results and Discussion

3.1 8PEG-VS-SH synthesis

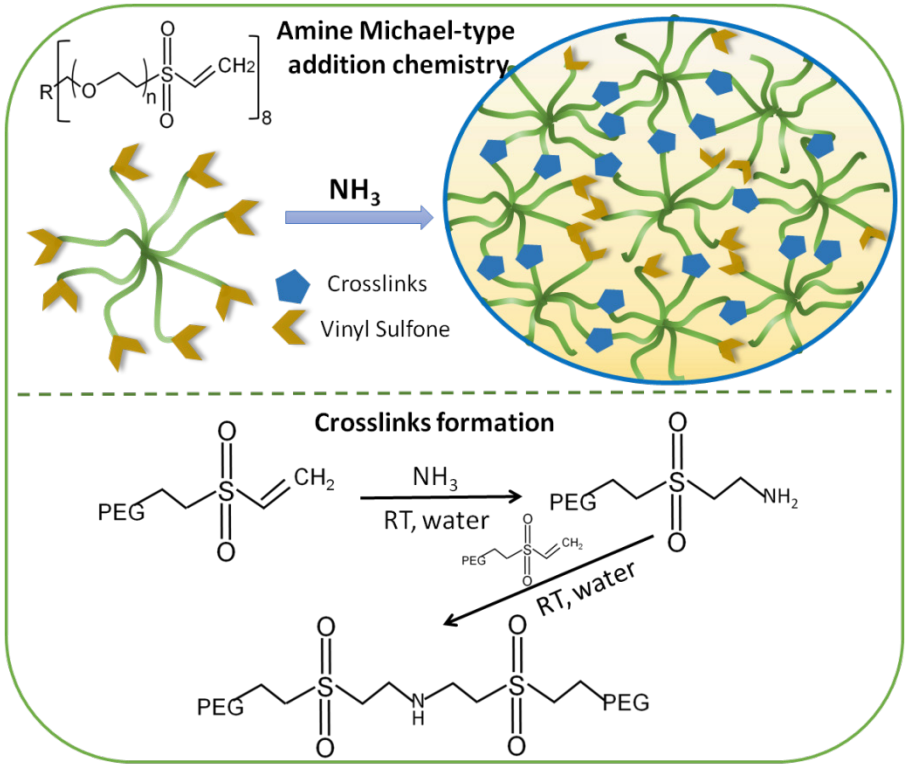

Figure 1: Schematic representation of novel hydrogels prepared through amine Michael-type addition chemistry.

In the present work, PEG hydrogels are used because of the renown bio-inertness and biocompatibility. Novel hydrogels composed of star-shaped PEG molecules (having 8 arms with vinyl sulfone end groups; 8PEG-VS) are readily formed in situ by mixing of two aqueous solutions: 8PEG-VS with 50% water content and an ammonium hydroxide solution (5%, compared with 8PEG-VS) via amine Michael-type addition between vinyl sulfone and amine groups (Figure 1). In this reaction, NH_3 molecule acts as the cross-linker, which at the same time acts as a catalyst because of its very basic nature. The advantage of using NH_3 as cross-linker is the ease to remove its excess after the reaction by evaporation. Moreover, due to the inefficient chemical reactivity of NH_3 with vinyl sulfone in aqueous solution, partial vinyl sulfone groups are left for further functionalization.

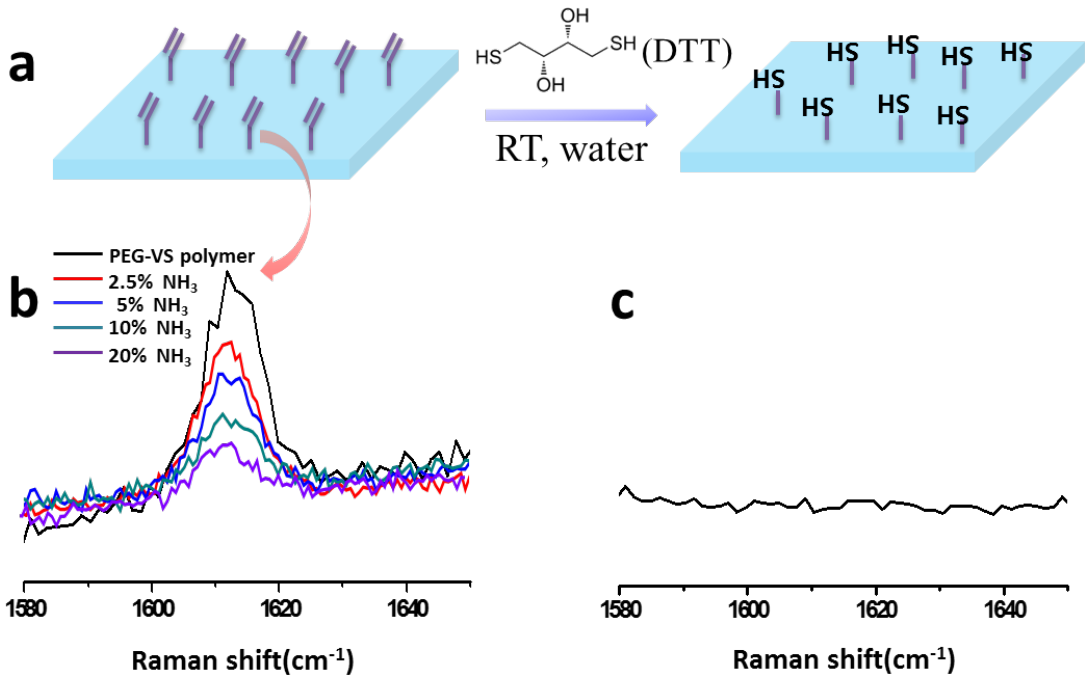

Figure 2: Schematic presentation for the synthesis of 8PEG-VS-SH hydrogel (a), Raman spectra of residual vinyl sulfone groups of 8PEG-VS hydrogels with different amount of NH_3 addition (b) and Raman spectrumof 8PEG-VS-SH hydrogel (c).

The Raman spectra shown in Figure 2b are normalized according to the intensity of the peak at 1480 cm^{-1} that corresponds to the C-O vibrations, because the content of C-O groups in the hydrogels is constant. As can be observed, the intensity of the peak at 1612 cm^{-1}, which is attributed to the C=C vibrations of the unreacted vinyl sulfone groups, decreases with increasing the amount of NH_3. 20% of the unreacted vinyl sulfone groups are left after the formation of hydrogels when 20% of NH_3 is used. After the addition of DTT, the absence of the peak at 1612 cm^{-1} shown in Figure 2c indicates complete consumption of vinyl sulfones due to Michael addition chemistry between thiols and vinyl sulfones. As reported, the two reactants in a 1:1 ratio will result in the complete consumption of vinyl sulfones, implying that thiol groups are more reactive than amine groups.[20] After addition of excess amount of DTT, the peak at 1612 cm^{-1} is absent from the Raman spectrum shown in Figure 2c, implying that the corresponding C=C bonds from the gel have been totally consumed and fully reacted with thiols from DTT, and thereby a novel 8PEG-VS-SH hydrogel has been successfully synthesized.

3.2 Transfer Au NPs from silicon wafers onto PEG-VS-SH hydrogels

The approach of transferring Au NPs from silicon wafers onto PEG-VS-SH hydrogels is schematically depicted in Figure 3. Au NPs deposited on silicon wafer via electrostatic interactions between positively charged amino groups on silicon wafer and negatively charged citrate-stabilized Au NPs. As shown in Figure 3a, amino groups are introduced onto silicon wafer through silanization of APTES via Chemical Vapor Deposition (CVD), which is the most potentially reproducible method for producing high density, homogeneously functionalized silane monolayer on silicon substrate surfaces. Due to electrostatic interactions, Au NPs with the diameters of 20 nm and 42 nm can be homogeneously deposited on silicon wafers, respectively.

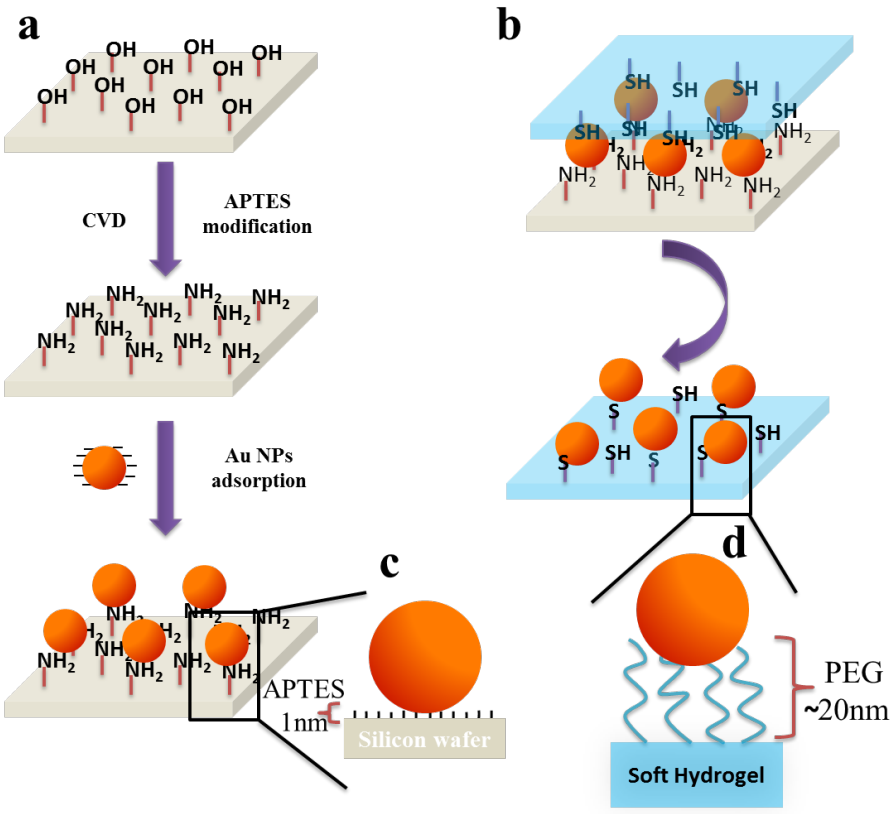

Figure 3: General scheme of transferring Au NPs with different densities from APTES modified silicon wafer to the surface of 8PEG-VS-SH hydrogels.

Next, the structured surface is firmly contacted with thiolated hydrogels (PEG-VS-SH) for 30 s (Figure 3b). The -SH linker molecules that are covalently attached to the Au NPs as well as

the interaction between relatively flexible PEG polymer chains can couple the Au NPs to the hydrated PEG-VS-SH hydrogels. Separation of the hydrogel from the original support (Figure 3b) results in a gel surface decorated with the structures originated from the silicon wafer, in essence transferring the inorganic structures from the silicon wafer to the hydrogel support.

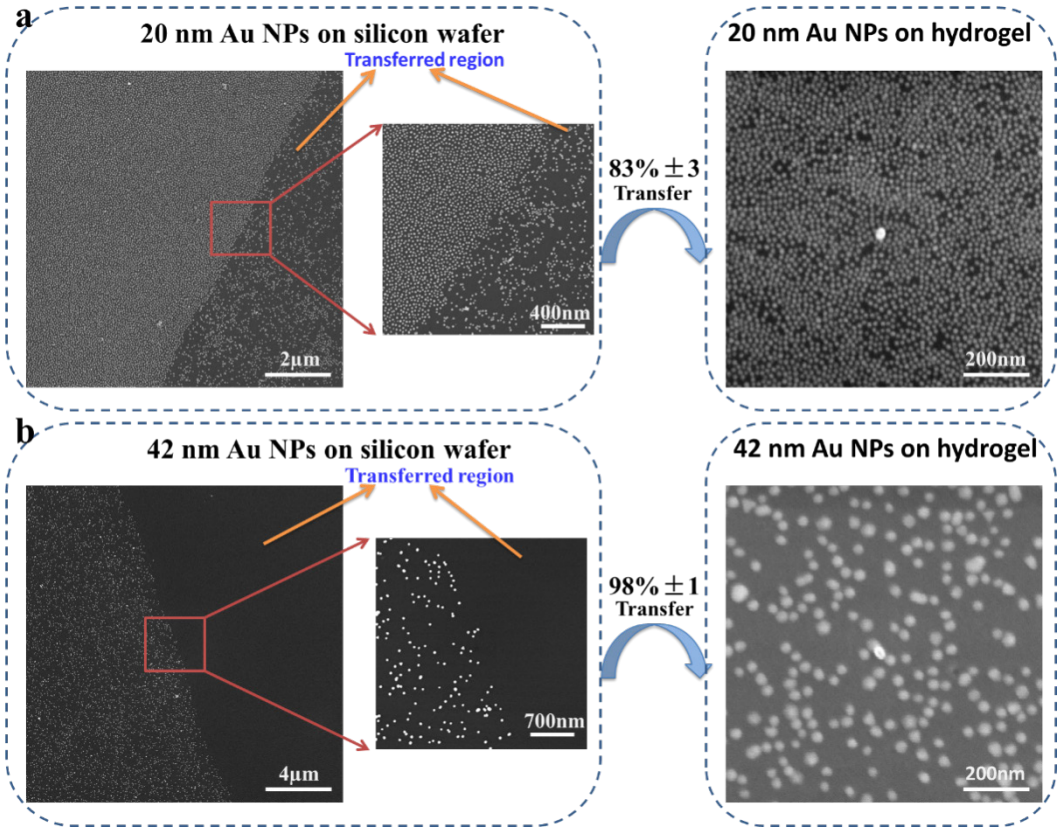

Figure 4: SEM images of Au NPs transferred from the surface of silicon wafers onto hydrogels. (a) 20 nm Au NPs, (b) 42 nm Au NPs.

In order to investigate the transfer efficiency of our novel method, SEM is utilized to characterize and count Au NPs on the silicon before and after transferring. Please note that the area of hydrogel in SEM images is actually more than 4 times larger than the silicon wafer, since they are in dried state during SEM measurements, therefore there are many more Au NPs on surface of hydrogel than on the silicon wafer under the same view with same magnification. In Figure 4b, 42 nm Au NPs can hardly be observed on the silicon wafer, indicating that the vast majority of Au NPs, up to 98%, have been transferred from silicon wafer to hydrogel through Au-S covalent bond by the nano-contact transfer method. In comparison, the transfer efficiency of Au NPs with diameter of 20 nm from silicon to hydrogel

can reach 83% (Figure 4a), implying that the smaller Au NPs cannot fully contact with hydrated hydrogels during the transferring process, possibly because of less contact areas.

3.3 Characterization of different density of Au NPs on hydrogels

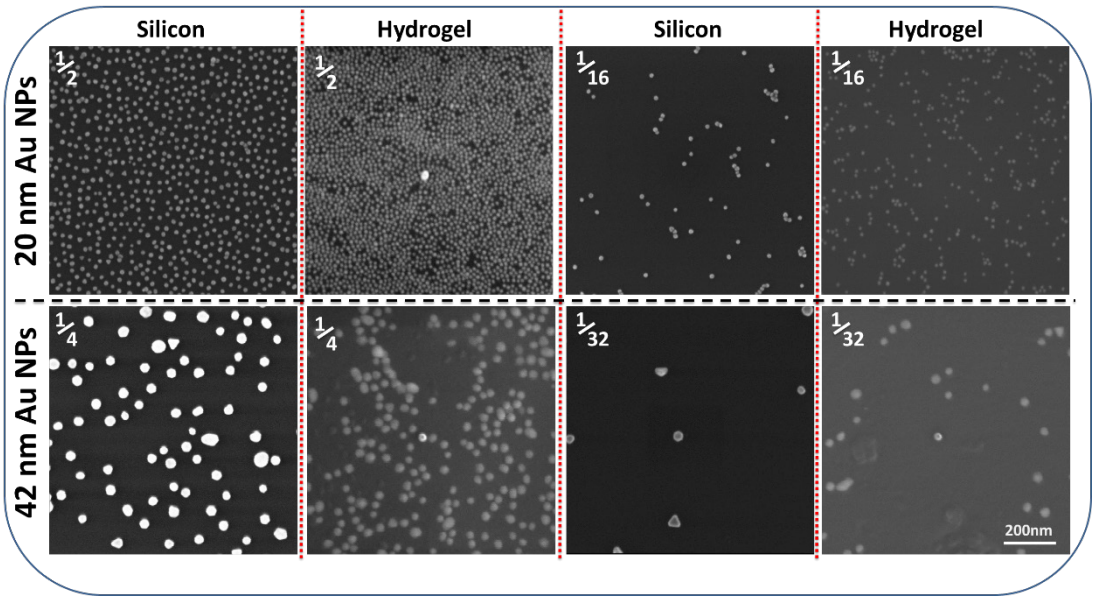

Figure 5: Representative SEM images of Au NPs deposited onto APTES modified silicon wafers and thiolated hydrogels (same scale in all images). 1/2, 1/4, 1/16 and 1/21 stand for the concentration of Au NPs.

Due to the high transferring efficiency and strongly covalent Au-S bonds, Au NPs with different densities on 8PEG-VS-SH hydrogels can be obtained. Firstly, Au NPs in suspension with different concentration are deposited on APTES modified silicon wafer, leading to Au NPs with different densities adsorbed on silicon as shown in Figure 5 and 6. After transfer lithography, Au NPs with different densities are immobilized onto PEG-VS-SH hydrogels. Samples obtained from different diluted Au NP solutions are denoted as 1/2, 1/4, 1/8, 1/16 and 1/32 of the concentration of 20 nm or 42 nm Au NPs on silicon or gel. The densities (number/μm^2) of Au NPs are shown in Figure 6. As the concentration of Au NPs deposited on silicon increases, the corresponding density of Au NPs on silicon and hydrogels increases accordingly.

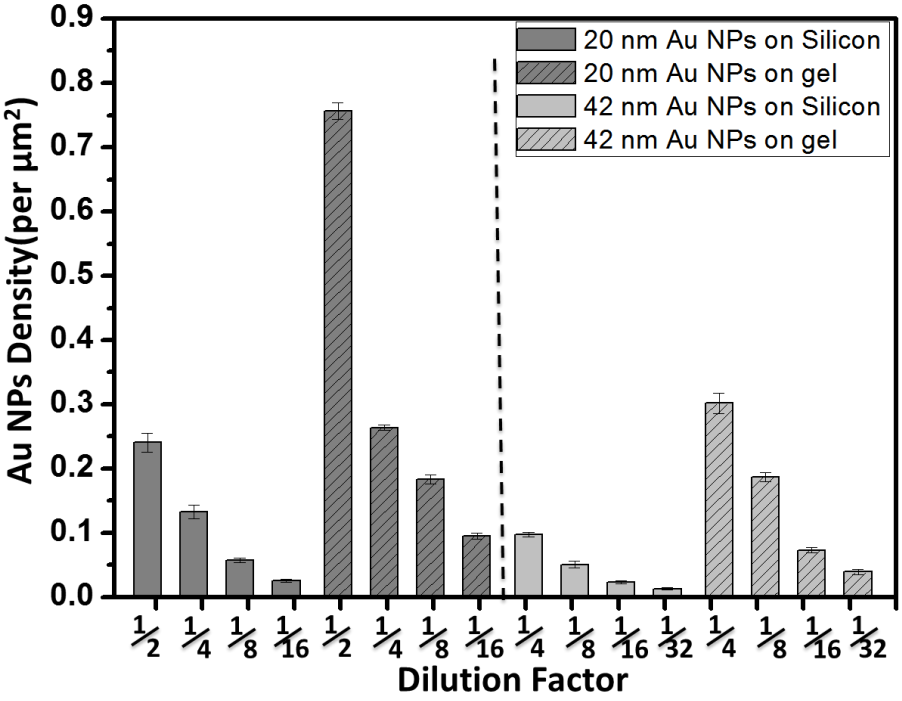

Figure 6: Quantitative results of 20 nm and 42 nm Au NPs deposited onto APTES modified silicon wafers and thiolated hydrogels.

In order to distinguish the optical difference between various densities of Au NPs on the surface of 8PEG-VS-SH hydrogels, UV-vis spectroscopy has been used to characterize hydrogels with different densities of Au NPs. In Figure 7a from top to bottom, the concentration of Au NPs is 1 C, 1/2 C, 1/4 C and 1/8 C, respectively. As the density of Au NPs deposited on the hydrogels decreases, the intensity of the peak for Au NPs correspondingly decreases as well. In addition, the SPR peaks of Au NPs on hydrogels are blue-shifted, due to the enlarged inter-particle distance, leading to degeneration of plasmon coupling between the neighboring Au NPs.

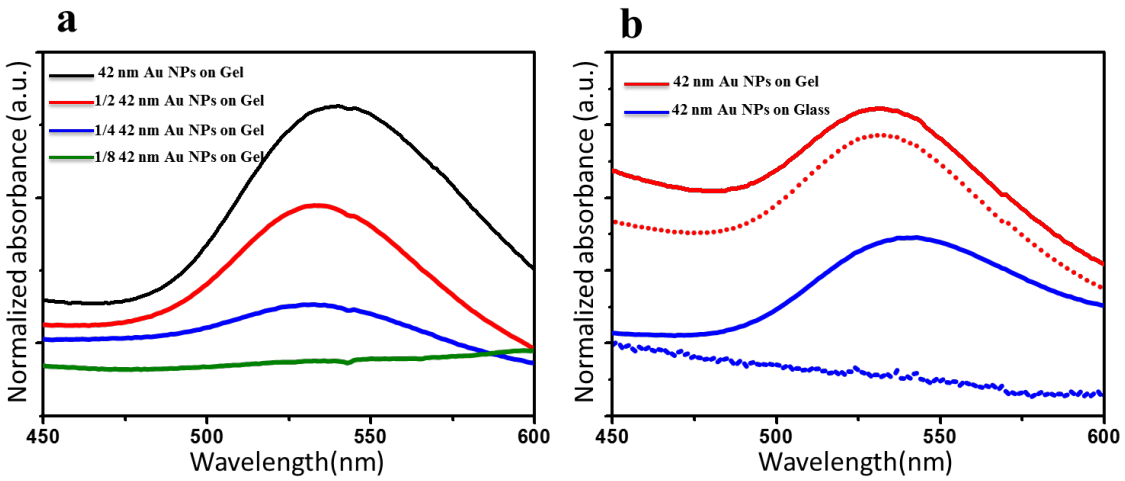

Figure 7: (a) UV-vis spectra of different density of 42 nm Au NPs on the surface of 8PEG-VS-SH hydrogels. (b) UV-vis spectra of 42 nm Au NPs on hydrogels (red lines) and glass (blue lines) (solid lines represent Au NPs on the substrate before sonication, dotted lines represent Au NPs on the substrate after sonication treatment for 5 min).

After Au NPs are transferred onto hydrogels, UV-Vis spectroscopy is utilized to characterize the stability of Au NPs binding with the hydrogels. Due to the transparency of glass, Au NPs modified on glass prepared by the same procedure is used for UV-vis absorption test. In Figure 7(b), solid lines stand for the immobilized Au NPs on hydrogel (red line) and glass (blue line), and dotted lines stand for the corresponding samples after sonication treatment for 5 min. After the hydrogels are ultrasonicated for 5 min, the same characteristic peaks at ~535 nm can be observed from UV-vis spectra, indicating Au NPs are still bound on the surface of hydrogels. In comparison, the characteristic peak is absent in the spectra of glass with Au NPs after ultrasonication for 5 min, which means Au NPs are detached from the glass. The results reveal that the attachment of Au NPs to the PEG-VS-SH hydrogel is strong and stable. This substrate for immobilizing Au NPs is very useful in our further experiments when incubated with L-929 cells in aqueous solution.

3.4 Cells adhesion and spreading on hydrogels

It is well-known that the surface of gold may bind to cell adhesion controlling proteins and thus facilitate the adhesion of cells.[27] Au NPs with two different diameters of 20 nm and 42 nm with a series of densities on the 8PEG-VS-SH hydrogel have been prepared to investigate

L-929 cell adhesion. The representative bright-field micrographs shown in Figure 8 reveal that L-929 cells adhere to and spread on Au NPs/PEG-VS-SH hydrogels after incubation for 24 h.

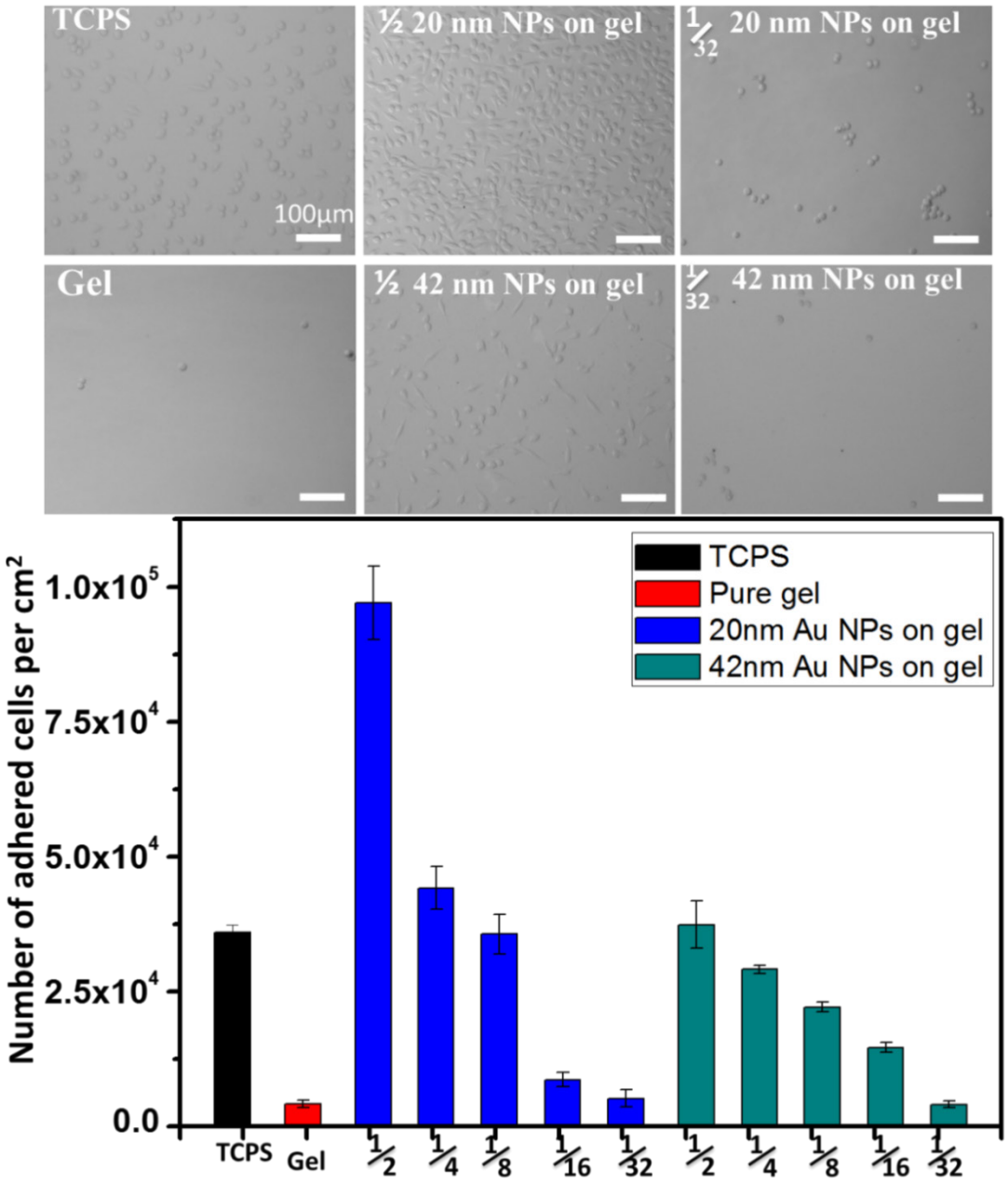

Figure 8: Optical images of L-929 cells and number of L-929 cells on the surface of TCPS, pure hydrogel and Au NPs/PEG-VS-SH hydrogels.

Based on the properties of anti-adhesive PEG-VS-SH hydrogel as well as the Au NPs without any specific functionalization, cell adhesion can hardly be expected on the as-synthesized composite hydrogels. However, remarkable cell adhesion can be observed on these hydrogels from Figure 8. The cells are spindle-shaped when cultured with high density of Au NPs, while

they are round-shaped when cultured with low density of Au NPs. The overall number of cells adhered to the substrate decreases with the decrease of the densities of Au NPs immobilized on the surface of hydrogel. The number of adhered cells on Au NPs composite hydrogels (d_{Au} = 20 nm, concentration of 1/2 Au NPs) is two times more than that on the TCPS. In addition, the cells can proliferate on the hydrogels with high density of Au NPs compared to the control on TCPS during the cultivation.

We consider a number of possible explanations for such remarkable cell adhesion on Au NPs composite hydrogels (8PEG-VS-SH):

(1) The surface hydrophilicity has been found to be an important factor for cell adhesion. For instance, Dowling *et al.* concluded that cell adhesion decreased with an increase in hydrophobicity of the fluorinated PS surfaces, and optimum cell adhesion was observed at the water contact angle of 64°.[33] The water contact angle for 8PEG hydrogels is 48 ± 6°. After incorporation of Au NPs onto the surface of hydrogels may result in an increase in the water contact angle, thereby favoring the cell adhesion.

(2) It is well known that the variation of the stiffness properties and surface roughness correlate with the changes in the cell adhesion.[34] Fibroblasts prefer to adhere on the surface with increased stiffness and larger roughness. After incorporation of Au NPs onto the surface of hydrogels, an increase in the stiffness and roughness of composite hydrogels may induce cell adhesion, whereas the TCPS substrates exhibit a very smooth surface.

(3) Cell adhesion is also influenced by surface topographies in the micrometer and nanometer range.[35] As reported, cells can align along microgrooves or similar topographical features on a surface. Arnold *et al.* investigated the cells adhesion on the Au-nanodot-patterned interfaces with different spacing distance, and found that local dot–dot separation is critical for inducing cell adhesion and focal adhesion assembly. Separation of ≤ 58 nm between the dots allows effective adhesion.[36] By measuring the distance between the Au NPs from SEM image shown in Figure 5, the inter-Au NPs distances on the as-synthesized composite hydrogels are

determined to be around 40 nm. Thus, this is an appropriate length scale for effective cell adhesion, which is in good agreement with literature report.[36]

(4) Besides the aforementioned factors, another physical parameter which can influence cell adhesion is the surface elasticity. Most cells are in close contact to a much softer surface in vivo conditions in comparison with standard in vitro substrates. And PEG hydrogels with an elastic modulus of 0.27 ± 0.05 Mpa is significantly softer than TCPS (E > 1 GPa).[37] Thus, the possible discrepancies in cell adhesion might be more likely caused by differences in other factors rather than the substrate elasticity.

However, more experiments need to be performed in future to prove our hypotheses. For instance, the surface wettability, stiffness, roughness and topographies of the nanocomposite hydrogels need to be investigated in future.

In general, these factors in combination might result in an environment, where proteins from the medium can accumulate and accommodate themselves on or between the nanoparticles, slightly be embedded in the soft surface of PEG chains. Thus, we propose that protein adsorption is enabled and this in turn results in the observed cell adhesion. In order to verify this, protein adsorption must be quantified. Finally, the remaining -SH groups on the functional gels might interact chemically with proteins, or even bind them covalently.

3.5. Cytocompatibility of Au NPs/PEG-VS-SH hydrogels

Figure 9 shows the representative fluorescent images of Live/dead staining assays of L-929 cells after cultured Au NPs/PEG-VS-SH hydrogels with different densities of Au NPs. In Live/dead staining assay, dead cells appear red, whereas living cells appear green when observed with a fluorescence microscope. Red dead cells can hardly be observed on any of the hydrogels, demonstrating that no cytotoxicity to L-929 cells originates from 8PEG-VS-SH hydrogels with either high or low density Au NPs on the surface. Thus, these cyto-compatible hydrogels are very promising for tissue engineering.

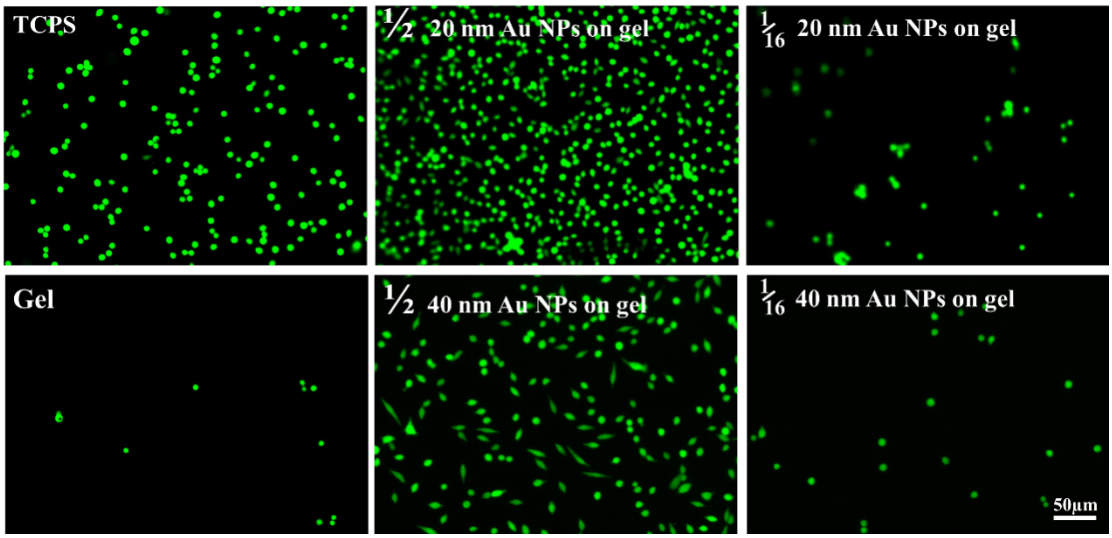

Figure 9. Live-dead assay indicating viable (green) and dead (red) L-929 cells on TCPS, pure PEG-VS-SH hydrogels and Au NPs/PEG-VS-SH hydrogels after 24 h of incubation. (same scale in all images)

4. Conclusion

In this study, novel 8PEG-VS-SH hydrogels have been synthesized and further functionalized by amine Michael-type addition reactions – first with ammonia and then with DTT – to yield hydrogels with high affinity for gold. Furthermore, Au NPs with different densities have been transferred from silicon wafers to the surface of hydrogels with a transfer efficiency of up to 98% through the strong Au-S bond between Au NPs and hydrogels. The stability of the Au NPs on the hydrogels has been proved by UV-vis spectroscopy after sonication treatment for 5 min; the Au NPs still remain on the surface of hydrogels. More importantly, nanocomposite PEG-VS-SH hydrogels offer a substrate to control the cell adhesion and spreading of fibroblast L-929 cells. The results implied that Au NPs played an important role in cell adhesion, with more Au NPs on hydrogels, inducing more cell adhesion. Therefore, Au NPs could act as a controllable substance in tissue engineering and biomedical applications.

5. References

(1) Xu, H.; Hong, R.; Lu, T.; Uzun, O.; Rotello, V. M. Recognition-Directed Orthogonal Self-Assembly of Polymers and Nanoparticles on Patterned Surfaces. *J. Am. Chem. Soc.* **2006**, *128* (10), 3162–3163.

(2) Park, H.-Y.; Schadt, M. J.; Wang, L.; Lim, I.-I. S.; Njoki, P. N.; Kim, S. H.; Jang, M.-Y.; Luo, J.; Zhong, C.-J. Fabrication of Magnetic Core@shell Fe oxide@Au Nanoparticles for Interfacial Bioactivity and Bio-Separation. *Langmuir* **2007**, *23* (17), 9050–9056.

(3) Nurgaziyeva, E. K.; Tatykhanova, G. S.; Mun, G. A.; Khutoryanskiy, V. V; Kudaibergenov, S. E. Catalytic Properties of Gel-Immobilized Gold Nanoparticles in Decomposition of Hydrogen Peroxide. *Proc. Int. Conf.* **2015**, *4* (2), 1–4.

(4) Niazov, T.; Pavlov, V.; Xiao, Y.; Gill, R.; Willner, I. DNAzyme-Functionalized Au Nanoparticles for the Amplified Detection of DNA or Telomerase Activity. *Nano Lett.* **2004**, *4* (9), 1683–1687.

(5) Baeissa, A.; Moghimi, N.; Liu, J. Hydrogel Porosity Controlling DNA-Directed Immobilization of Gold Nanoparticles Revealed by DNA Melting and Scanning Helium Ion Microscopy. *RSC Adv.* **2012**, *2* (7), 2981.

(6) Dam, D. H. M.; Lee, H.; Lee, R. C.; Kim, K. H.; Kelleher, N. L.; Odom, T. W. Tunable Loading of Oligonucleotides with Secondary Structure on Gold Nanoparticles through a pH-Driven Method. *Bioconjug. Chem.* **2015**, *26* (2), 279–285.

(7) Hu, M.; Chen, J.; Li, Z.-Y.; Au, L.; Hartland, G. V; Li, X.; Marquez, M.; Xia, Y. Gold Nanostructures: Engineering Their Plasmonic Properties for Biomedical Applications. *Chem. Soc. Rev.* **2006**, *35* (11), 1084–1094.

(8) Pardo-Yissar, V.; Gabai, R.; Shipway, A. N.; Bourenko, T.; Willner, I. Gold Nanoparticle/hydrogel Composites with Solvent-Switchable Electronic Properties. *Adv. Mater.* **2001**, *13* (17), 1320–1323.

(9) Su, Jing，He, Xiaoxiao，Wang, Yonghong，Wang, K.; Chen, Z.; Yan, G. A Sensitive Signal-on Assay for MTase Activity Based on Methylation-Responsive Hairpin-Capture DNA Probe. *Biosens. Bioelectron.* **2012**, *36* (1), 123–128.

(10) Kumar, P.; Choithani, J.; Gupta, K. C. Construction of Oligonucleotide Arrays on a Glass Surface Using a Heterobifunctional Reagent, Triethoxysilylpropyl-3-Amine (NTMTA). *Nucleic Acids Res.* **2004**, *32* (10), 9.

(11) Tang, L.; Wang, Y.; Liu, Y.; Li, J. DNA-Directed Self-Assembly of Graphene Oxide with Applications to Ultrasensitive Oligonucleotide Assay. *ACS Nano* **2011**, *5* (5), 3817–3822.

(12) Glass, B. R.; Arnold, M.; Spatz, J. P. Micro-Nanostructured Interfaces Fabricated by the Use of Inorganic Block Copolymer Micellar Monolayers as Negative Resist for Electron-Beam Lithography. *Adv. Drug Deliv. Rev.* **2003**, *13* (7), 569–575.

(13) Kim, S.; Chu, C. Synthesis and Characterization of Dextran–Methacrylate Hydrogels and Structural Study by SEM. *J. Biomed. Mater. Res.* **2000**, *49* (4) 517–527.

(14) Cruise, G. M.; Scharp, D. S.; Hubbell, J. A. Characterization of Permeability and Network Structure of Interfacially Photopolymerized Poly (Ethylene Glycol) Diacrylate Hydrogels. *Biomaterials* **1998**, *19*, 1287–1294.

(15) Huang, J.; Grater, S. V; Corbellini, F.; Rinck, S.; Bock, E.; Kemkemer, R.; Kessler, H.; Ding, J.; Spatz, J. P. Impact of Order and Disorder in RGD Nanopatterns on Cell Adhesion. *Nano Lett.* **2009**, *9* (3), 1111–1116.

(16) Graeter, S. V.; Ding, J.; Spatz, J. P. Mimicking Cellular Environments by Nanostructured Soft Interfaces. *Nano Lett.* **2007**, *7* (5), 1413–1418.

(17) Phelps, E. a.; Enemchukwu, N. O.; Fiore, V. F.; Sy, J. C.; Murthy, N.; Sulchek, T. a.; Barker, T. H.; García, A. J. Maleimide Cross-Linked Bioactive PEG Hydrogel Exhibits Improved Reaction Kinetics and Cross-Linking for Cell Encapsulation and In Situ Delivery. *Adv. Mater.* **2012**, *24* (1), 64–70.

(18) Seliktar, D. Designing Cell-Compatible Hydrogels for Biomedical Applications. *Science* **2012**, *336*, 13–17.

(19) Vernon, B.; Tirelli, N.; Ba, T.; Haldimann, D.; Hubbell, J. A.; Al, V. E. T. Water-Borne , in Situ Crosslinked Biomaterials from Phase-Segregated Precursors. *J. Biomed. Mater. Res. - Part A* **2002**, *13* (1), 448–458.

(20) Missirlis, D.; Spatz, J. P. Combined E Ff Ects of PEG Hydrogel Elasticity and Cell-Adhesive Coating on Fibroblast Adhesion and Persistent Migration. *Biomacromolecules* **2014**, *15* (1), 195–205.

(21) Zhang, Z.; Loebus, A.; de Vicente, G.; Ren, F.; Arafeh, M.; Ouyang, Z.; Lensen, M. C. Synthesis of Poly(ethylene Glycol)-Based Hydrogels via Amine-Michael Type Addition with Tunable Stiffness and Postgelation Chemical Functionality. *Chem. Mater* **2014**, *26*, 3624–3630.

(22) Tang, J.; Peng, R.; Ding, J. Biomaterials The Regulation of Stem Cell Differentiation by Cell-Cell Contact on Micropatterned Material Surfaces. *Biomaterials* **2010**, *31* (9), 2470–2476.

(23) Gumbiner, B. M. Cell Adhesion: The Molecular Basis of Tissue Architecture and Morphogenesis. *Cell* **1996**, *84* (3), 345–357.

(24) Stevens, M. M.; George, J. H. Exploring and Engineering the Cell Surface Interface. *Science* **2005**, *310* (5751), 1135–1138.

(25) Kyung, M.; Rich, M. H.; Lee, J.; Kong, H. A Bio-Inspired , Microchanneled Hydrogel with Controlled Spacing of Cell Adhesion Ligands Regulates 3D Spatial Organization of Cells and Tissue. *Biomaterials* **2015**, *58*, 26–34.

(26) Engler, A. J.; Sen, S.; Sweeney, H. L.; Discher, D. E. Matrix Elasticity Directs Stem Cell Lineage Specification. *Cell* **2006**, *126* (4), 677–689.

(27) Deeg, Janosch A ; Louban, I.; Aydin, D.; Selhuber-unkel, C.; Kessler, H.; Spatz, J. P. Impact

of Local versus Global Ligand Density on Cellular Adhesion. *Nano Lett.* **2011**, *11*, 1469–1476.

(28) Wang, X. Li, S.; Yan, C.; Liu, P.; Ding, J. Fabrication of RGD Micro/Nanopattern and Corresponding Study of Stem Cell Differentiation. *Nano Lett.* **2015**, *15*, 1475–1467.

(29) Massia, S. P.; Stark, J. Immobilized RGD Peptides on Surface-Grafted Dextran Promote Biospecific Cell Attachment. *J. Biomed. Mater. Res.* **2001**, *56* (3), 390–399.

(30) Cavalcanti-Adam, E. A.; Spatz, J. P. Receptor Clustering Control and Associated Force Sensing by Surface Patterning : When Force Matters. *Nanomedici* **2015**, *10* (5), 681–684.

(31) Lutolf, M. P.; Lauer-Fields, J. L.; Schmoekel, H. G.; Metters, a T.; Weber, F. E.; Fields, G. B.; Hubbell, J. a. Synthetic Matrix Metalloproteinase-Sensitive Hydrogels for the Conduction of Tissue Regeneration: Engineering Cell-Invasion Characteristics. *Proc. Natl. Acad. Sci. U. S. A.* **2003**, *100* (9), 5413–5418.

(32) Bast, N. G.; Comenge, J.; Puntes, V. Kinetically Controlled Seeded Growth Synthesis of Citrate-Stabilized Gold Nanoparticles of up to 200 Nm : Size Focusing versus Ostwald Ripening. *Langmuir* **2011**, *27*, 11098–11105.

(33) Dowling, D. P.; Miller, I. S.; Ardhaoui, M.; Gallagher, W. M. Effect of Surface Wettability and Topography on the Adhesion of Osteosarcoma Cells on Plasma-Modified Polystyrene. *J. Biomater. Appl.* **2011**, *26* (3), 327–347.

(34) Ye, K.; Wang, X.; Cao, L.; Li, S.; Li, Z.; Yu, L.; Ding, J. Matrix Stiffness and Nanoscale Spatial Organization of Cell-Adhesive Ligands Direct Stem Cell Fate. *Nano Lett.* **2015**, *15* (7), 4720–4729.

(35) Norman, J. J.; Desai, T. A. Methods for Fabrication of Nanoscale Topography for Tissue Engineering Scaffolds. *Ann. Biomed. Eng.* **2006**, *34* (1), 89–101.

(36) Arnold, M.; Spatz, J. P. Activation of Integrin Function by Nanopatterned Adhesive Interfaces. *ChemPhysChem* **2004**, *5*, 383–388.

(37) Miyamoto, S.; Teramoto, H.; Coso, O. a; Gutkind, J. S.; Burbelo, P. D.; Akiyama, S. K.; Yamada, K. M. Integrin Function : Molecular Hierarchies of. *J. Cell Biol.* **1995**, *131* (3), 791–805.

Chapter 6

Surface Patterning of Au NPs on 8PEG-VS-SH Hydrogel Surface to Control Cell Adhesion

Abstract

In this work, we develop an approach to micro-pattern gold nanoparticles (Au NPs) on 8-arm poly(ethylene glycol)-vinyl sulfone thiol (**8PEG-VS-SH**) hydrogels, and these patterned Au NPs stripes have been applied in controlling cell adhesion. Firstly, the Au NPs were patterned on silicon wafers, and then transferred onto 8PEG-VS-SH hydrogels. The patterned, micrometer-sized Au NPs stripes with different spacing distances (20 μm and 50 μm, respectively) were created by a micro-contact deprinting method. After transferring these micro-patterns Au NPs stripes onto 8PEG-VS-SH hydrogels, they have been used for cell adhesion of the murine fibroblasts L-929. The cells can adhere to and spread on those patterned stripes in an ordered way.

1. Introduction

In recent decades, due to the unique electronic and photonic properties as well as easy functionalization, gold nanoparticles (Au NPs) have been utilized in physical[1,2] and biomedical fields.[3,4] With the increasing development of nanotechnology, the ability to generate patterns of Au NPs on substrate is important for biosensor,[5] optics,[6] catalysis,[7] and biomaterial applications.[8]

To control cell behavior by designing the appropriate environment is very important to understand biological systems.[9] Control of cell adhesion is crucial for tissue engineering and fundamental studies in cell biology like cell–cell, cell–substrate and cell–medium interactions.[10] Biomaterials modified by cell recognition motives (*e.g.* fibronectin protein) are used to control the interaction between cells and synthetic substrates. Besides biochemical functionalization, cell behavior can be influenced by the stiffness, nanoscale topography and microscopic surface patterning of the substrate.[11,12,13] For example, Ding *et al.* showed that micropatterns of peptide via micropatterned Au NPs enable cell localization on the background of poly(ethylene glycol) (PEG) hydrogels.[14] It is highly interesting to assemble nanoparticles to create desired regions for cell adhesion.[10,15]

As research continues, many methods to pattern nanoparticles have been successfully developed. All these methods can be generally categorized as “top-down” and “bottom-up” methods. However, some of them are time consuming and require expensive devices, and the obtained patterns consist of unordered, agglomerated, or densely compacted Au NPs.[16]

Most efforts in cell micropatterning have focused on microfabrication techniques that are based on silicon or glass substrates, which limit applications to tissue engineering. PEG hydrogels, which possess an inert and protein-repellent surface have demonstrated to be especially useful as a background platform for the *in vitro* investigation of cell behavior, when applied in biosensor systems and tissue engineering.[17,18] In this chapter, we report a novel technique to pattern regularly arranged Au NPs on silicon wafers, and the Au NPs patterns can be transferred to the 8PEG-VS-SH hydrogel by a “micro-contact deprinting method”. These

micro-patterned Au NPs composite hydrogels enable us to control cell adhesion of murine fibroblasts L-929 in an ordered way following the patterned Au NPs stripes.

2. Experimental Section

2.1 Materials

Isopropanol, acetone, (3-aminopropyl) triethoxysilane (APTES), ammonia (25%), hydrogen peroxide (H_2O_2 30%), concentrated sulfuric acid (H_2SO_4 98%) and toluene were purchased from Carl Roth. PEG-PPG-PEG (block polymer), acryloyl chloride, 2-iminothiolane hydrochloride, vinyl sulfone, DL-dithiothreitol (DTT) and fluorescein diacetate (FDA) were purchased from Sigma-Aldrich. RPMI 1640, fetal bovine serum (FBS), 1% penicillin/streptomycin and Trypsin-EDTA were purchased from PAA Laboratories GmbH. Propidium iodide (PI ≥ 94%) and phosphate buffer saline (PBS) containing K_2HPO_4 and KH_2PO_4 were purchased from Fluka. 8-arm PEG with a molecular weight of 15 KDa was purchased from Jenkem technology USA. Silicon wafers (polished on one side) were obtained from Microchemicals, and silicon masters were purchased from Amo GmbH (Aachen). Ultrapure deionized water was used for all solution preparation. All glassware was cleaned with Aqua Regia (V_{HNO3}:V_{HCl} = 1:3).

All chemicals used as received unless stated otherwise. Solvents were of at least analytical grade quality. Ultrapure deionized water was used for all solution preparation.

2.2 Apparatus

Silicon masters were made by Amo GmbH in special sizes. The UV lamp (λ = 366 nm, Vilber Lourmat GmbH) was used for UV curing. SEM measurements were performed on DSM 982 offered by ZEISS Company, the optical parts of the microscope from Gemini Optics. The hydrogels were carbon coated prior to measurements, which were performed using an Inlens detector operated at 20 KV. Optical images were obtained using a Carl Zeiss fluorescent microscope (Göttingen Company). Fluorescence microscopy Axio Observer Z1 was used to achieve optical sectioning through the fluorescent sample. Images were taken using an AxioCam MRm digital camera and analyzed using the Axio Vision V4.8.1 software package (Carl Zeiss, Göttingen, Germany).

2.3 Synthesis of 8PEG-VS-SH hydrogel

8PEG-VS-SH hydrogel was successfully synthesized, and the synthesis process has been introduced in Chapter 5, section 2.5.

2.4 Fabrication of micro-patterned block polymer hydrogel replicas

PEG-PPG-PEG (block polymer, 4400Da, Sigma–Aldrich) replica with micropatterns of lines were prepared by replication from silicon masters (width × distance × height = 20 × 10 × 5, 50 × 10 × 5 μm) as shown in Figure 1, which comprise patterned stripes constructed into microscale lines. Silicon wafers were rinsed with acetone, water, and isopropanol and dried under a mild stream of nitrogen before use. Prior to the replication the cleaned silicon masters were fluorinated with trichloro (1*H*, 1*H*, 2*H*, 2*H*-perfluorooctyl) silane 97% (Sigma-Aldrich). The viscous liquid of block polymer was dispensed on the silicon master (Figure 1), covered with a thin glass coverslip and exposed to UV light (λ = 366 nm Vilber Lourmat GmbH) for 15 min using a working distance of 10 cm, in a nitrogen-filled glovebox. After formation of polymeric film, it was mechanically peeled off from silicon master by tweezers.

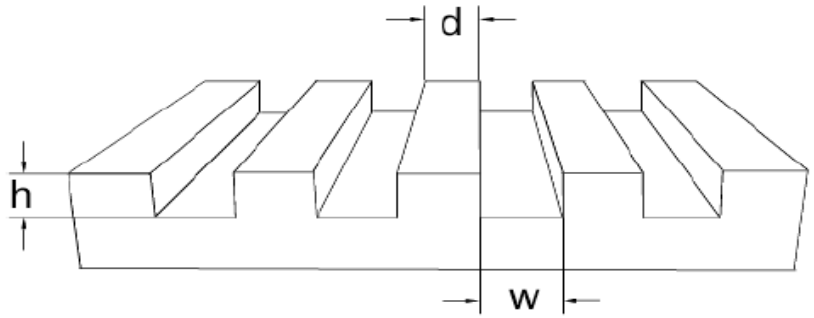

Figure 1: Schematic of a patterned silicon master.

2.5 Transfer the patterned Au NPs from silicon wafer to 8PEG-VS-SH hydrogels

After ultrasonication in a mixture of acetone and water (V/V = 1:1) for 20 min, the silicon wafers were immersed in Piranha solution (mixture of H_2SO_4 and H_2O_2 with V/V = 7:3) for

30 min. They were washed thoroughly with Milli-Q water and isopropanol, and then dried under a stream of pure nitrogen gas. Afterwards, the as-prepared silicon wafers were placed inside a small Teflon chamber filled with a solution of APTES (100 μL). APTES was then introduced into the sealed chamber with raising the pressure of the deposition chamber.[19] After 2 hours of reaction, the silicon wafers were washed with anhydrous toluene (×3) and isopropanol (×1), and immediately dried with nitrogen followed by evacuation. Then, deposition of Au NPs onto silicon wafers was carried out as the procedure described in details in Chapter 5, section 2.7.

The patterned block polymer stamp was contacted with the Au NPs on silicon wafers for about 60 s, and then withdrawn carefully to create Au NPs patterns on silicon wafers. Subsequently, 8PEG-VS-SH hydrogel was placed to contact with the silicon wafers with patterned Au NPs for 30 s. Afterwards, it was peeled off carefully and immediately, and then put into a petri dish. The hydrogel was washed for 3 times with deionized water in order to remove the non-adsorbing Au NPs. The final samples were kept in water in swollen state for cell culture, and other samples were kept at room temperature for 12 h in dried state for SEM measurements.

2.6 Cell culture

Murine fibroblasts L-929 were kindly provided by Dr. J. Lehmann (Fraunhofer Institute for Cell Therapy and Immunology IZI, Leipzig). L-929 cells were cultured in 75 cm^2 cell culture flasks containing RPMI 1640 supplemented with 10% fetal bovine serum (FBS) and 1% penicillin/streptomycin (PS, 100×, all PAA Laboratories GmbH) at 37 °C and 5% CO_2 in a humidified incubator. The cells were grown until confluence, washed with Dulbecco's phosphate buffered saline solution and treated with Trypsin-EDTA (PAA Laboratories GmbH). After incubation for 2-5 min at 37°C, the detached cells were suspended in cell culture medium. The cell suspension was transferred into a falcon tube (VWR International GmbH) and centrifuged for 3 min at 1300 rpm, 4 °C. Finally, the cell pellet was resuspended in fresh medium and cells were counted using a hemocytometer (Paul Marienfeld GmbH & Co. KG). Cell culture medium was refreshed every second day. The cells were taken out from incubator at 3 h, 24 or 96 h for taking images in microscopy.

2.7 Incubation with L-929 cells

After spraying ethanol (70 % V/V) on both sides of hydrogels, they were washed carefully by deionized water and waited for drying in the sterile bench. Afterwards, they were put into each 8-well plates with 300 μL of a cell suspension containing 20 000 cells/mL L-929 cells, and incubated at 37 °C, 5% CO_2 atmosphere and 100% humidity. The adhered cells were detected by optical microscopy after incubation for 3 h, 24 h and 96 h, respectively.

3. Results and Discussion

3.1 Synthesis of 8PEG-VS-SH hydrogel with patterned Au NPs

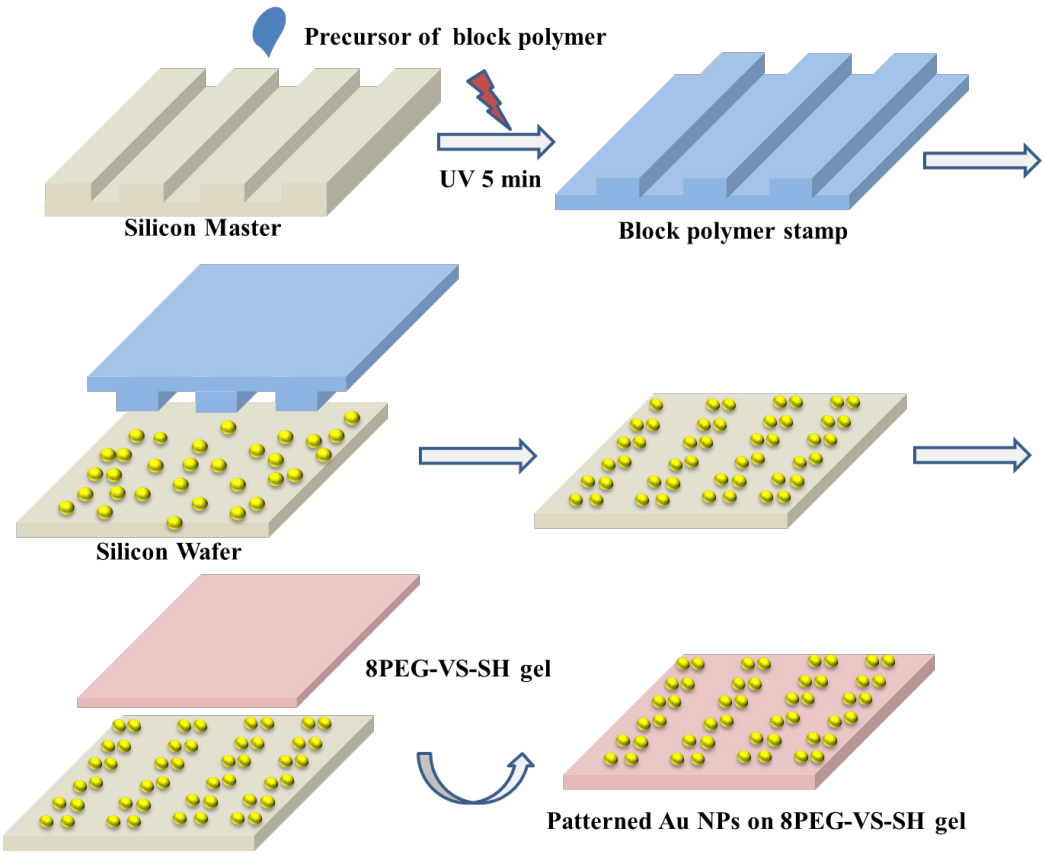

Scheme 1: Schematic diagram of patterning Au NPs on the surface of 8PEG-VS-SH hydrogels in an ordered stripe.

The strategy to prepare micro-patterns of Au NP arrays on the surface of PEG-VS-SH hydrogels is shown in Scheme 1. Firstly, APTES that is rich in amino groups, is chemically modified to the silicon wafers by Chemical Vapor Deposition (CVD) method. Au NPs are then immobilized on the surface of silicon wafers due to the electrostatic interactions between amino groups and negatively charged Au NPs. As studied and introduced in Chapter 4, block polymer hydrogel can efficiently transfer Au NPs from silicon wafers. Therefore, block polymer stamp has been subsequently fabricated and used to create patterned Au NPs stripes on the surface of silicon wafer. Because the block polymer stamp is in a patterned way, only the regions where the stamp directly contacts with the substrate, the Au NPs can be taken off.

After peeling off the stamp, the remaining Au NPs thus represent a patterned array on the surface of the silicon wafer. At last, the patterned Au NPs are transferred from silica wafers onto the surface of the 8PEG-VS-SH hydrogels. This strategy is successful, because the flexibility of the block polymer stamp makes large contact area between block polymer stamps and Au NPs modified silicon via this nano-contact transfer method, leading to higher adhesive force between Au NPs and hydrogels, thereby guaranteeing the patterned Au NPs on the silicon wafer. Then, Au-S bond between Au NPs and 8PEG-VS-SH hydrogels is stronger than the electrostatic interactions between positively charged amino groups on silicon wafer and negatively charged citrate-stabilized Au NPs.

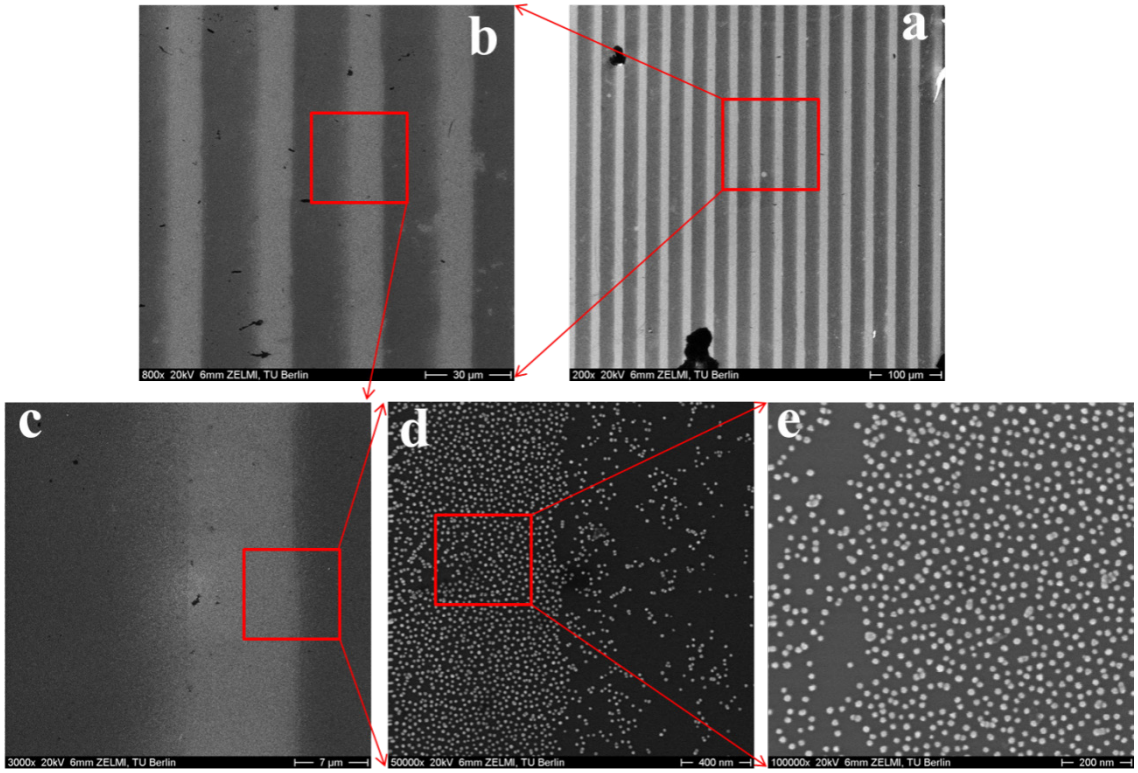

Figure 2: SEM images of patterned Au NPs on the surface 8PEG-VS-SH hydrogels. Scale bar (a) 100 µm; (b) 30 µm; (c) 7 µm; (d) 400 nm; (e) 200 nm. The size of Au NPs is 20 nm, and the distance between patterned stripes is 20 µm in the swollen state.

Two types of patterned Au NPs on the hydrogels have been obtained by using this approach. Au NPs with different sizes (20 and 42 nm) and silicon masters with different width (20 and 50 µm) have been applied in this work. SEM has been used to characterize the as-obtained patterned structure on hydrogels.

When Au NPs with 20 nm in diameter and silicon wafers with 20 µm in width have been used, patterned Au NPs stripes are formed on the hydrogels, which can be recognized as straight grey lines from Figure 2a-c. These patterned Au NPs stripes consist of a densely packed Au NPs without formation of multilayers (Figure 2d and e).

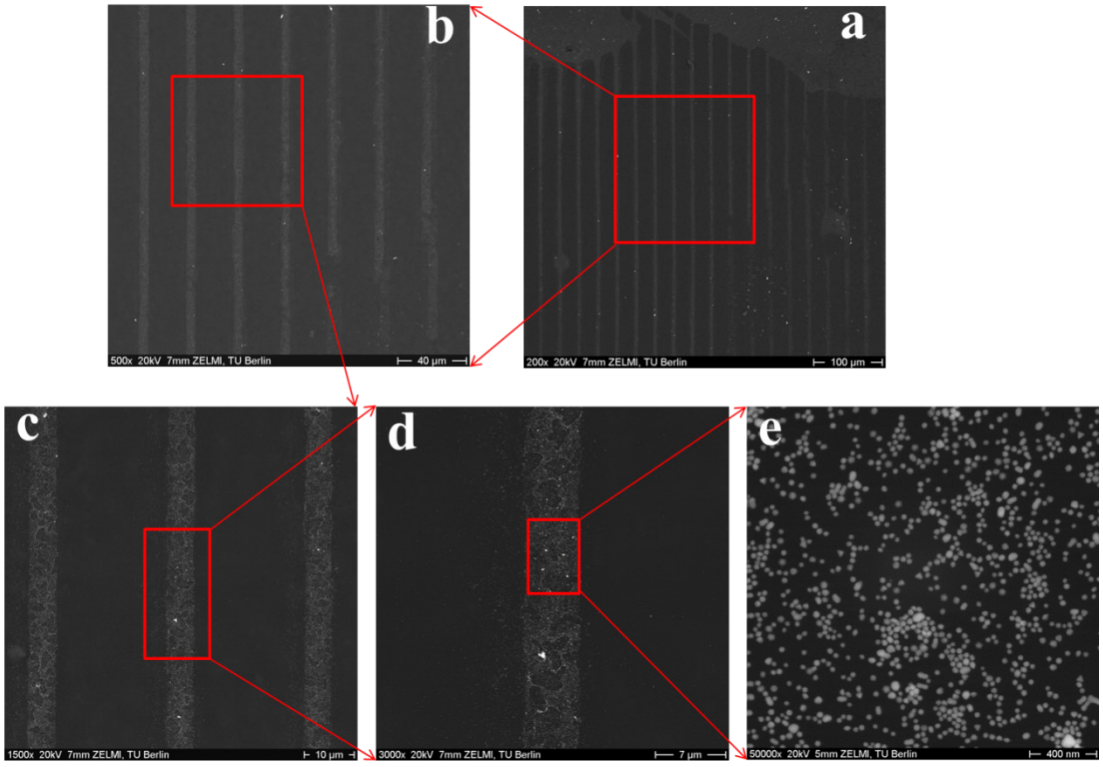

Figure 3: SEM images of patterned Au NPs on the surface of 8PEG-VS-SH hydrogels. Scale bar (a) 100 µm; (b) 40 µm; (c) 10 µm; (d) 7 µm; (e) 400 nm. The size of Au NPs is 42 nm, the width of stripe is 10 µm and the distance between patterned stripes is 50 µm in the swollen state.

When Au NPs with 42 nm in diameter and silicon wafers with 50 µm lines have been used, similar results are obtained. Straight grey lines with lines of 10 µm in width (distance between stripes is 50 µm) can be recognized from Figure 3 a-c, indicating that patterned Au NPs stripes are formed on the hydrogels. At higher magnification, it can be seen that the Au NPs are well distributed on the hydrogels.

In general, for this patterning fabrication method some problems such as broken or collapsed patterns as well as partly missing patterns that are peeled-off together with the mold can be avoided. Moreover, this versatile strategy may also be used for patterning heterogeneous

nanoparticles for various applications.

3.2 Cellular behavior on the patterned Au NPs hydrogels

The ability to culture cells on substrates with control over their size and spatial arrangement has facilitated fundamental studies in cellular research. To pattern cells is ideal to address fundamental issues like cell to cell interactions and cell to ECM interactions. When cells are placed on the substrate, the shape of the cells will largely depend on the size and shape of the adhesive patterns. In this way, the degree of cell extension or spreading can be manipulated. In the present work, the cells are expected to be adhered on the patterned Au NPs stripes in an ordered way after incubation for a certain time (Scheme 2).

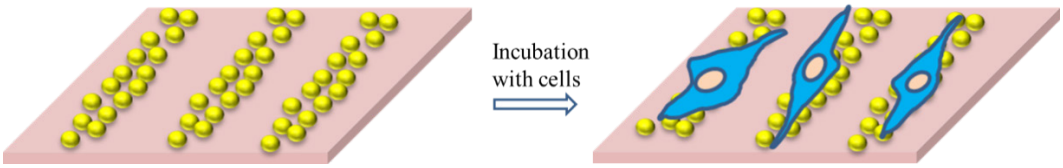

Scheme 2: General scheme of the patterned Au NPs stripes on the surface of 8PEG-VS-SH hydrogels to control cell adhesion and spreading.

3.2.1 Cell adhesion and cell spreading

Cell adhesion process comprises three stages: attachment, spreading, and formation of focal adhesions and stress fibers.[20,21] At the first stage, cells are very sensitive to the environmental conditions. Any variation in the environment will result in their attachment or detachment from the substrate.[22,23] For instance, the variation of the rigidity properties and surface roughness correlates with the changes of cell adhesion.[24,25]

In order to investigate the influence of the incubation time on the cell adhesion and spreading, different incubation times have been applied. The cellular behavior of L-929 cells on the surface of 8PEG-VS-SH hydrogels with patterned 20 nm Au NPs stripes (10 μm in width and 20 μm in distance) has been firstly investigated. As can be observed from Figure 4a, the L-929 cells tend to adhere to the patterned Au NPs stripes after incubation for 3 h (Figure 4b), whereas cells can hardly be observed on the surface of the pure hydrogel without Au NPs

(Figure 4a). With increasing the incubation time to 24 h, the cells start to spread along the patterned Au NPs stripes (Figure 4c). After incubation for 48 h, cells cover the whole pattern lines (Figure 4d), while the morphology of cells changes from round to spindle-like, indicating that the patterned Au NPs on 8PEG-VS-SH hydrogels have a great impact on the murine fibroblasts L-929 cell adhesion and spreading.

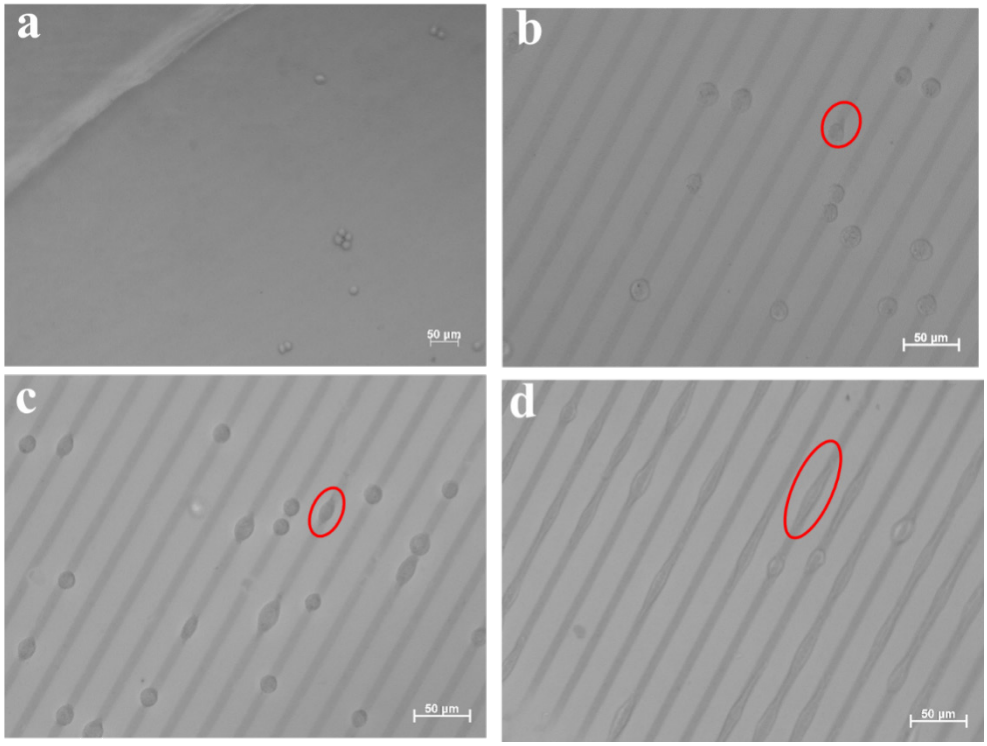

Figure 4: Optical images of L-929 cells after incubation with patterned Au NPs (d = 20 nm) on the surface hydrogels (20 µm in distance of the inter-stripes) for different incubation time: (b) 3 h, (c) 24 h and (d) 48 h, respectively. Red circles refer to L-929 cell growing on the patterned Au NPs stripes.

The cellular behavior of L-929 cells on the surface of 8PEG-VS-SH hydrogels with patterned 42 nm Au NPs stripes (10 µm in width and 50 µm in distance) has been further investigated. Figure 5a shows that the cells adhere to the patterned Au NPs lines after 3 hours of incubation. This phenomenon is distinctly different from L-929 cells cultured on TCPS, where the cells grow with random distribution. Similarly, the cells tend to grow along the direction of the patterned Au NPs stripes after incubation for 24 h (Figure 5b). With increasing the incubation time to 48 h, cell proliferation leads to a slight increase in cell number. Cells agglomerate and form clusters consisting of several individual cells along the direction of the patterned Au NPs

stripes (Figure 5c). The patterned Au NPs stripes, indeed, induce cell alignment and promotes cell adhesion, spreading and proliferation along the patterned direction.

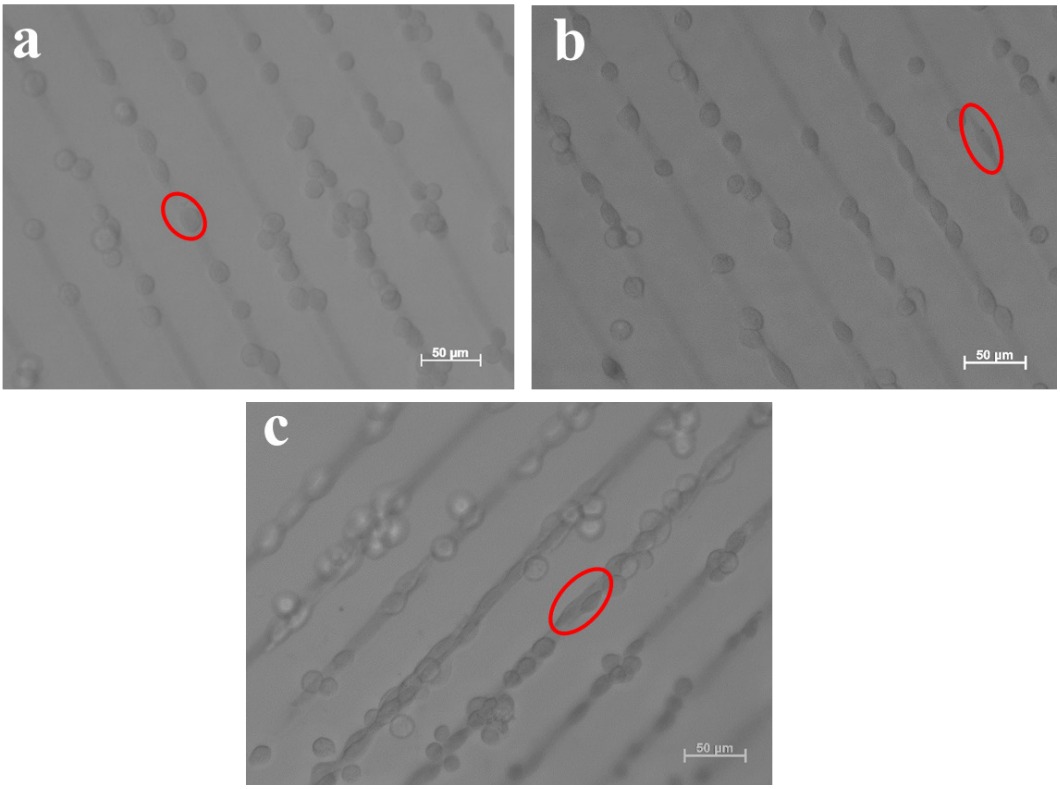

Figure 5: Optical images of L-929 cells incubated with patterned Au NPs (d = 42 nm) on the surface of hydrogels (50 µm in distance of the inter-stripes) for different incubation time: (a) 3 h, (b) 24 h and (c) 48 h, respectively. Red circles refer to L-929 cell growing on the patterned Au NPs stripes.

The result demonstrates that the patterned Au NPs stripes can be transferred to the 8PEG-VS-SH hydrogel to promote cell adhesion and spreading in an ordered way. After incorporation of Au NPs onto the surface of hydrogels, an increase in the stiffness and roughness of composite hydrogels may induce cell adhesion. In addition, surface topographies in the micrometer and nanometer range may also induce cell adhesion. The present study shows that the patterned Au NPs stripes can be used for controlling a cellular response, and affect the morphology, adhesion of the fibroblasts cells. More importantly, patterning cells on the substrate is useful for the development of tissue engineering and fundamental studies in cell biology.

3.2.2 Cell viability

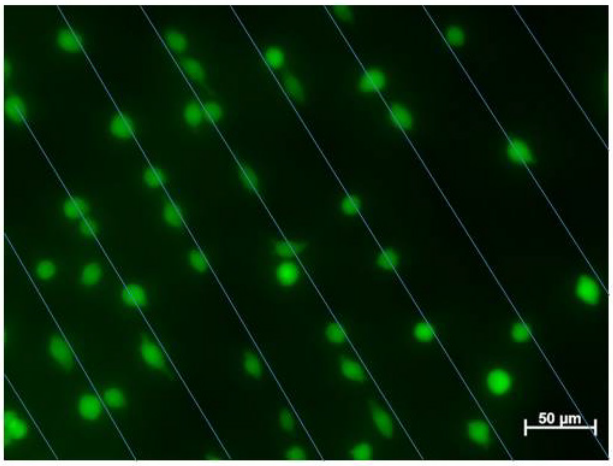

Figure 6: Fluorescent images of L-929 cells after being cultured on the surface of 8PEG-VS-SH hydrogel with patterned Au NPs (d = 42 nm) stripes (50 µm in distance of the inter-stripes) for 24 h. Straight lines were drawn to represent the patterned Au NPs below the cells.

Live/dead staining assay has been used to study the cell viability after incubation with patterned Au NPs stripes for a certain time. In Live/dead staining assay, dead cells appear red, whereas living cells appear green when observed with a fluorescence microscope. As shown in Figure 6, all the cells appear to be green, indicating that the patterned Au NPs stripes are non-cytotoxic to L-929 cells. This is due to the fact that all the Au NPs are firmly immobilized on the surface of hydrogels without entering the cells.

4. Conclusions

In the present study, a simple, time-saving and cost-effective protocol has been developed to create micropatterned Au NPs on the surface of functional PEG hydrogel. This “micro-contact deprinting method” provides a new way to pattern Au NPs onto hydrogel. On this hydrogel with patterned Au NPs, L-929 cells can adhere to and spread on the patterned Au NPs stripes in an ordered way. Therefore, these cyto-compatible hydrogels with patterned Au NPs stripes can be applied for controlling cell adhesion, and they are a very promising candidate for applications in tissue engineering.

5. References

(1) Tiwari, P. M.; Vig, K.; Dennis, V. a.; Singh, S. R. Functionalized Gold Nanoparticles and Their Biomedical Applications. *Nanomaterials* **2011**, *1* (1), 31–63.

(2) Giljohann, D. A.; Seferos, D. S.; Daniel, W. L.; Massich, M. D.; Patel, P. C.; Mirkin, C. A. Gold Nanoparticles for Biology and Medicine. *Angew. Chem. Int. Ed.* **2010**, *49* (19), 3280–3294.

(3) Saha, K.; Agasti, S. S.; Kim, C.; Li, X.; Rotello, V. M. Gold Nanoparticles in Chemical and Biological Sensing. *Chem. Rev.* **2012**, *112* (5), 2739–2779.

(4) Dykman, L.; Khlebtsov, N. Gold Nanoparticles in Biomedical Applications: Recent Advances and Perspectives. *Chem. Soc. Rev.* **2012**, *41* (6), 2256.

(5) Du, Y.; Luo, X.-L.; Xu, J.-J.; Chen, H.-Y. A Simple Method to Fabricate a Chitosan-Gold Nanoparticles Film and Its Application in Glucose Biosensor. *Bioelectrochemistry* **2007**, *70* (2), 342–347.

(6) Nanoarrays, G.; Manipulate, T.; Zhu, M.; Baffou, G.; Meyerbro, N. Adhesion. *ACS Nano* **2012**, 8, 7227–7233.

(7) Tao, Y.; Ju, E.; Ren, J.; Qu, X. Bifunctionalized Mesoporous Silica-Supported Gold Nanoparticles: Intrinsic Oxidase and Peroxidase Catalytic Activities for Antibacterial Applications. *Adv. Mater.* **2015**, *27* (6), 1097–1104.

(8) Cheng, Z. a; Zouani, O. F.; Glinel, K.; Jonas, A. M.; Durrieu, M.-C. Correction to Bioactive Chemical Nanopatterns Impact Human Mesenchymal Stem Cell Fate. *Nano Lett.* **2013**, *13* (10), 4996.

(9) Geiger, B.; Spatz, J. P.; Bershadsky, A. D. Environmental Sensing through Focal Adhesions. *Nat. Rev. Mol. Cell Biol.* **2009**, *10* (1), 21–33.

(10) Yap, F. L.; Zhang, Y. Protein and Cell Micropatterning and Its Integration with Micro/nanoparticles Assembly. *Biosens. Bioelectron.* **2007**, *22* (6), 775–788.

(11) Saha, K.; Keung, A. J.; Irwin, E. F.; Li, Y.; Little, L.; Schaffer, D. V; Healy, K. E. Substrate Modulus Directs Neural Stem Cell Behavior. *Biophys. J.* **2008**, *95* (9), 4426–4438.

(12) Discher, D. E.; Janmey, P.; Wang, Y.-L. Tissue Cells Feel and Respond to the Stiffness of Their Substrate. *Science* **2005**, *310* (5751), 1139–1143.

(13) Dulgar-Tulloch, A. J.; Bizios, R.; Siegel, R. W. Human Mesenchymal Stem Cell Adhesion and Proliferation in Response to Ceramic Chemistry and Nanoscale Topography. *J. Biomed. Mater. Res. - Part A* **2009**, *90* (2), 586–594.

(14) Wang, X.; Li, S.; Yan, C.; Liu, P.; Ding, J. Fabrication of RGD Micro/Nanopattern and Corresponding Study of Stem Cell Differentiation. *Nano Lett.* **2015**, *15* (3), 1457–1467.

(15) Huang, J.; Grater, S. V; Corbellini, F.; Rinck, S.; Bock, E.; Kemkemer, R.; Kessler, H.; Ding, J.; Spatz, J. P. Impact of Order and Disorder in RGD Nanopatterns on Cell Adhesion. *Nano Lett.* **2009**, *9* (3), 1111–1116.

(16) Chen, J.; Mela, P.; Möller, M.; Lensen, M. C. Microcontact Deprinting: A Technique to Pattern Gold Nanoparticles. *ACS Nano* **2009**, *3* (6), 1451–1456.

(17) Seliktar, D. Designing Cell-Compatible Hydrogels. *Science* **2012**, *336*, 1124–1129.

(18) Tibbitt, M. W.; Anseth, K. S. Hydrogels as Extracellular Matrix Mimics for 3D Cell Culture. *Biotechnol. Bioeng.* **2009**, *103* (4), 655–663.

(19) Zhang, F.; Sautter, K.; Larsen, A. M.; Findley, D. a.; Davis, R. C.; Samha, H.; Linford, M. R. Chemical Vapor Deposition of Three Aminosilanes on Silicon Dioxide: Surface Characterization, Stability, Effects of Silane Concentration, and Cyanine Dye Adsorption. *Langmuir* **2010**, *26* (18), 14648–14654.

(20) Murphy-Ullrich, J. E. The de-Adhesive Activity of Matricellular Proteins: Is Intermediate Cell Adhesion an Adaptive State? *J. Clin. Invest.* **2001**, *107* (7), 785–790.

(21) Kruss, S.; Erpenbeck, L.; Amschler, K.; Mundinger, T. a; Boehm, H.; Helms, H.-J.; Friede, T.; Andrews, R. K.; Schön, M. P.; Spatz, J. P. Adhesion Maturation of Neutrophils on Nanoscopically Presented Platelet Glycoprotein Ibα. *ACS Nano* **2013**, *7* (11), 9984–9996.

(22) Kolesnikova, T. A.; Kohler, D.; Skirtach, A. G.; Möhwald, H. Laser-Induced Cell Detachment, Patterning, and Regrowth on Gold Nanoparticle Functionalized Surfaces. *ACS Nano* **2012**, *6* (11), 9585–9595.

(23) Ye, K.; Wang, X.; Cao, L.; Li, S.; Li, Z.; Yu, L.; Ding, J. Matrix Stiffness and Nanoscale Spatial Organization of Cell-Adhesive Ligands Direct Stem Cell Fate. *Nano Lett.* **2015**, *15* (7), 4720–4729.

(24) Kloxin, A. M.; Kloxin, C. J.; Bowman, C. N.; Anseth, K. S. Mechanical Properties of Cellularly Responsive Hydrogels and Their Experimental Determination. *Adv. Mater.* **2010**, *22* (31), 3484–3494.

(25) Guilak, F.; Cohen, D. M.; Estes, B. T.; Gimble, J. M.; Liedtke, W.; Chen, C. S. Control of Stem Cell Fate by Physical Interactions with the Extracellular Matrix. *Cell Stem Cell* **2009**, *5* (1), 17–26

Summary and Outlook

The general objective of this thesis is to exploit the cytotoxicity of gold nanoparticles (Au NPs) in cell-biological applications. Owing to the cyto-compatibility of hydrogels, novel Au NPs-based composite hydrogels have been designed and investigated as substrate for biomedical applications in cell adhesion and spreading. The present thesis is organized as follows:

In **chapter 2**, spherical Au NPs with diameters of 4.5, 12, 30, 50 and 60 nm, respectively, have been synthesized and characterized. Trypan blue assay, Live/dead staining assay and MTT assay methods have been selected to test their cytotoxicity for murine fibroblasts L-929 and murine osteoblasts MC3T3-E1, respectively. Among the as-synthesized Au NPs, Au NPs with 4.5 nm in diameter have been proved to be highly toxic to L-929 cells since the viability of L-929 cells is around 15%. It has been observed that Au NPs not only destroy the cell membrane integrity, but also damage mitochondria. In contrast, the Au NPs show lower toxic effects to MC3T3-E1 cells than that of L-929 cells. In addition, the toxicity of Au NPs decreases with the increase of the size, especially for 60 nm Au NPs, which are comparatively nontoxic. In general, the toxicity of Au NPs strongly depends on their size.

In **Chapter 3**, novel pH-responsive genipin-crosslinked chitosan-gold nanocomposite hydrogels have been developed incorporating 4.5 nm Au NPs due to their high cytotoxicity. At acidic environment (pH 6.4), the swelling ratio of as high as 365% can be reached for these pH-responsive composite hydrogels, resulting in the release of 4.5 nm Au NPs from the nanocomposite hydrogels. The released Au NPs cause harm to cancer cells (i.e. human hepatocellular carcinoma Hep G2), which has been confirmed by fluorescence microscopy *in vitro*. While the Au NPs are well kept in the nanocomposite hydrogels at neutral environment (pH 7.4), they can act as substrate for promoting cell adhesion and proliferation of the L-929 cells. These chitosan-gold nanocomposite hydrogels can be used in biomedical applications (*e.g.* cancer treatment).

The work presented in **Chapter 4** focuses on immobilization of Au NPs onto hydrogels. Au NPs have been firstly distributed on silicon wafers, and then been transferred to 3BC-UV, PEG_{575}-UV, 8PEG-UV and 8PEG-VS-SH hydrogels by soft lithographic method, respectively. 98% of transfer efficiency can be achieved for immobilizing Au NPs on 3BC-UV and 8PEG-VS-SH hydrogels. A monolayer of Au NPs is formed and homogeneously distributed on the surface of 3BC-UV and 8PEG-VS-SH hydrogels. These nanocomposite hydrogels show an excellent stability; even if the composite hydrogels are ultrasonicated for 15 min, the detachment of Au NPs from these composite hydrogels can hardly be observed. In contrast, the other two hydrogels PEG_{575}-UV hydrogel and 8PEG-UV cannot immobilize any Au NPs on their surface by this direct transfer method.

As explained in chapter 4, Au NPs on PEG-VS-SH hydrogels have been immobilized due to the strong Au-S bond. In **chapter 5**, owing to the cyto-compatibility and high transfer efficiency of Au NPs of 8PEG-VS-SH hydrogels, the nanocomposite hydrogels have been investigated as novel substrates to control L-929 cell adhesion. It was found that the overall number of L-929 cell adhered on the composite hydrogels can be well controlled by the density of Au NPs on the hydrogel; increasing the density of Au NPs leads to the increase of cell adhesion. Such performance can be mainly attributed to the following features. Au NPs immobilized on the hydrogels provide stiffness and roughness to adhere cells, facilitating the cell adhesion. Thus, these novel nanocomposites represent a promising biomaterial for controlled cell adhesion in tissue engineering and biomedical application.

In **Chapter 6**, **a "**micro-contact deprinting method" has been developed for designing a new type of patterned nanocomposite hydrogels (Au NPs on 8PEG-VS-SH hydrogel), on which Au NPs were patterned in an organized way (10 μm in width and 20 or 50 μm in distance of the inter-stripes). The obtained patterned Au NPs stripes on the hydrogels have been investigated for their ability to induce localized cell adhesion and spreading of L-929 cells. It has been observed that cells not only adhere to these micro-patterned nanocomposite substrates, but also spread in an ordered way along the patterned Au NPs stripes. The present work provides a facile and effective method for transferring patterned Au NPs from silicon

wafers to hydrogel surface. Most importantly, the novel composite hydrogels can act as a useful platform for biotechnological research, making it a promising candidate for the design of tissue engineering substrates, in particular for nerve regeneration substrate where the guidance of axons regenerating over large distances is of vital importance.

Abstract

Gold nanoparticles (Au NPs) play an important role in chemistry, biology, engineering and medicine due to their unique optical properties, ease of synthesis, and flexibility of (bio)chemical functionalization. Knowledge about their potential toxicity is essential before these nanomaterials can be used in real clinical settings, particularly, if they are incorporated into hydrogels as nanocomposite hydrogels for advanced biomedical applications. The main goals pursued in this thesis are the development synthesis of Au NPs with variable size, their controlled immobilization on poly(ethylene glycol)-based hydrogels, and the investigation of cellular responses to these nanocomposite hydrogels.

In the present work, Au NPs with different sizes are synthesized and characterized. The cytotoxicity of these as-obtained Au NPs are conducted *in vitro* with murine fibroblasts and osteoblasts using Trypan blue assay, Live/dead staining assay and MTT assay, respectively. Au NPs with 4.5 nm in diameter show significant cytotoxicity, while larger NPs are less cytotoxic. These small Au NPs have consequently been selected to fabricate novel pH-responsive hydrogel systems, i.e. genipin cross-linked chitosan-gold nanocomposite hydrogels that could release the toxic substances at lower pH values. The novel nanocomposite hydrogels indeed are found to feature a higher swelling degree at pH 6.4 as compared with that at pH 7.4. It has been demonstrated that the 4.5 nm Au NPs are released from the gels when cultured with human hepatocellular carcinoma Hep G2 (acidic environment), inducing cell death. Meanwhile, they can work as substrate to promote adhesion and proliferation of murine fibroblasts in neutral environment.

Besides the incorporation of Au NPs into genipin-crosslinked chitosan hydrogels, the immobilization of Au NPs on the surface of PEG-based hydrogels has been investigated. To that end, a soft lithographic method was developed ("nanocontact transfer lithography") to transfer Au NPs from silicon wafers to soft hydrogels. A correlation between the density of the immobilized Au NPs on the surface of 8PEG-VS-SH hydrogel and the cell adhesion of murine fibroblasts is observed.

In addition to the random distribution of Au NPs on PEG-hydrogels, patterned Au NPs on hydrogels are fabricated by another soft lithography method (i.e. “micro-contact deprinting”). These patterned Au NPs on PEG- hydrogels are also used to control cell adhesion. Cell adhesion can be directed following the patterned Au NPs lines in an ordered way.

These gold nanocomposite hydrogels provide a useful platform to further develop the control of cellular behavior on new materials for biomedical and tissue engineering applications.

Zusammenfassung

Gold Nanopartikeln (Au NPs) spielen eine bedeutende Rolle in Chemie, Biologie, Ingeieurwesen und Medizin aufgrund ihrer einzigartigen optischen Eigenschaften, leichten Synthese und Flexibilitat in der (bio)chemischen Funktionalisierung. Kenntnis über ihre potentielle Toxizität ist notwendig bevor diese Nanomaterialien in realen klinischen Einstellungen angewendet werden, insbesondere wenn sie inkorporiert werden in Hydrogele als Nanokomposite Hydrogele für neue biomedizinische Anwendungen. Die Hauptziele, die in dieser Arbeit verfolgt werden, sind die Entwicklung der Synthese von Au NPs mit verschiedenen Größen, ihre Immobilisierung in Polyethylenglykol-basierte Hydrogele und die Untersuchung der zellulären Reaktionen zu diesen Nanokompositen Hydrogelen.

In der vorliegenden Arbeit werden Au NPs mit verschiedenen Größen synthetisiert und charakterisiert. Die Zytotoxizität der erhaltenen Au NPs sind ausgeführt *in vitro* mit murinen Fibroblasten und Osteoblasten jeweils mittels Trypanblau Analyse, Lebend/Tot Färbung Analyse und MTT Analyse. Au NPs mit einer Durchmesser von 4.5 nm zeigen eine signifikante Zytotoxizität, während größere Au NPs weniger toxisch sind. Diese kleinen Au Nps sind folglich ausgewählt um neue, pH-responsive Hydrogelsysteme zu bilden, z.B. Genipin quervernetzte Chitosan-Gold Nanokomposite Hydrogele, die die toxischen Substanzen bei kleineren pH Werten freilassen. Diese neuen Nanokomposite Gele weisen höhere Schwellungsgrade bei pH 6.4 im Vergleich zu pH 7.4 auf. Es wird gezeigt, dass die 4.5 nm großen Au NPs aus den Gelen freigesetzt werden wenn sie mit humanen Hepatomzellen Hep G2 (saure Umgebung) kultiviert werden, die den Zelltod verursacht. Inzwischen können sie als Substrate verwendet werden, die die Zelladhäsion und Proliferation von murinen Fibroblasten in natürlicher Umgebung fördert.

Zusätzlich zu der Inkorporation von Au NPs in Genipin-quervernetzte Chitosan-Gold Nanokomposite Hydrogele ist die Immobilisierung von Au NPs auf die Oberfläche von PEG-basierten Hydrogelen untersucht worden. Hierzu ist eine softlithographische Methode entwickelt („Nanokontakt Transfer Lithography“) um die Au NPs von Siliziumwafern auf

weiche Hydrogele zu transferrieren. Eine Beziehung zwischen der Dichte der immobilisierten Au NPs auf der Oberfläche von 8PEG-VS-SH Hydrogelen ond der Zelladhesion von murinen Fibroblasten wird beobachtet.

Zusätzlich zu der zufälligen Verteilung von Au NPs auf PEG-Hydrogele, werden strukturierte Au NPs auf Hydrogele mittels weiterer softlithographischer Methode (z.B. „Mikrokontakt Rückdrucken“) erzeugt. Diese strukturierten Au NPs auf PEG-Hydroglen sind ebenfalls benutzt um Zelladhäsionen zu kontrollieren. Es wird gezeigt, dass die Strukturen die Zelladhäsion steuern indem sich die Zellen regelmäßig den strukturierten Au NPs Linien folgen.

Diese Gold Nanokomposite Hydrogele bieten eine brauchbare Plattform für die weitere Entwicklung bei der Kontrolle von zellulären Verhalten gegenüber neuen Materialien für biomedizinische und gewebetechnische Anwendungen.

List of publications

Publications resulting from this thesis

1. **Fang Ren**, Marga C. Lensen. „Genipin Cross-linked Chitosan-Gold Nanocomposite Hydrogels for Cancer Treatment Applications". *Manuscript in preparation*.

2. **Fang Ren**[+], Zhenfang Zhang[+], and Marga C. Lensen. „Facile Transfer of Gold Nanoparticles to Functional Hydrogels and the Effect on Cell Adhesion". Submitted to *Chemistry of Materials.*

3. **Fang Ren**[+]**,** Zhenfang Zhang[+], and Marga C. Lensen. „Surface Patterning of Au NPs on 8PEG-VS-SH Hydrogel Surface to Control Cell Adhesion". *Planned to be submitted to Small.*

Additional publications and manuscripts

1. Zhenfang Zhang[+], Axel Loebus[+], Gonzalo de Vicente, **Fang Ren**, Manar Arafeh, Zhaofei Ouyang and Marga C. Lensen. „Synthesis of Poly (ethyleneglycol)-based hydrogels via amine-Michael type addition with tunable stiffness and post-gelation chemical functionality". *Chemistry of Materials* **2014**, 26, 3624−3630.

2. Zhenfang Zhang, Fabian Kruse, **Fang Ren**, Cigdem Alkan, Inez M. Weidinger and Marga C. Lensen. „Instant hot spots created via flexible gold nanoparticles on polymeric hydrogels greatly enhance Raman scattering". Submitted to *Angewandte Chemie International Edition.*

Contribution to Scientific Conferences

Genipin Cross-linked Chitosan/Gold Nanocomposite Hydrogel for Cancer Treatment Applications. **Fang Ren**, Gonzalo de Vicente Lucas, Zhenfang Zhang, Marga C. Lensen. *Materials Science Engineering MSE* **2014**, Darmstadt.

Surface Patterning of Gold Nanoparticles on Functional PEG-based Hydrogels to Control Cell Adhesion. **Fang Ren**, Zhenfang Zhang, Marga C. Lensen. *Polydays* **2014**, Berlin.

PEG-based Hydrogels patterned with Gold Nanoparticles for Biosensor Applications. Cigdem Yesildag, Arina Tyushina, Christoph Bartsch, **Fang Ren**, Zhenfang Zhang, Marga C. Lensen. *EuroBiomat* **2015**, Munich.

Acknowledgement

First and foremost, I would like to thank my supervisor Professor Dr. Marga C. Lensen for giving me the opportunity to work on this versatile, interesting subject, for allowing me to follow my own ideas, and for being always available for helpful and inspiring guidance and discussions in every stage of the writing of this thesis.

Further, I also want to thank the China Scholarship Council (CSC) for financial support.

And all the colleagues at Lensen Lab, I thank for all their kindness, advice and help. Especially thank to Dr. Zhenfang Zhang for his productive teamwork and invaluable suggestions throughout the course of this research with a number of collaborations.

In addition, I wish to thank the BIG-NSE.

Beyond that, I want to express my gratitude to the persons, Prof. Dr. Roderich Sussmuth, Dr. Wei Song, Fabian Kruse, who helped in several instrumental analysis and measurement during the course of this thesis.

Last but not least, I am indebted to my boyfriend Jie Cao and my family, for their support, patience and empathy in these years.